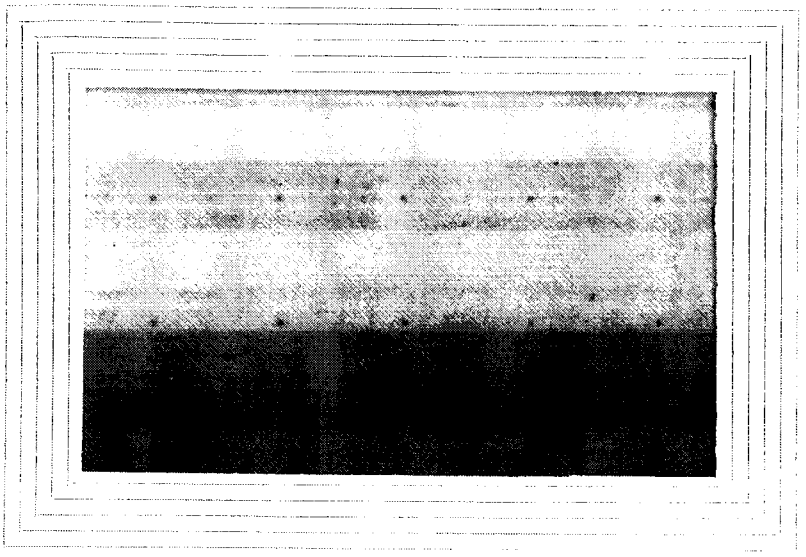

P-133

Department of Physics and Astronomy
Brigham Young University
Provo, Utah 84602

FINAL REPORT

Pioneer 10 and 11 (Jupiter and Saturn)

Magnetic Field Experiments

Prepared under grant NAG 2-145

by Brigham Young University

for

Ames Research Center

NASA

October, 1986

Principal Investigator: Douglas E. Jones

Technical Monitor: Richard O. Fimmel

Summary

This final report covers work conducted by Brigham Young University personnel in the analysis and interpretation of magnetic field data obtained by the vector helium magnetometer (VHM) during the encounters of Jupiter (Pioneer 10 and 11) and Saturn (Pioneer 11). We have principally directed our efforts in an attempt to understand the puzzling characteristics of the Jovian and Saturnian magnetospheric magnetic fields. An apparent substorm (including thinning of the dayside "tail" current sheet) has been observed at Jupiter, as well as evidence suggesting that at the magnetopause the cusp is at an abnormally low latitude. The characteristics of Saturn's ring current as observed by Pioneer 11 were dramatically different from those suggested by the Voyager observations. Most importantly, very strong perturbations in the azimuthal ring current magnetic field suggest that the plane of the ring was not in the dipole equatorial plane, being tilted 5 - 10° relative to the dipole and undergoing significant changes during the encounter. When these changing currents were corrected for, an improved planetary field determinations was obtained. In addition, the ring and azimuthal currents at Saturn displayed significantly different time dependences. The time dependent characteristics observed in the radial current system suggest that at least a portion of the magnetospheric currents may behave in a manner similar to the predicted perturbations of a rapidly rotating plasma-field configuration. Theoretical studies of the interaction of Saturn's corotationg magnetospheric plasma with Titan's atmosphere have been started. Such a study may lead to a better understanding of the anomalous behavior observed in the field as Pioneer 11 passed corotationally downstream, and above the orbit, of Titan.

A list of publications and papers presented resulting from this grant are listed at the end of this report. Four additional papers are in preparation, portions of which are included in this report. This grant covered the period January 1, 1982 thru September 30, 1986, and funds were received sufficient to support the equivalent of about 1 1/2 faculty man years.

The Jovian Magnetosphere and Magnetospheric Currents

Douglas E. Jones (and Barry T. Thomas, JPL)

In our early studies of the Jovian magnetosphere and magnetospheric currents we concentrated primarily on the ρ component of the field, and utilized only the outbound Pioneer 10 data (Jones et al., 1975, 1976, 1980a). Subsequent attempts to interpret the z and ϕ component suggested that in those portions observed by Pioneers 10 and 11, either a "tail-like" current sheet or a local time dependent radial current sheet was present in the dayside magnetosphere (Goertz et al., 1976, Parish et al., 1980, Connerney, 1981, Jones et al., 1981). A critical test to distinguish between these two possibilities is not possible at the present time because observations of the magnetosphere in the required noon to dusk quadrant have not been made.

In a more comprehensive study, a model combining a disc current, a dusk-dawn current sheet in both the tail and dayside regions, and an image dipole (to simulate magnetopause currents) was utilized (Fig. 1). For both the tail and dayside sheet currents, a semi-infinite current sheet was assumed to extend to infinity in the dawn-dusk direction, being restricted only in the sunward and tailward dimensions. Although this model is not realistic for either the dayside or tail regions, nevertheless it was relatively easy to work with and qualitatively provided an indication of the type of currents likely needed to explain the data in the development of a more sophisticated model.

Preliminary studies of this model used a visual fit to the three vector components of the perturbation field ($\vec{B}_{total} - \vec{B}_{planetary}$) rather than a computer algorithm. Field line plots of the magnetospheric field due to the derived currents plus that of a planetary dipole displayed a tendency for the cusp to be at a relatively low latitude of 25-40^{o} as compared to a value nearer 80^{o} for earth (Jones et al., 1983). This low latitude feature was most apparent when the currents required to fit the outbound Pioneer 10 data were used. The Pioneer 11 outbound data (Figure 2) are clearly seen to be consistent with the possible existence of a low-latitude cusp. In fitting the Pioneer 10 outbound data segment it was not necessary to have the tail-like sheet extend into the dayside more than several Jovian radii because most of this pass occurred behind the dawn line. When the tail-like dayside current

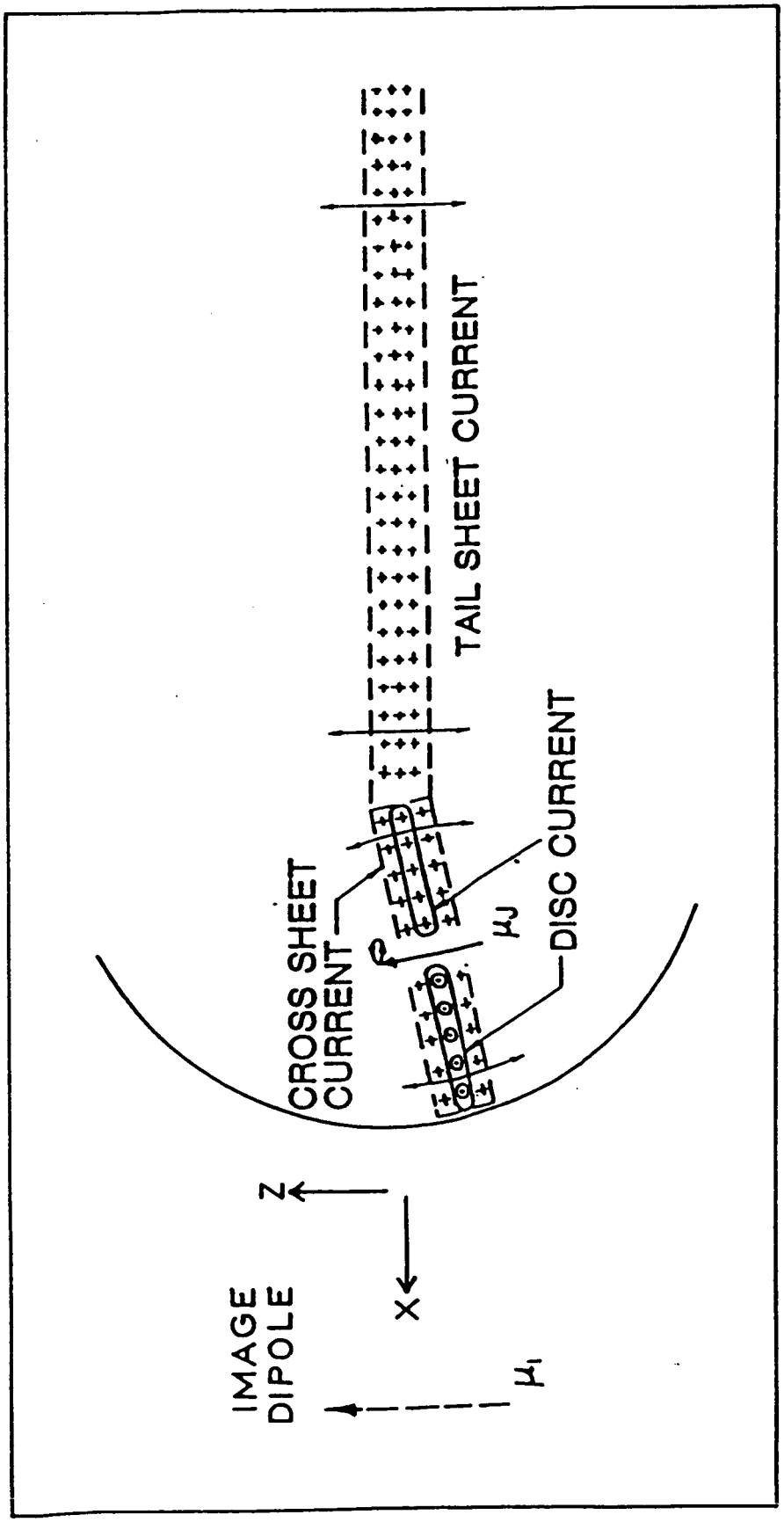
TAIL SHEET CURRENT
CROSS SHEET CURRENT
DISC CURRENT
μ_J
Z
X
IMAGE DIPOLE
μ_I

Figure 1

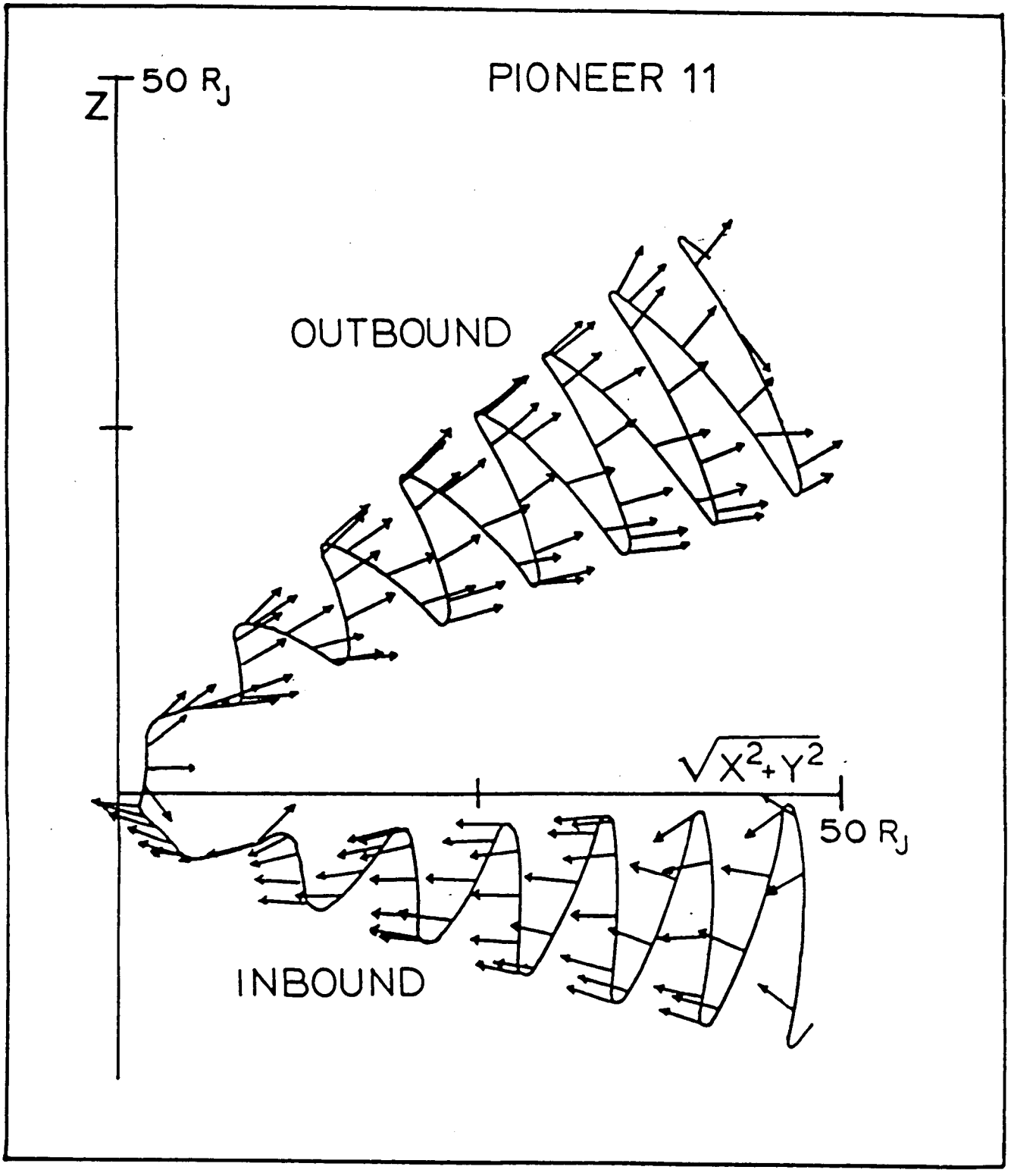

Figure 2

sheet was allowed to extend into the dayside region only enough to provide a good fit to this data segment alone, the resulting cusp latitude was much more earth-like. Hence, it was concluded that the low latitude cusp may simply result from the formation of a tail-like current sheet in the dayside magnetosphere.

The location of a planetary cusp is dependent upon the field sources inside the magnetosphere and the solar wind pressure at the magnetopause boundary. For a simple dipole field source, a uniform external field oriented opposite the direction of the planetary dipole results in two cusps, one at each pole. If the uniform field is parallel to the dipole moment, the cusp is a circle in the equatorial plane. Studies of the case of a dipole field in the presence of a rectilinear pressure due to the impinging solar wind show that the resulting cusp is similar to the case of the dipole in a uniform field that is anti parallel to the dipole moment, but shifted 10 - 20^{o} from the pole in the direction towards the solar wind source. It can be shown that a dipole field in the presence of a uniform field oriented orthogonal to the dipole moment, and reversing direction with respect to the dipole equator (i.e., a sheet or tail like field) locates the magnetopause cusp at a colatitude angle θ given by $\tan^{-1} = \sqrt{2}$, or a latitude of about 35^{o} (Fig. 3). Addition of a ring or disc current will tend to extend the equatorial magnetopause and probably increase the latitude of the cusp (inverse r dependent current density), whereas a solar wind approaching the planet on the same side of the magnetosphere as the cusp, should, as in the case of the simple dipole (i.e., the earth), lower the latitude of the cusp. The presence of other fields (north ward, south ward) will correspondingly shift the cusp to lower or higher latitudes, respectively.

Considerable research has been done in searching for IMF control of the latitudinal position of the magnetospheric cusp. (See reviews by Burch [1979] and Shepherd [1979].). Recently, Carbury and Meng (1986a, 1986b) have found that IMF B_z and AE both affect the low altitude cusp latitude, the latitude varying between 67 and 78 degrees. The behavior of the latitude of the cusp at the magnetopause boundary was unknown at this time, however. During quiet times no apparent correlation between these parameters and cusp latitude was observed (Carbury and Meng, 1986a). No mention is made in terms of a possible solar wind pressure dependence of the cusp laitude, however. It is also

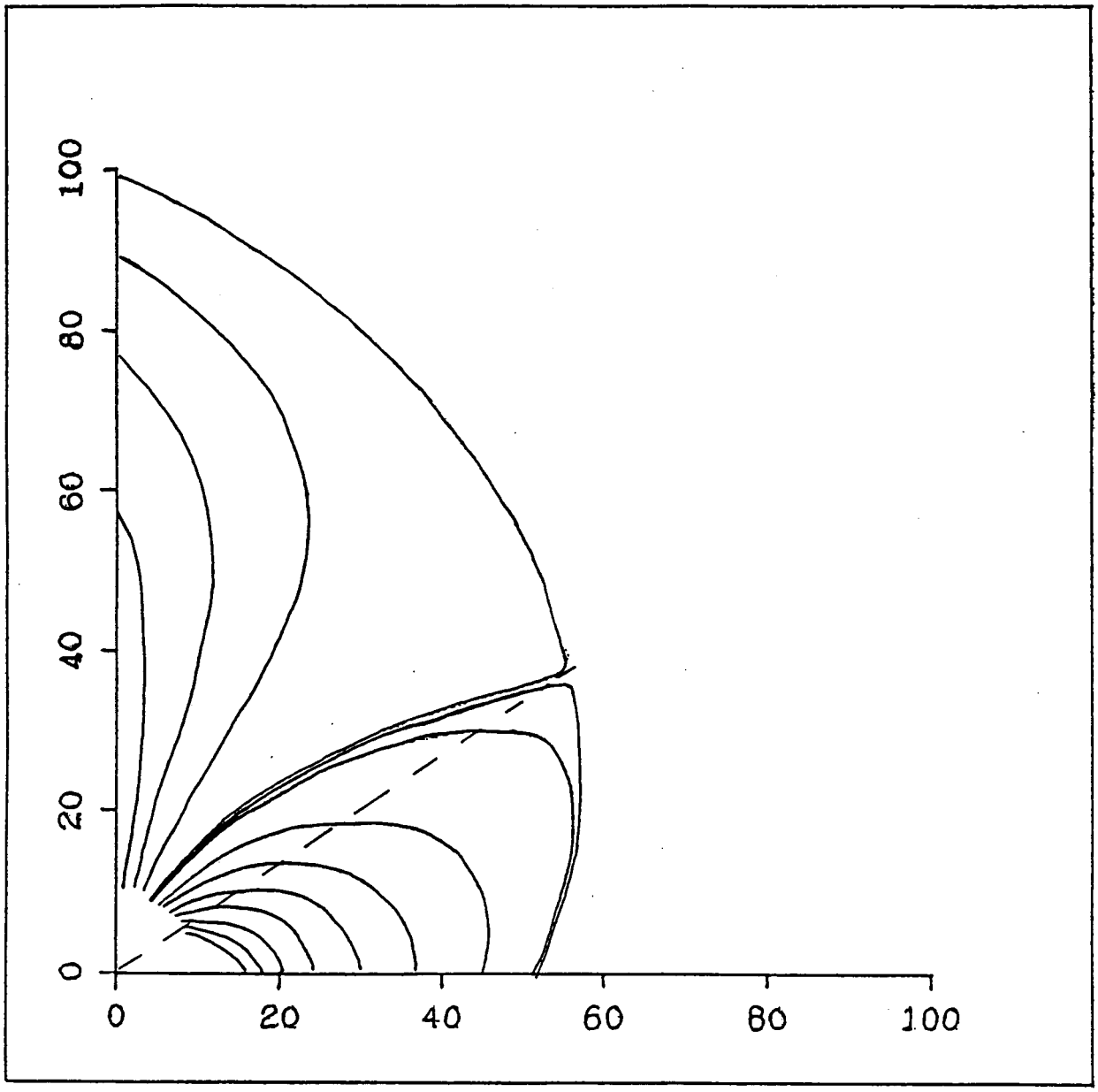

Figure 3

possible that some other parameter, directly related to equatorial magnetospheric currents (dawn-dusk?) might be important. We should note that immediately after the final outbound penetration of the magnetopause by Pioneer 11 the interplanetary field had a southward component, and therefore this factor may also have contributed to the observed low latitude cusp, although the magnitude of the field was low (~ 0.3 - .5 nT).

Jovian model magnetospheres based upon a more comprehensive fitting of the Pioneer data sets also suggest low cusp magnetic latitudes (Fig. 4). As noted above, a major feature of these model magnetospheres, in addition to the warped current disc (Jones et al., 1980a), has been a tail-like dawn dusk sheet current required in the sunlit portion of the magnetosphere (Jones et al., 1981). This current flows in opposition to the disc current in the dayside magnetosphere, and parallel to it in the tail region. Such a current adds a uniform field of the type noted above and therefore should lower the latitude of the cusp, the lowering being further enhanced by the positive z component of a realistic, divergenceless sheet field.

A large number of models fitting the Pioneer 10 and 11 data have been studied using a computer algorithm to minimize the data-model field residuals. One such set of model magnetopause and corresponding cusp configurations are displayed in Figure 4 (Thomas and Jones, 1984). Another model studied added high latitude "return" currents, as such a model is a more realistic representation of the actual current configuration likely to exist. A cusp latitude of 23^{o} for such a model has been determined. Note that this is the latitude at the magnetopause and not where bifurcation of the field lines occur at the planetary surface (which is nearer 80^{o}). A number of other models of this general type have also been studied.

Several comments about the fitting procedure and model currents should be made as they could critically affect the resulting location of the magnetopause cusp. In the development of the model fits from which the magnetopause shapes were derived, the noisy data close to the outbound magnetopause was excluded, i.e., no attempt was made to fit the data right up to the point evident in the data where the spacecraft entered the magnetosheath. Consequently, the location of the cusp, as determined by the latitude where the model field lines bifurcate, is based upon field lines extrapolated some 15-20 Jovian radii beyond the fitting region, and as a result, the location of the

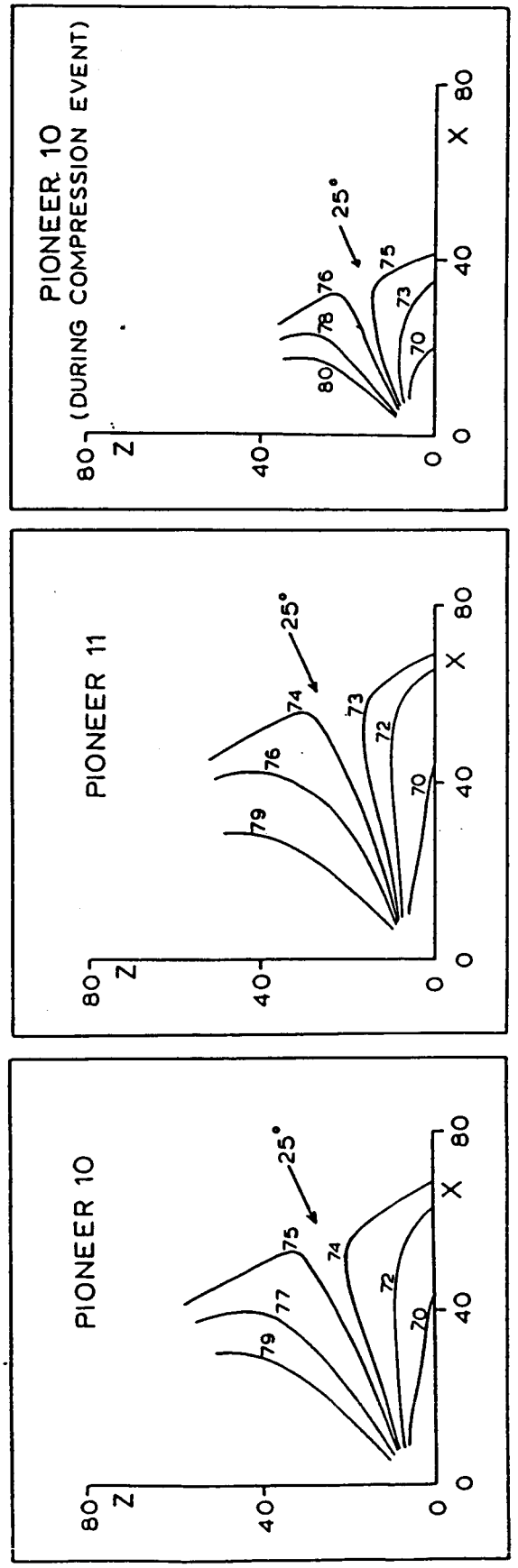
PIONEER 10
Z
80
40
0
0
40
80
X
25°
79
77
75
74
72
70
(a)
PIONEER 11
Z
80
40
0
0
40
80
X
25°
79
76
74
73
72
70
(b)
PIONEER 10
(DURING COMPRESSION EVENT)
Z
80
40
0
0
40
80
X
25°
80
78
76
75
73
70
(c)

Figure 4

cusp might be considered to be model dependent. Another unrealistic feature of these models is the obvious extension of both the tail and dayside current sheets beyond the equatorial magnetopause. The shape of the magnetospause (and therefore the latitude of the cusp) will be dependent upon where the image dipole is placed in the minimization process. Although other modelling studies of magnetopause shapes using image dipoles have set the image dipole distance at approximately 4-6 times the planet-magnetopause distance (Hones, 1963), we did not to constrain the model in this manner in the preceding studies.

We have continued our model studies of these data with a more realistic dayside dusk-to-dawn current sheet, replacing the semi-infinite ribbon currents by one confined to a parabolic envelope, and using a finite width tail current sheet. A function minimization routine was used as before (Thomas and Jones, 1984). For this model the image distance and dayside sheet extent are allowed to be variables. The dawn-dusk extent of the current sheet was assumed to be either 3 or 4 times the subsolar distance. Runs for which this ratio was 3 provided a slightly poorer fit, but we do not believe that our model studies are able to provide a unique determination of the shape of the magnetosphere in the magnetic equatorial plane. Such parameters as the disc tilt, thickness, and twist parameters were observed to optimize rapidly and remain relatively fixed during the runs resulting in the following: tilt = 11.17^{o}, Disc current thickness = 2.5 * 0.9 R_J (assumed Gaussian variation), R_{in} = 12.66, start longitude for twisting = 39.61^{o}, Twist rate = $0.96^{o}/R_J$. The tail length was arbitrarily set at 1.5 times R_{out}. The relevant parameters for combined Pioneer 11 inbound and outbound data set are displayed in Table 1, and the derived field lines of one model are shown in Figure 5.

The corresponding cusp latitude is found to be at about 27^{o}, or about the same as that found using the semi-infinite current sheet reported by Thomas and Jones (1984) (compare Figures 4 and 5). However, it is noted that if the image distance is fixed at 300 R_J, i.e., 4 to 5 times the observed subsolar distance for the Jovian magnetosphere or consistent with the assumed location of the image dipole in the early terrestial modelling reported by Hones (1963), the cusp moves up to nearly 32^{o}. At the same time, the rms error of the fit for the fixed image distance case is degraded by less than 1 part in several thousand. Some change in cusp latitude on the order of 1 or 2 degrees

Table 1

Pioneer 11 inbound/outbound (15-45 R_J)

(variable image distance and sheet extent; parabolic ratio = 3.0)

A	α	ratio M_I/M_J	dist R_J	j_{sheet} nT	sheet R_J	R_{out} R_J	β	rms nT
0.741	2.03	6.1	144.7	1.96	125.2	64.8	0.250	2.26

* times 3.65×10^{15}

Table 2

Pioneer 11 inbound/outbound: 20-45 R_J

(image distance 300 R_J, sheet extent = R_{out}; parabolic ratio = 4)

j_o (nT) nT	α	ratio M_I/M_J	j_{sheet} nT	R_{out} R_J	β	rms nT
.767	1.930	120.6	2.423	55.9	0.202	1.70

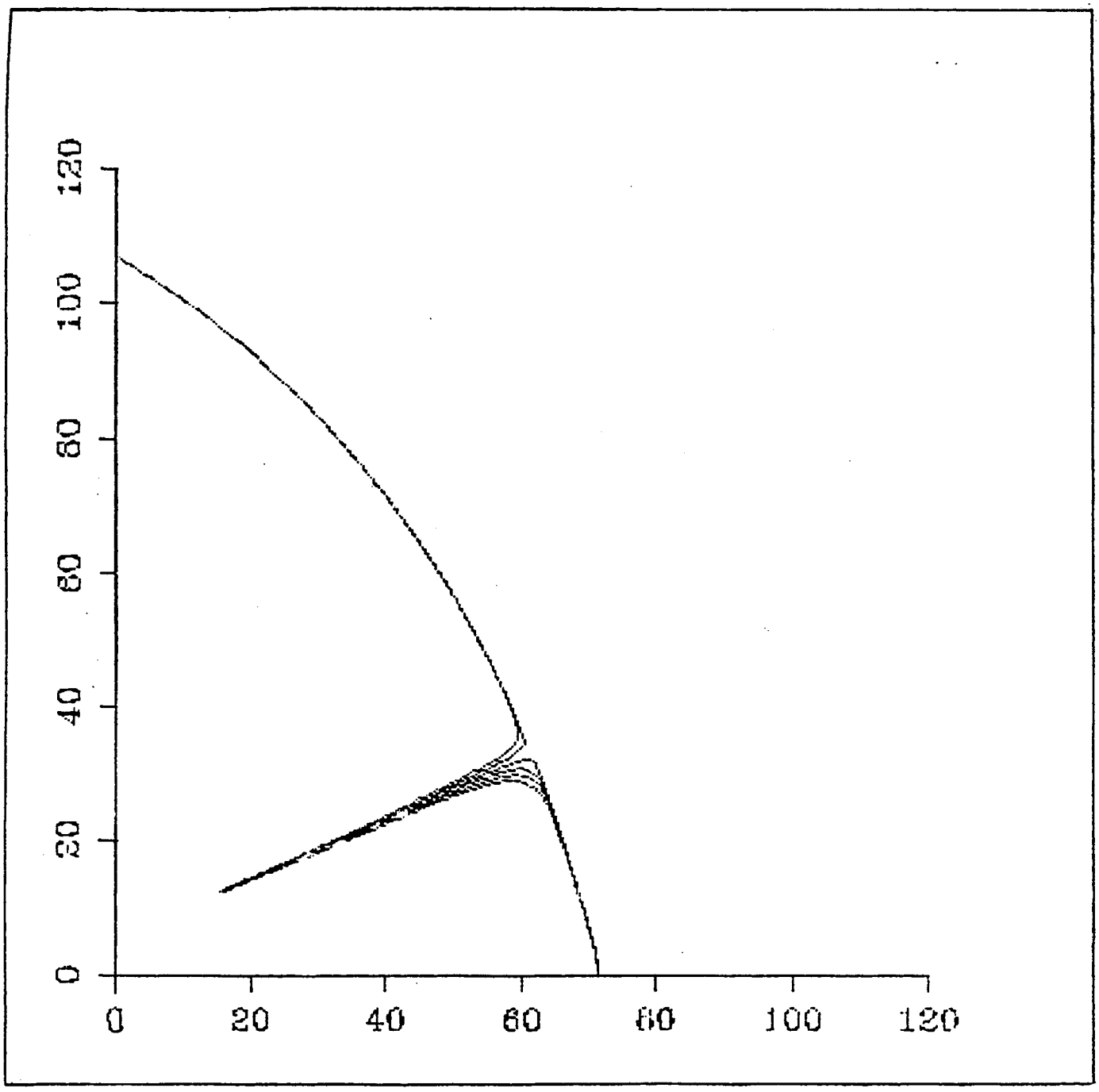

Figure 5

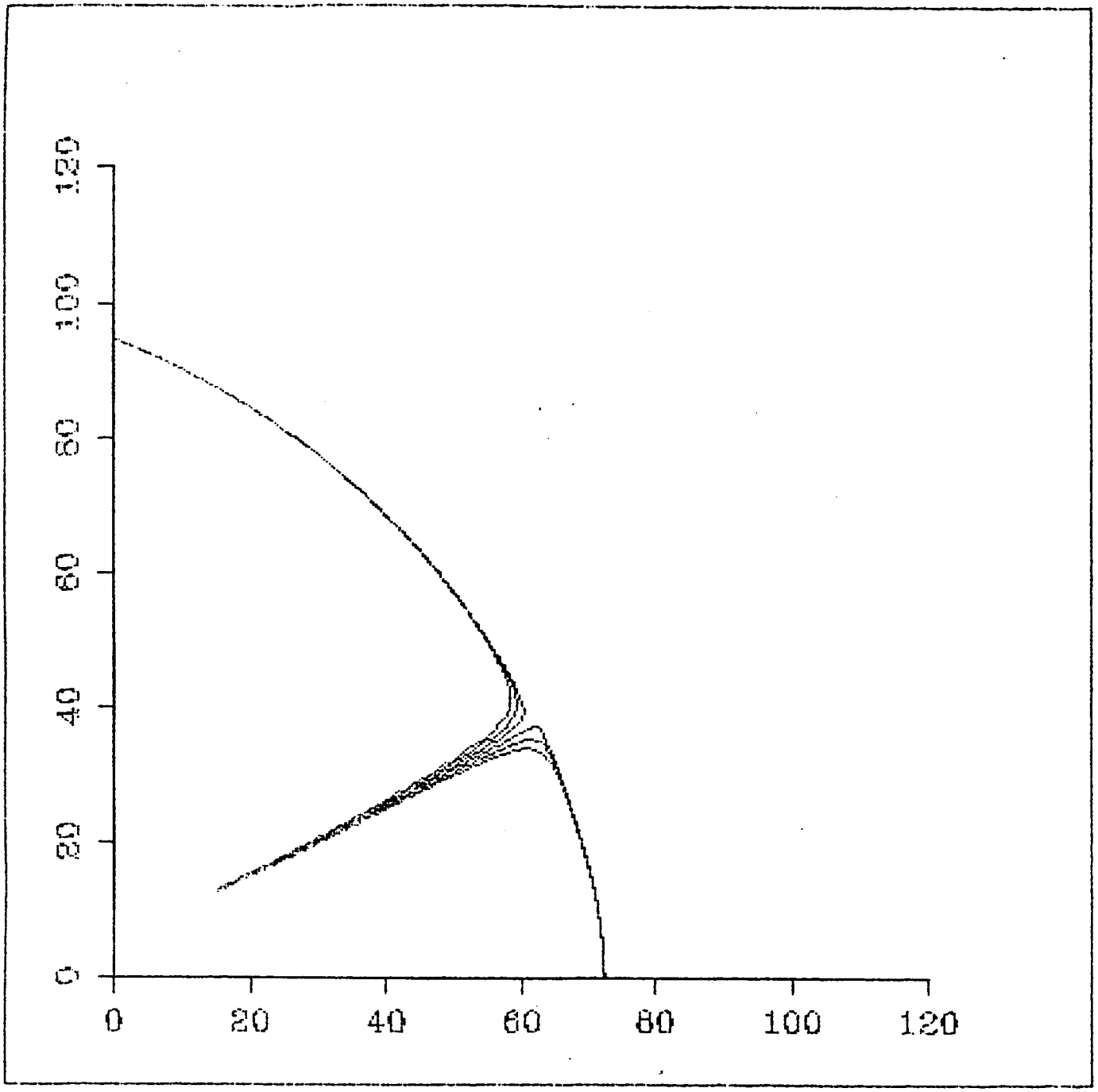

Figure 6

is also noted if the dayside sheet extent is allowed to be a variable. A comparison of the variable versus fixed image distance and dayside sheet extent can be seen by comparing Tables 1 and 2, and Figures 5 and 6 (note that the data intervals differ also).

In addition to fitting the data prior to the first outbound magnetopause crossing, we have fit the magnetosphere data interval just prior to the final outbound penetration of the magnetopause, i.e., the outbound interval between 62 and 80 R_J. This interval was of interest because contrary to the suggested trend of the field within 57 R_J, where a clear separation of the field lines consistent with a cleft region in the magnetosphere is observed, the field lines in the last magnetosphere interval all show a definite southward trend. Combining these data with that obtained closer suggests a possible field configuration consistent with the results suggested of the 3-d MHD studies of Wu (1983, 1985) and Wu and Walker (1985), wherein a counter flowing current segment is predicted to occur just beyond the location of a nominal cusp. However, the nature of the data beyond 62 R_J out to the last outbound magnetopause crossing are also consistent with a different interior current configuration. Applying no constraints to the model, we have attempted to determine the current parameters best fitting the outer interval. The cusp is located at a much higher latitude (i.e., more "earth-like") and appears to be due to the apparent disappearance of the dayside tail-like current sheet as the solar wind pressure decreased.

The manner in which the required model parameters change in fitting the Pioneer 10 inbound data before and after the magnetosphere was pushed closer to the planet than Pioneer 10 is suggestive of the manner in which the tail changes during a substorm at earth. This is seen in the very strong increase in dayside sheet current at the same time that a significant thinning of this sheet by a factor of at least 10 to 1 occurs (Table 3 and Figures 7 and 8). One notes that the current density in the sheet is increasing by a factor of some 6 X 11 = 66 as a result of an increase in current per unit R_J width by a factor of about 6, and a decrease in sheet thickness by a factor of about 11. This is in response to the effective increase in solar wind pressure equivalent to an image dipole ratio increase by a factor of about 4. It would appear that not only is there a need for a tail-like sheet in the dayside magnetosphere, but the manner in which it changes in response to an increase

Table 3

Distance interval	A	α	image ratio @ 300 R_J	jcs nT	thik R_J
beyond 60-85 R_J	0.375	1.21	157.6	0.883	1.35
within 20-45 R_J	0.344	2.85	663.3	4.94	.114

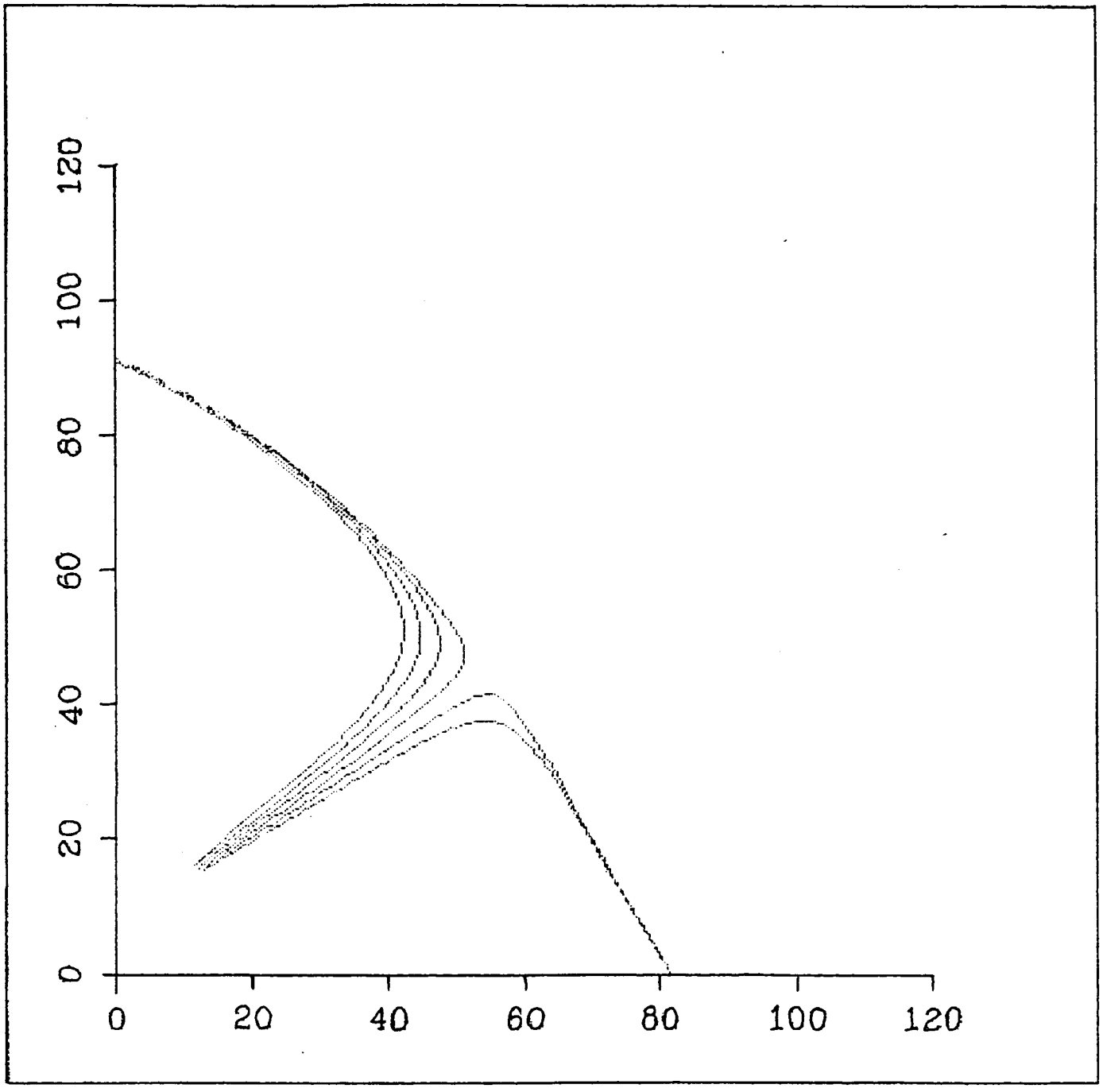

Figure 7

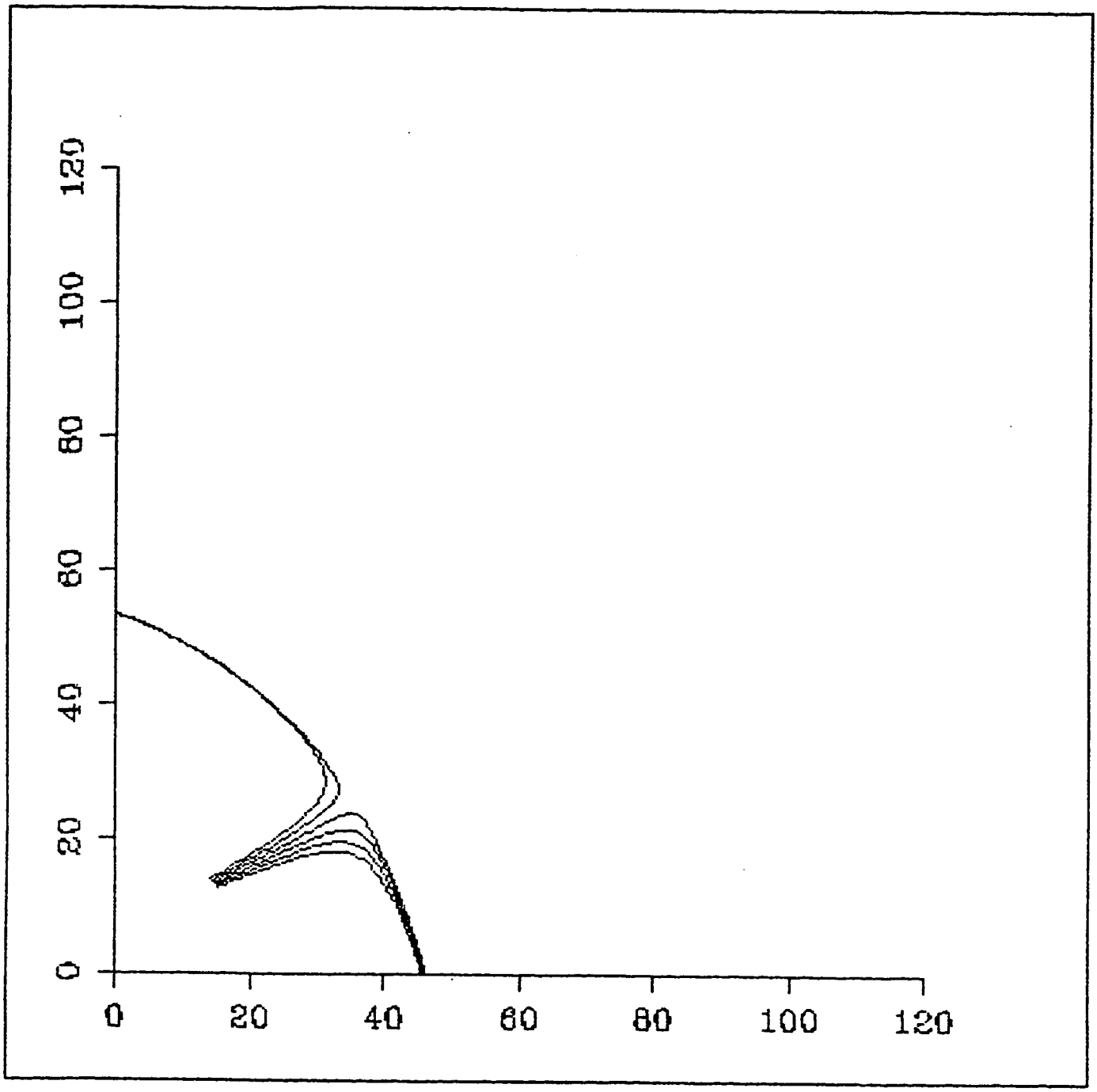

Figure 8

solar wind pressure is somewhat similar to the changes occurring in the terrestrial tail current sheet. At the same time, the inverse power law dependence of the Jovian ring current sharply increases resulting in an overall decrease in the current in the ring rather than an increase as observed at earth.

Polynomial B Model Studies

(Douglas E. Jones with Barry T. Thomas and Michael Rigler, JPL)

Another model magnetosphere that was studied utilized polynomial expressions for the rectangular (B_x, B_y, B_z) components of the perturbation magnetic field required in addition to the twisted azimuthal disc current, instead of one in which this addition magnetospheric current configuration was assumed and optimized. The model is sufficiently different that it was felt that such an approach might help answer the question regarding a possible model dependent cusp latitude.

Each component of the corresponding $\vec{B}$ is required to be divergenceless, and certain symmetries are imposed consistent with the geometry at Jupiter. For example, the general 3rd degree polynomial expression for B_x is

$$
\begin{aligned}
B_x = {} & A_0 + A_1 x + A_2 y + A_3 z + A_4 x^2 + \\
& A_5 y^2 + A_6 z^2 + A_7 xy \; A_8 xz + A_9 yz + \quad \Big] \text{2nd deg.} \\
& A_{10} x^2 y + A_{11} x^2 z + A_{12} x^3 + A_{13} y^2 x + \\
& A_{14} y^2 z + A_{15} y^3 + A_{16} z^2 x + A_{17} z^2 y + A_{18} z^3 \quad \Big] \text{3rd deg.}
\end{aligned}
$$

and similarly for B_y and B_z. After application of $\nabla \cdot \vec{B} = 0$, several types of effective sheet configurations were studied. These include:

Dusk-dawn sheet type constraint (even/odd functional dependence on coordinates)

1. B_x even y, odd z; B_y odd y,z; B_z even y,z (no constraint on tail)
2. B_x even x,y, odd z; B_y odd y,z; B_z even y,z

Radial sheet type constraint

B_x even x, odd y, odd z; B_y odd x, even y, odd z; B_z even x, y, z

For example, a dusk-dawn sheet-like polynomial function that was used had the form:

		2nd degree	3rd degree
B_x	=	$A_1 z + A_2 xz$	$+ A_8 y^2 z + A_9 x^2 z + A_{10} z^3$
B_y	=	$A_3 yz$	$+ A_{11} xyz$
B_z	=	$A_4 + A_5 x\ A_6 x^2 + A_7 y^2$	$+ A_{12} xy^2 - (2A_9 + A_{11})/2\, xz^2 - (A_2 + A_3)/2\, z^2$

Modifications of the above expression are also possible, i.e., one can set $A_2 = 0$ in the B_x expression, which forces other changes in order to satisfy the zero divergence requirement.

The results for several types of polynomial models are displayed in Table 4 (Thomas et al., 1984). For purposes of comparison four of the previous magnetosphere current models studied are also listed (first four entries). Magnetopause/cusp configurations predicted by the polynomial models are displayed in Figures 9-13. Figures 9 and 10 are the results for 2-degree sheet-like models, where Fig. 9 is for $A_2 = 0$, and Fig. 10 for $A_2 = 0$. Figure 11 results from a 2-degree radial-like disc current. Figures 12-15 are derived from 3-degree polynomial fits. Figures 12 and 13 are sheet-like, and differ in that Fig. 13 results if the coefficient of z^3 term is forced to be negative. The corresponding rms fit values are 1.62 and 1.69 nT. Figures 14 and 15 display the 3-degree results for radial-like current sheets, the latter forcing one of the coefficients.

An inspection of the magnetopause shapes in these figures make it clear that rms fitting in the data region should not be the major criterion used to decide which of the models is most realistic, particularly when considering the 3-degree polynomial functions. In fact, it is surprising that none of the 3-degree magnetopause shapes appear reasonable if our knowledge of the shape of the earth's magnetopause is correct. Additional consideration must be given to the abnormal character of the corresponding $\nabla \times B$ currents. This portion of the study suggests that the type of model affects the latitude of the cusp, but those models predicting a reasonable magnetopause shape generally have cusps at latitudes considerably lower than for earth.

Table 4

Polynomial Model Results

Model	σ nT	Cusp Latitude degrees
Model Magnetosphere Currents		
Tail, Sheet	1.84	26
Symmetric sheet (not tail)	1.74	23
Tail, sheet plus return sheet currents	1.73	23
Tail, no sheet ($\sigma = [(\Delta b_r^2 + \Delta b_z^2)/2]^{1/2}$)	2.29	22
Tail, 2nd Degree Polynomial: dusk-dawn sheet-like		
B_x even y, odd z; B_y odd y , z; B_z even y,z	1.82	39
B_x even x, y, odd z; B_y odd y, z; B_z even y, z	1.83	49.5
Tail, 3rd Degree Polynomial: sheet-like		
B_x even y, odd z; B_y odd y, z; B_z even y, z	1.62	32
B_x even x, y, odd z; B_y odd y, z; B_z even y, z	1.61	33
Tail, 3rd Degree Polynomial: radial-like	2.31	77

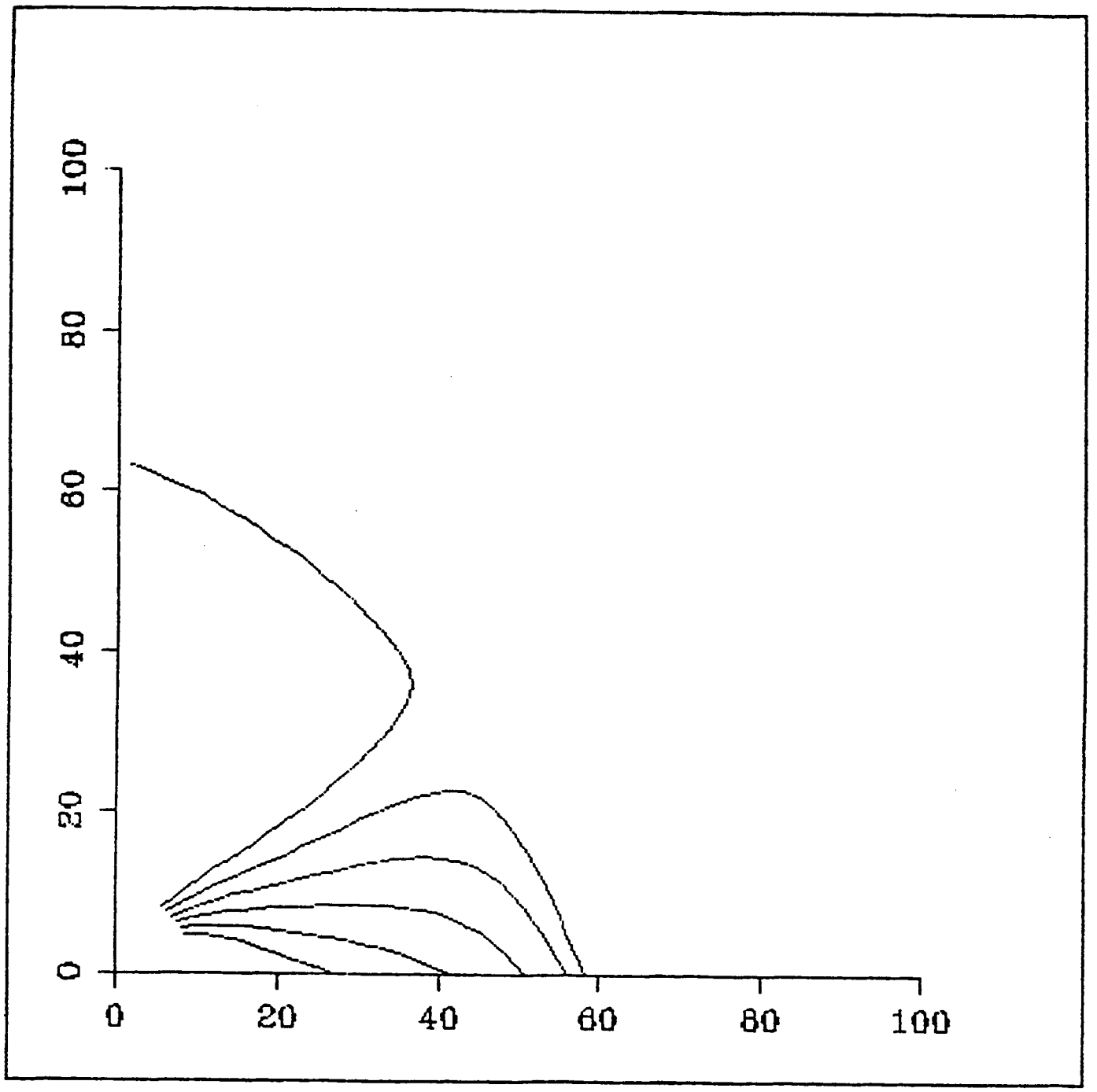

Figure 9

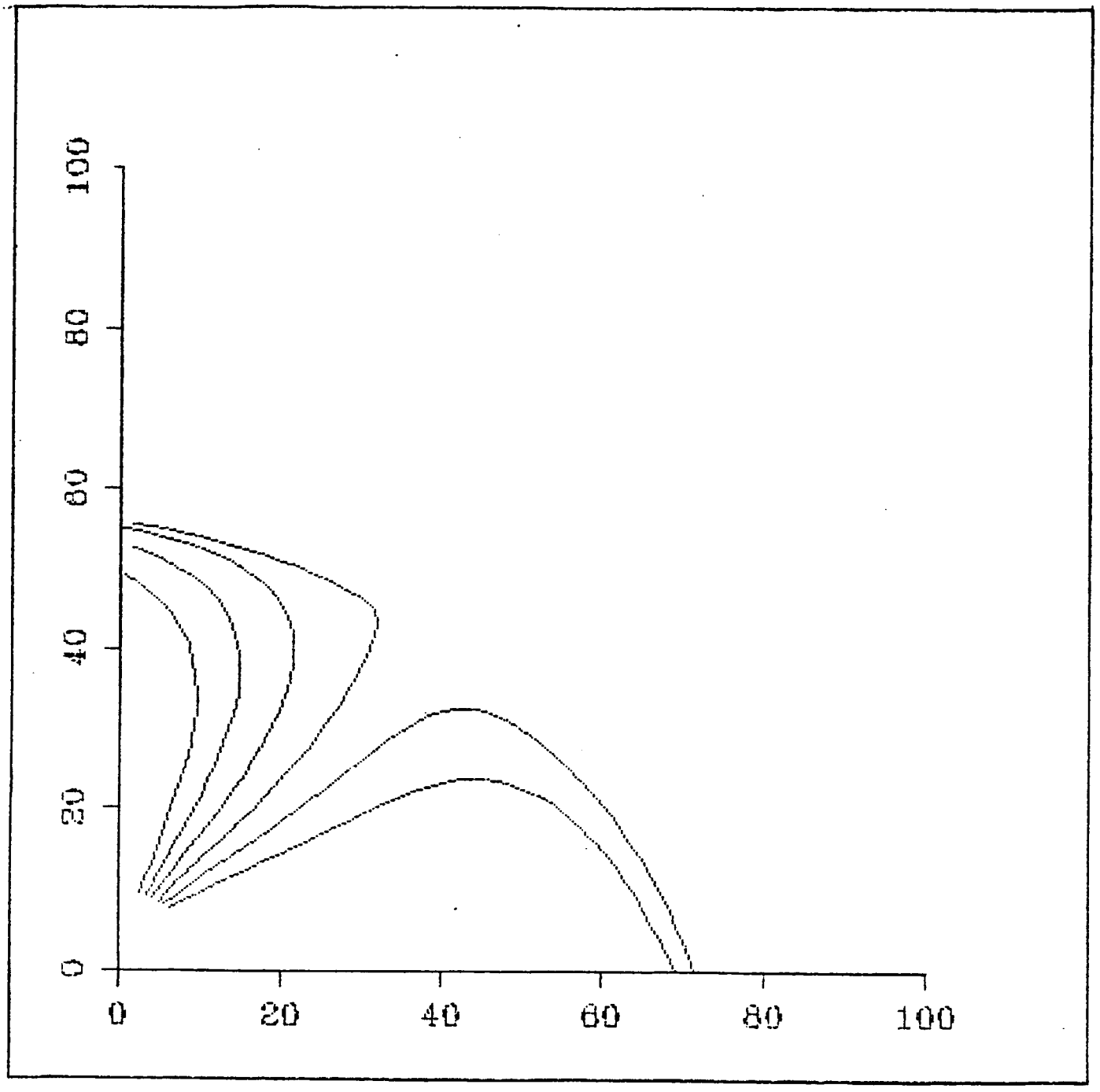

Figure 10

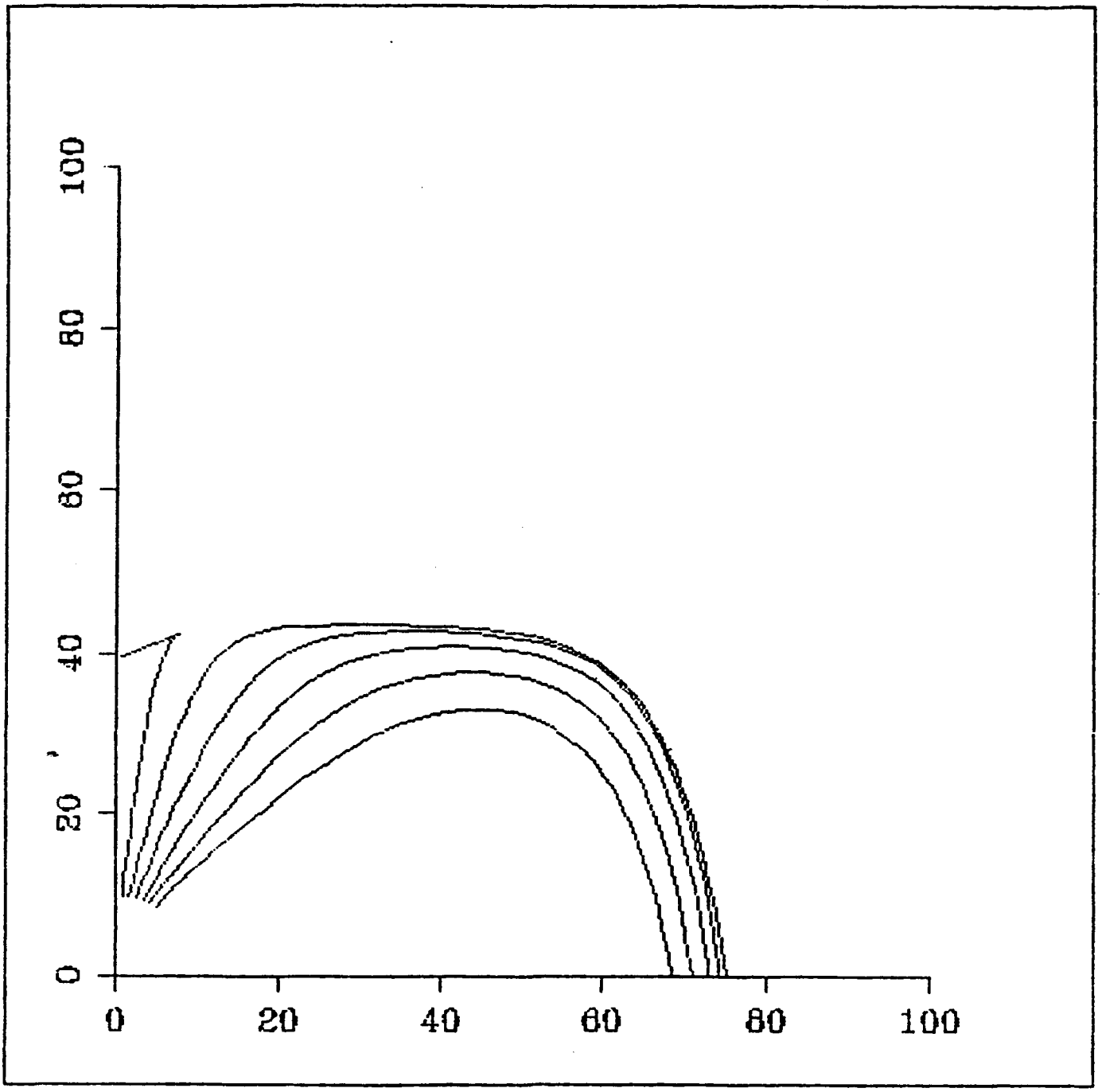

Figure 11

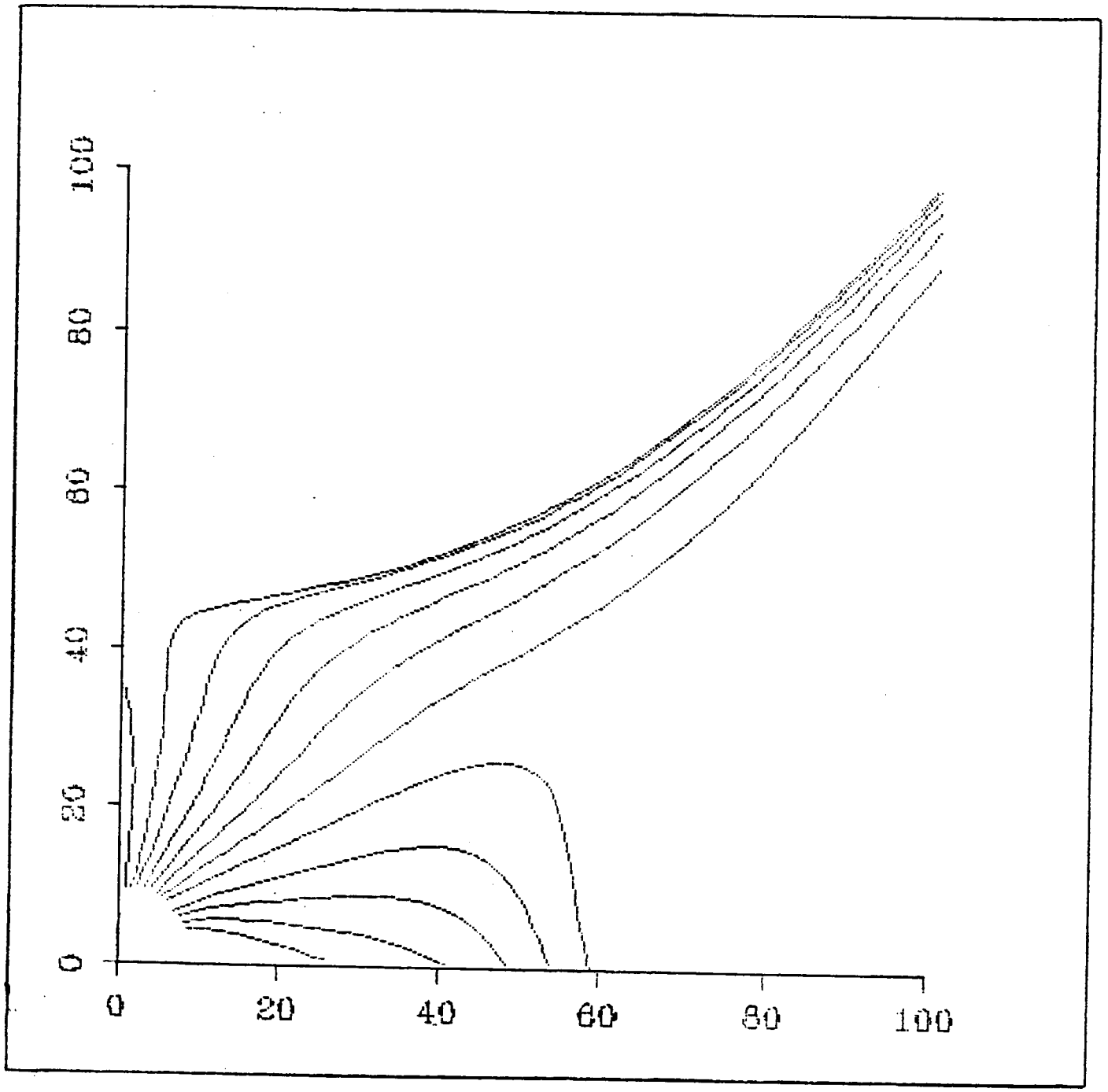

Figure 12

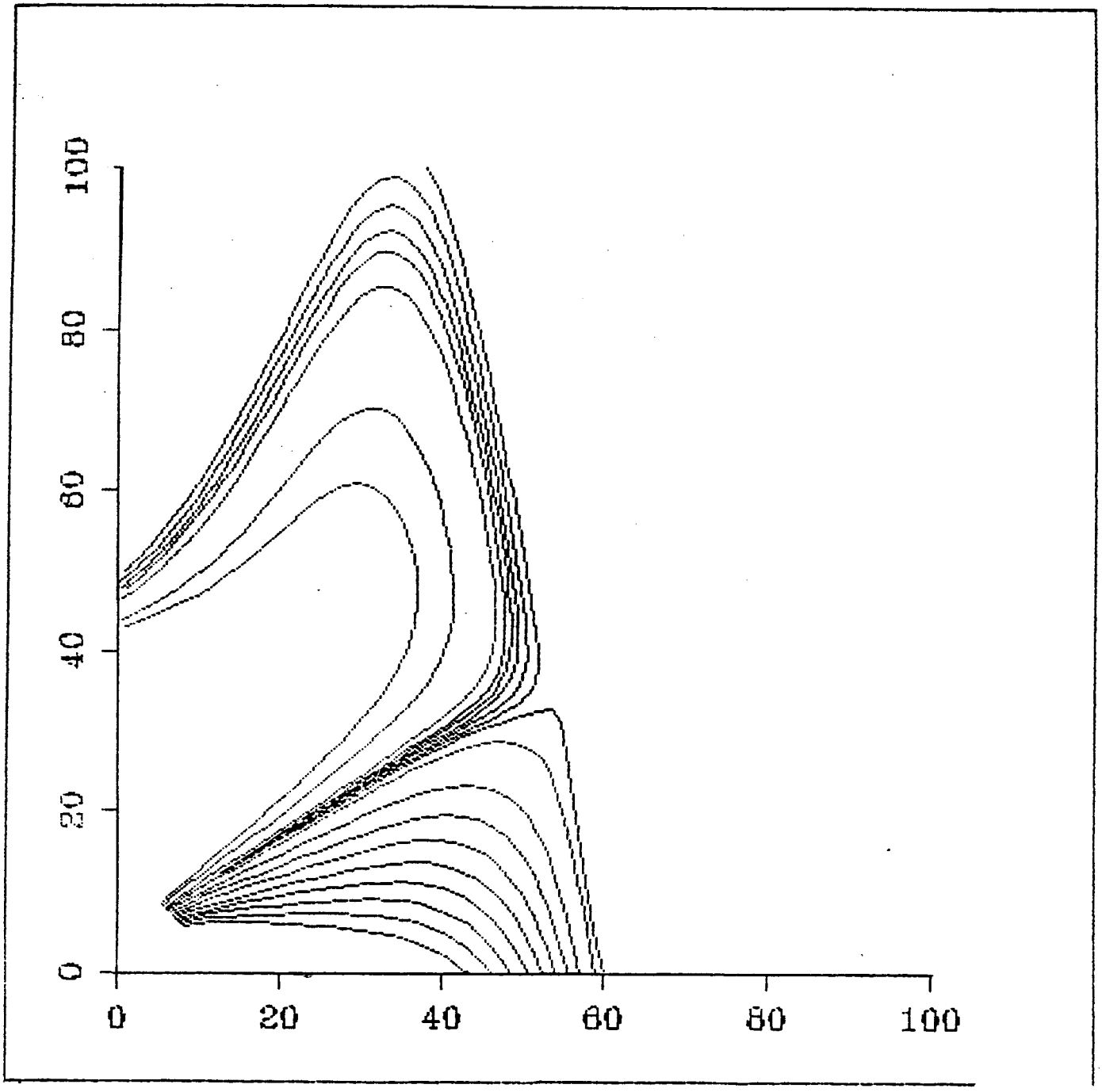

Figure 13

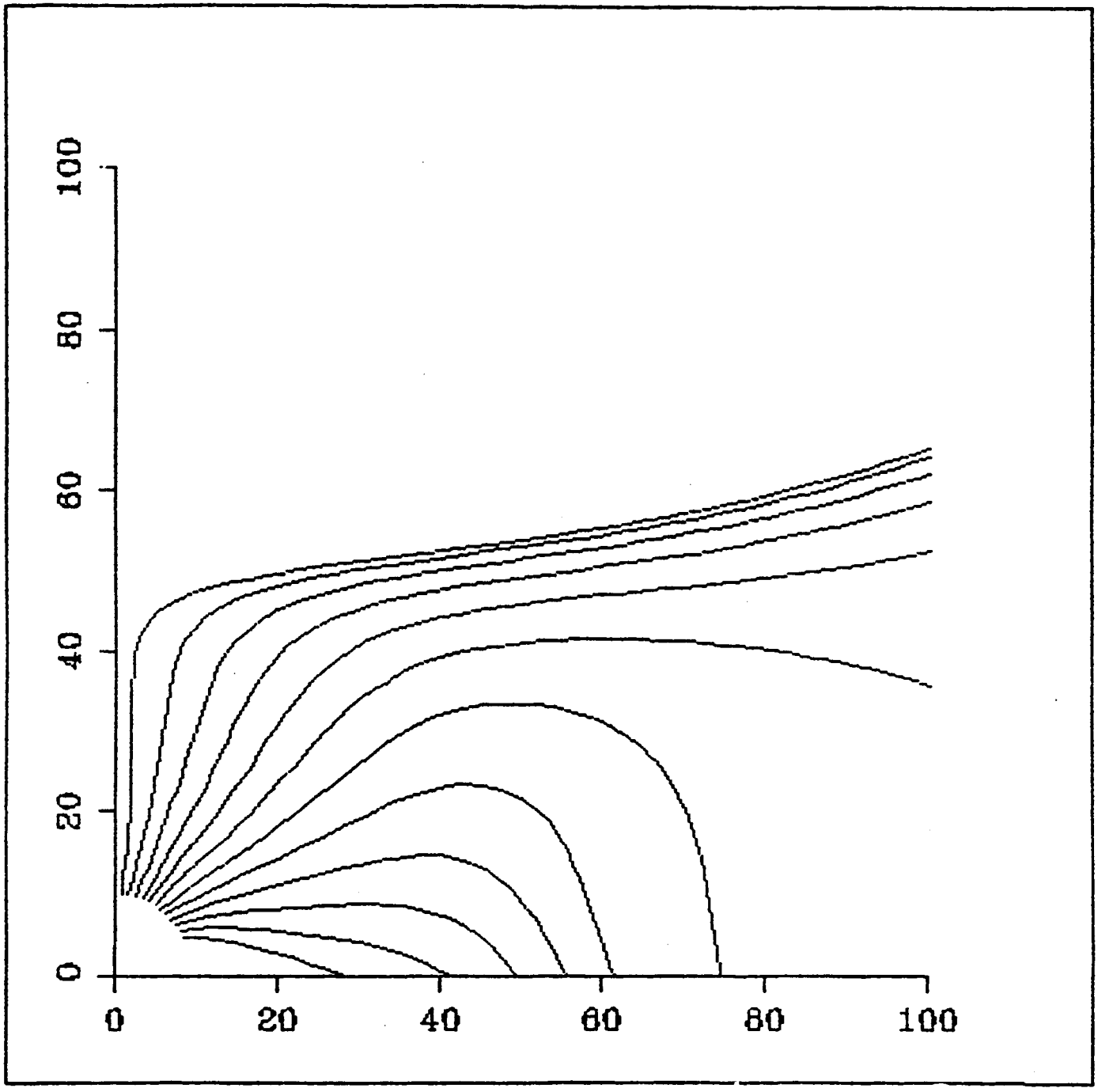

Figure 14

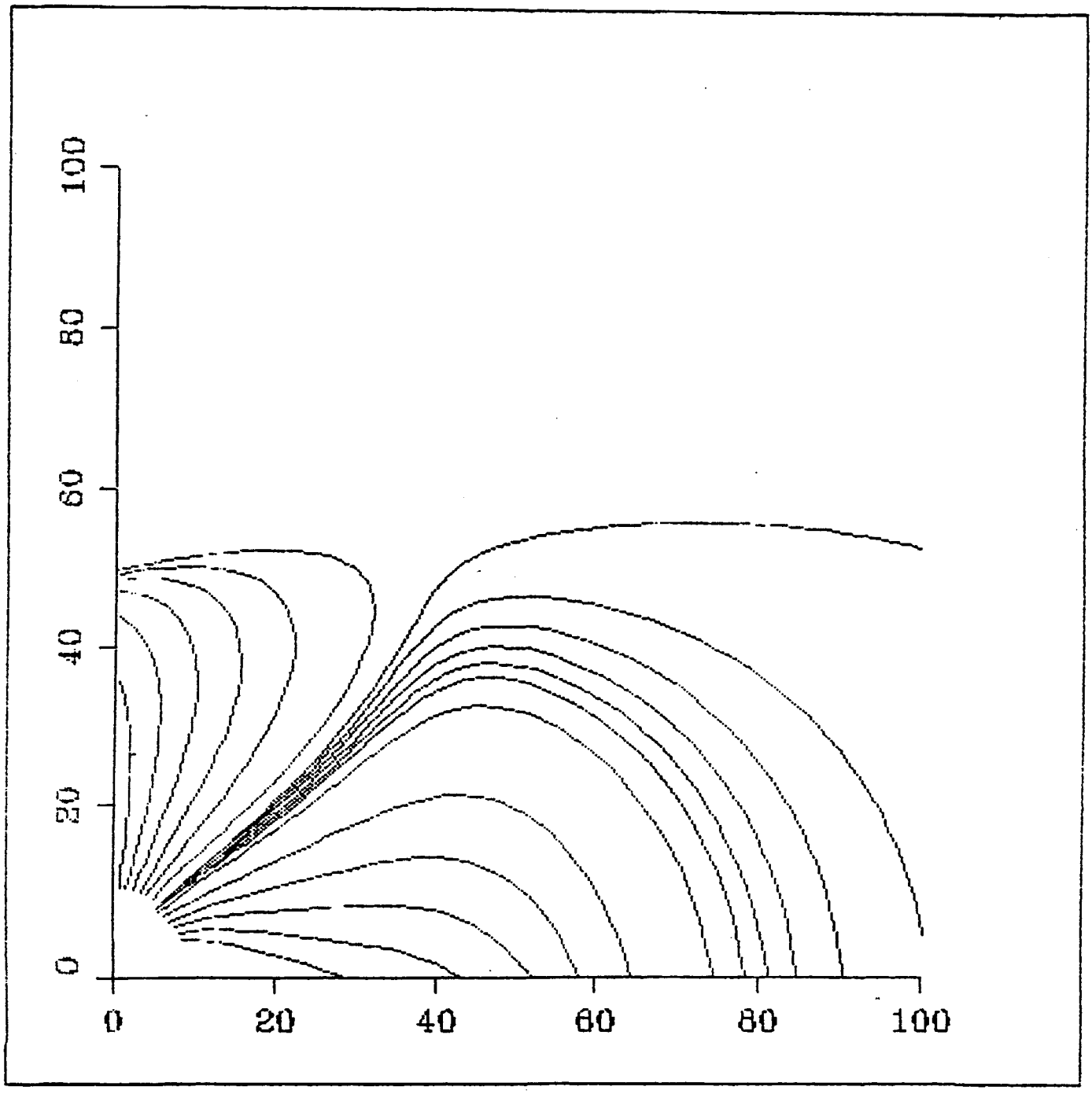

Figure 15

Pressure Balance

(Douglas E. Jones)

In developing the model magnetospheres discussed above no constraint of pressure balance at the magnetopause was imposed. Engle and Beard (1980) applied such a constraint in developing a model magnetosphere for Jupiter using techniques similar to those applied to the earth (Beard, 1960). In the Engle and Beard study an azimuthally symmetric current disc similar to that obtained by Jones et al.(1975, 1976) and Goertz et al. (1976) was added to the planetary field and the resulting field terminated by a uniform solar wind. The model disc current used was that obtained fitting the outbound Pioneer 10 data, and it may be the assumption of azimuthal symmetry of the disc that results in the earth-like high latitude cusp that was found. However, their model provides a poor fit to the outbound Pioneer 11 data near the magnetopause as can be seen in Figure 16 in which the Pioneer 11 field directions are also displayed. Requiring pressure balance at the magnetopause would seem to be a logical means of determining the most correct magnetopause configuration and therefore location of the cusp, but it should be remembered that the solar wind is only uniform just in front of the bow shock as thermalization and a non-uniformity of the flow develops in the magnetosheath. In addition, where the field lines near the cusp are parallel to the flow, the only source of pressure available to stand off the magnetosheath plasma would be high temperature plasma confined to the cusp "wells" which must also be added to the model.

In an attempt to assess the reasonableness of the model magnetopause configurations derived from the field/currents fit to the data we have computed the ratio $P(\alpha)/P_o$ versus α (α = MS latitude), where

$$p = nmV^2 \cos^2 \psi = \frac{B^2}{2\mu_o} = \frac{B_x^2 + B_z^2}{2\mu_o}$$

or, with substitution,

$$P/P_{sub\text{-}solar} = \frac{[B_x^2 + B_z^2] / B_z^2}{[(B_x^2 + B_z^2)^2 / B_z^2]_{sub\text{-}solar}}$$

ENGLE AND BEARD *

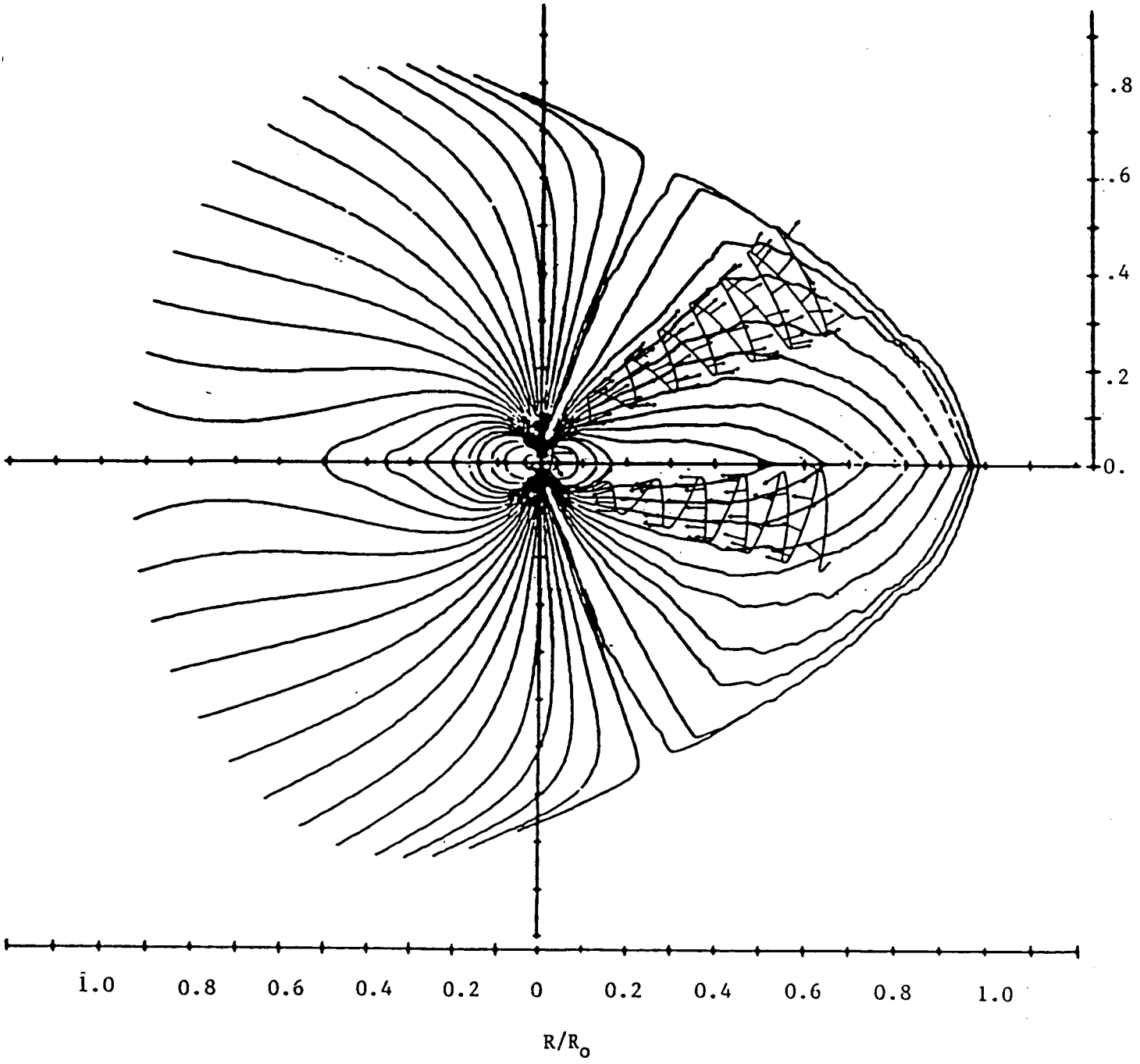

* WITH PIONEER 11 DATA

Figure 16

The manner in which the $P/P_{sub\text{-}solar}$ ratio varies with MS latitude for the several of the semi-infinite sheet and polynomial models studied is displayed in Figure 17. Considerable variability in the ratio is observed for all models, although the sheet and Euler (Stern, 1966; Goertz, 1976; Jones, 1976, 1976). models clearly display the smallest pressure variation. Figure 18 displays the results for the parabolic dayside current sheet models. Note, however, that the values plotted are not normalized to the subsolar value as they are in Figure 17. Of the various image distances used in the parabolic current sheet models, that near 185 R_J appears to provide reasonably similar pressure ratios either side of the cusp minimum. All of the models studied display a significant drop in the magnetic field pressure at and near the cusp, and it is assumed that thermal nkT pressure is needed to at least partially provide the additional amount needed.

A critical study that is clearly needed involves a pressure balance constrained fit to the Pioneer 11 outbound data. We have begun such a program. Our approach will start with a fit to the data combining a symmetric disc current, a parabolic dayside current sheet, earth-like tail configuration, and an image dipole. We will then modify the Beard pressure balance computer code previously developed for the earth for use at Jupiter, remove the image dipole, and allow the computer to establish the magnetopause shape and current distribution required to satisfy the constraint of pressure balance. The corresponding magnetospheric field configuration should provide a better answer to where the Jovian cusp is located, and in particular answer the question as to whether it is earth-like, or at a much lower magnetic latitude. In the process of developing this study effort, we will also attempt to assess the extent to which hot thermal plasma is present in and around the cusp, and in particular, determine if its presence significantly shifts the latitude of the cusp.

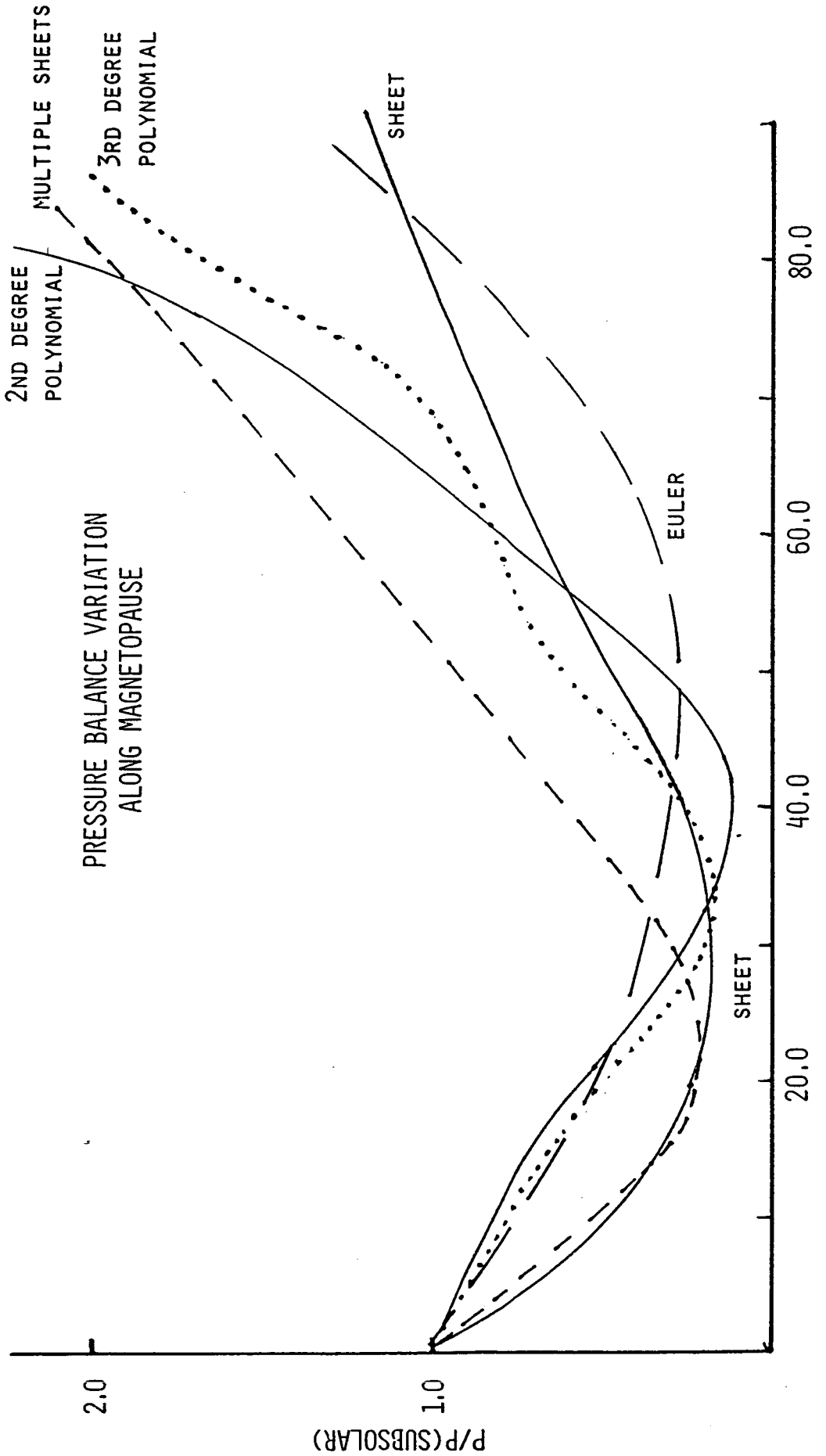
PRESSURE BALANCE VARIATION
ALONG MAGNETOPAUSE
2ND DEGREE
POLYNOMIAL
MULTIPLE SHEETS
3RD DEGREE
POLYNOMIAL
SHEET
EULER
SHEET
2.0
1.0
P/P(SUBSOLAR)
20.0
40.0
60.0
80.0
LATITUDE

Figure 17

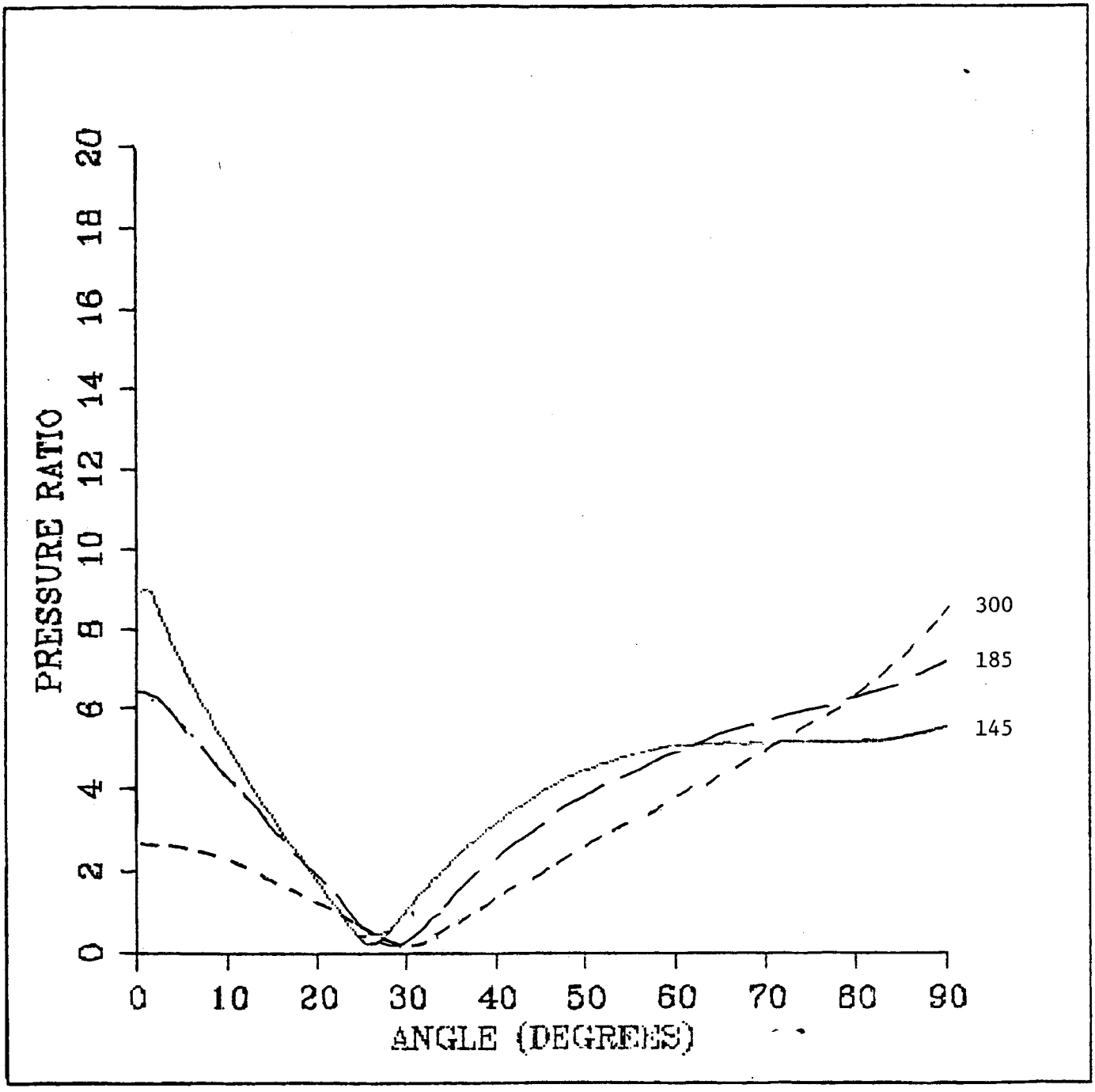
PRESSURE RATIO
0
2
4
6
8
10
12
14
16
18
20
0
10
20
30
40
50
60
70
80
90
ANGLE (DEGREES)
300
185
145

Figure 18

Energetic Particle Correlations

(Douglas E. Jones)

During its outbound passage, Pioneer 11 encountered periodic high fluxes of energetic particles at the low-latitude excursions of the trajectory (Simpson and McKibben, 1976; Filius, 1976; Van Allen, 1976; McDonald and Trainor, 1976). These observations have been interpreted as a clock-like global release of particles (Simpson and McKibben, 1976). We have suggested an alternate explanation for these results (Jones and Thomas, 1983; Thomas and Jones, 1984). On the outbound trajectory Pioneer 11 was primarily above the cusp on open field lines, and only at lowest latitude excursions did it penetrate the cusp or pass onto closed dayside field lines. Thus, the observed high fluxes could have been either particles escaping from the magnetosphere along the cusp, or, alternatively, a trapped population on the lower latitude closed field lines. Sentman et al (1975, 1978) have suggested that energetic particles undergo trans-L diffusion to high latitudes near the planet. We have recently received the Pioneer 11 energetic particle data from W. Filius of UCSD enabling us to test this important hypothesis. Goertz et al. (1976) concluded from an analysis of the outbound Pioneer 10 data that periodic decreases in the energetic particle flux occurred when the spacecraft encountered open field lines within the magnetosphere at magnetic latitudes below 20°. The existence of a low latitude separatrix between open and closed field lines in the near tail is consistent with a low-latitude cusp in the noon meridian. Referring to our model studies using only the outbound Pioneer 10 data as noted above, the Goertz et al. (1976) analysis suggests that at this time a taillike current sheet must have extended well into the dayside because such a configuration produces the type of low latitude cusp of that they need. Additional supporting evidence concerning a possibly abnormal cusp at Jupiter is provided in a recently published report of an analysis of the periodic amplitude variations in the Jovian continuum radiation, Kurth et al. (1986). They note that this radiation show structure suggesting preferred orientations of System III longitude with respect to the direction to the sun. Further, the importance of the dipole longitude-solar wind alignment to the amplitude of this radiation implies that the source region is near the magnetopause, and may tie the generation of the radio waves to the clock-like modulation of energetic electron fluxes from Jupiter. This type of mechanism would appear to be consistent with

our suggestion of a low latitude cusp, wherein the energetic particles are escaping from the Jovian magnetosphere. In order to quantify this suggestion we have begun an effort to correlate the occurance of Pioneer 11 energetic particle count maxima with trends observed in the measured field line directions.

Model Independent Studies of the Jovian Cusp Location

(Douglas E. Jones)

We have nearly concluded a study concerning the location of the Jovian cusp that is somewhat model independent. In this study the field vectors are transformed into a magnetospheric (MS) system that is based upon M, the dipole moment and the primary vector, and S, the direction to the sun (assumed to be anti-parallel to the solar wind velocity direction). In this system, Z is parallel to M, Y is formed by normalizing M X S, and X is obtained from Y X M. The magnetic field and position vector of the spacecraft are transformed into this MS system. The outward normal, n, to a parabola of revolution about the x-axis of this system (corresponding to an assumed semi-latus rectum/vertex distance ratio, Ak, as input) and passing through the MS coordinates of the spacecraft assuming the spacecraft is then determined and each point along the spacecraft is assumed to be on a magnetopause surface whose surface current, j_s, can then be determined from n X B. We have normalized this product, and assume that the cusp is located at points where the y component of this "surface current" revereses polarity for Pioneer 10 inbound and Pioneer 11 inbound and outbound, and where the x component reverses polarity for Pioneer 10 outbound. The model dependence of this study results from the assumption that the shape of the magnetopause is that of a paraboloid of revolution about the x axis of the magnetospheric coordinate system. This study supports the suggestion of a low latitude cusp at Jupiter.

Figures 19 through 21 display a sequence of spacecraft MS latitude and longitude angle versus $j_{sy}/[j_s]$ plots for Pioneer 11 outbound and for the distance interval of 15-40 R_J corresponding to parabola coefficients, (Ak), 1.2, 1.5, and 2.0. The inferred subsolar cusp latitude appears to be between 40 and 50 degrees for a parabola index of 1.2, 32-48 degrees for Ak = 1.5, and 25 - 35 for Ak = 2.0. Although the data are noisier, we have nevertheless applied this technique to the data intervals nearer the magnetopause. Figures 22 and 23 display the results for the 50-57 R_J and 62.2-68.9 R_J intervals corresponding to Ak value of 1.5. The former suggests a cusp at between 25 and 45°, and the latter between 35 and 40°. Applying this technique to the Pioneer 11 inbound, and both Pioneer 10 data sets provide results conisistent with the configuration inferred from the Pioneer 11 outbound data set.

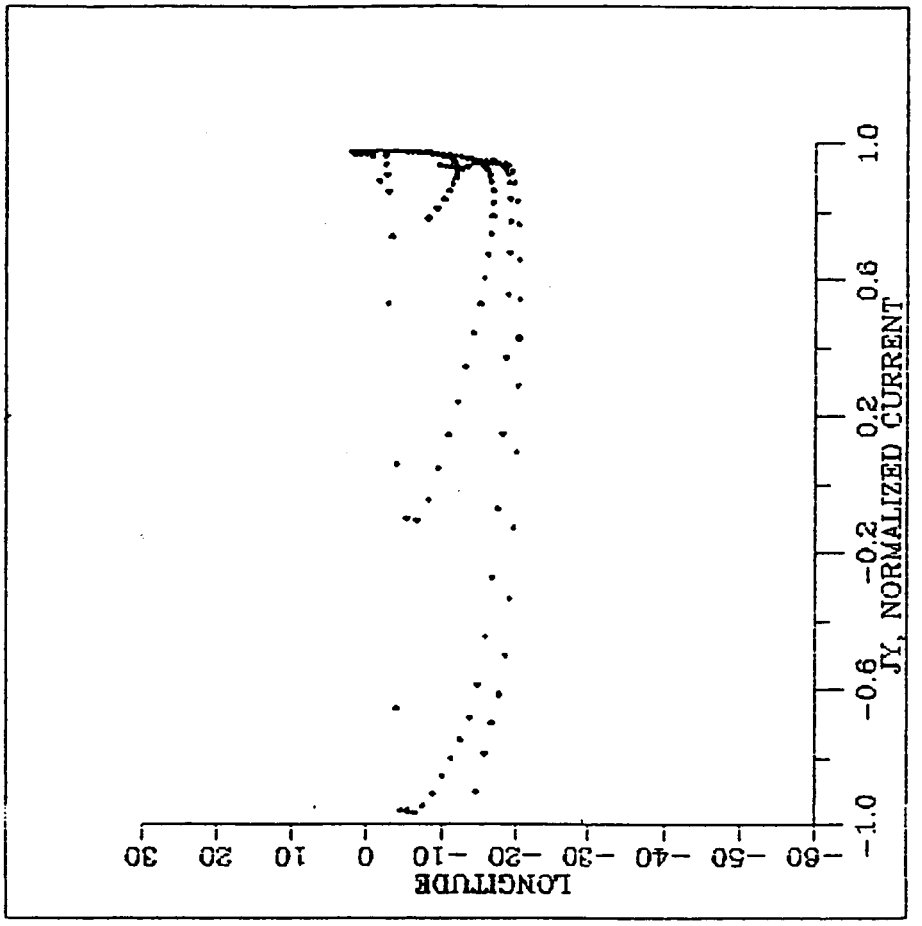

Figure 19b

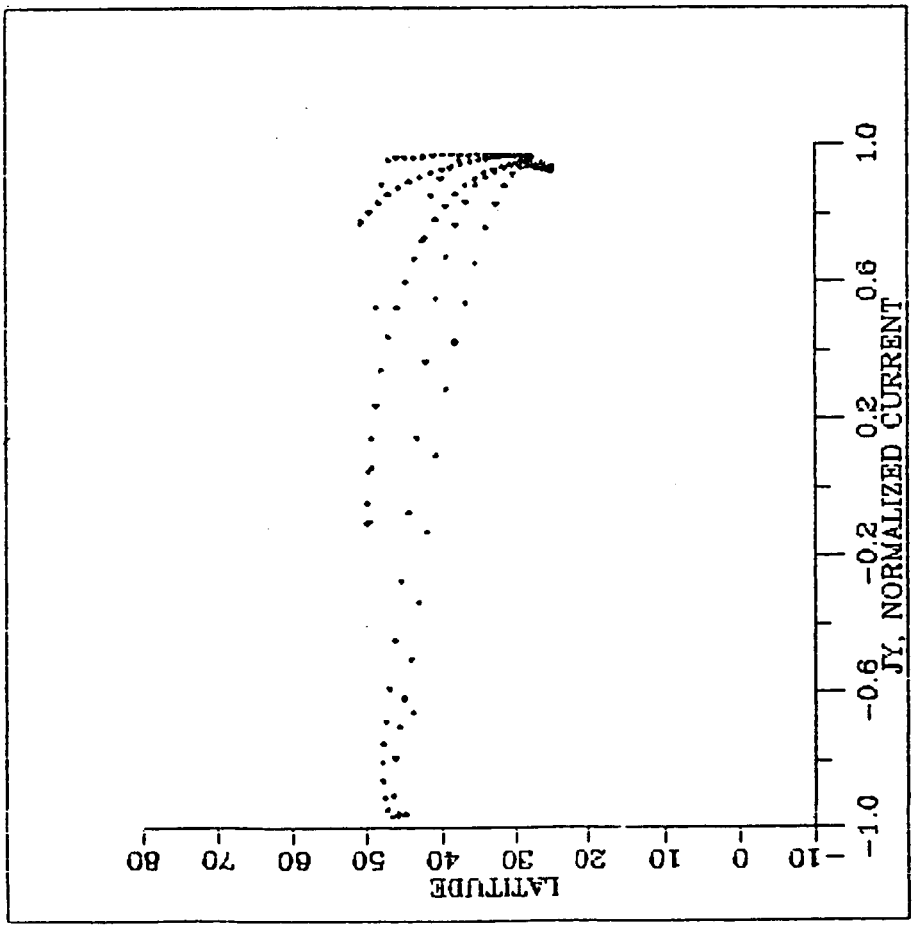

Figure 19a

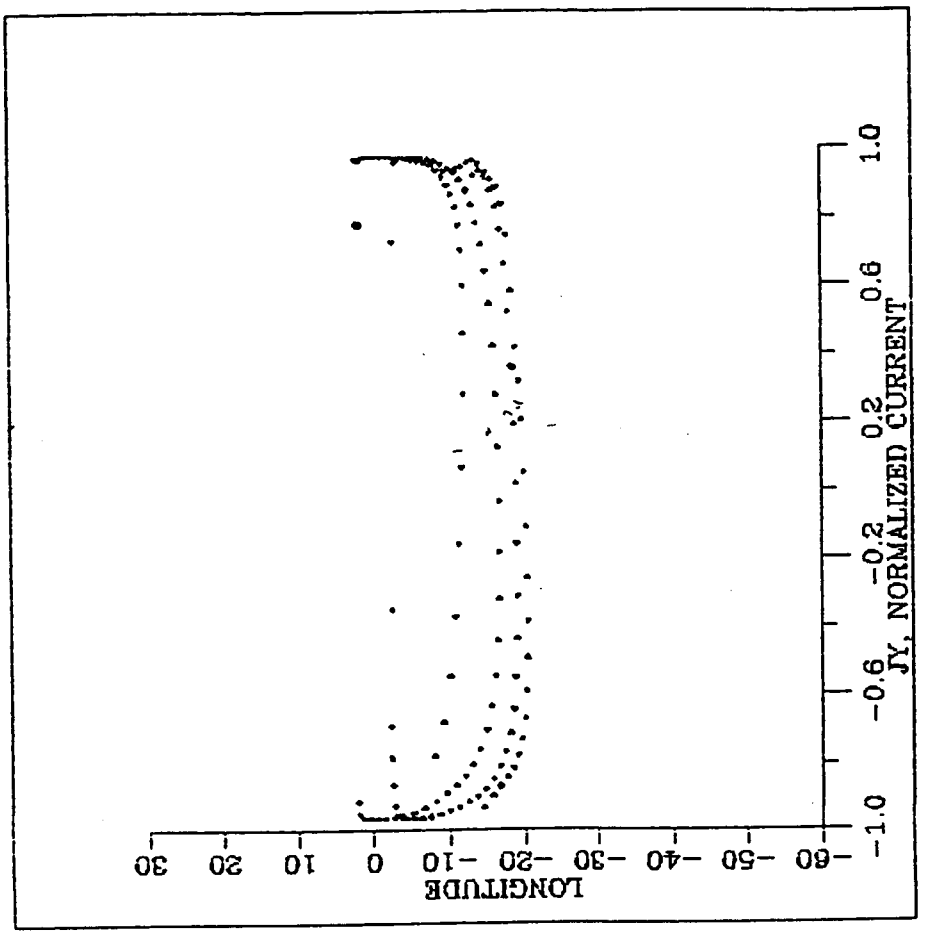

Figure 20b

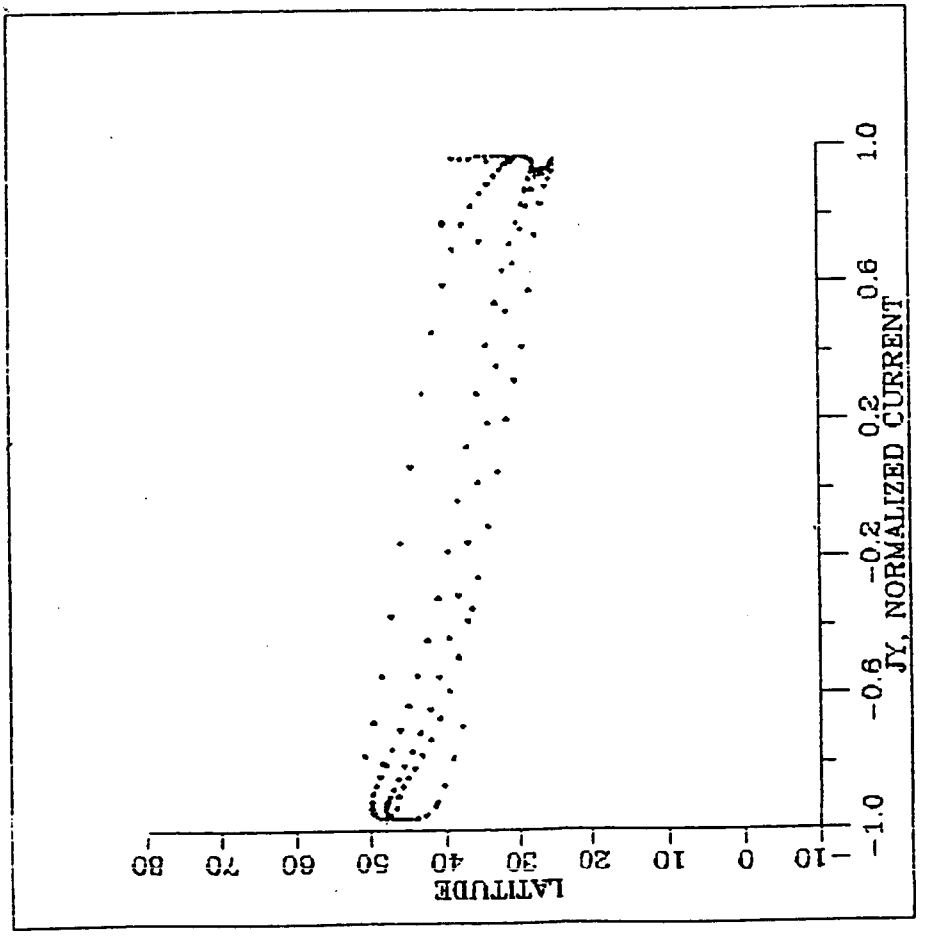

Figure 20a

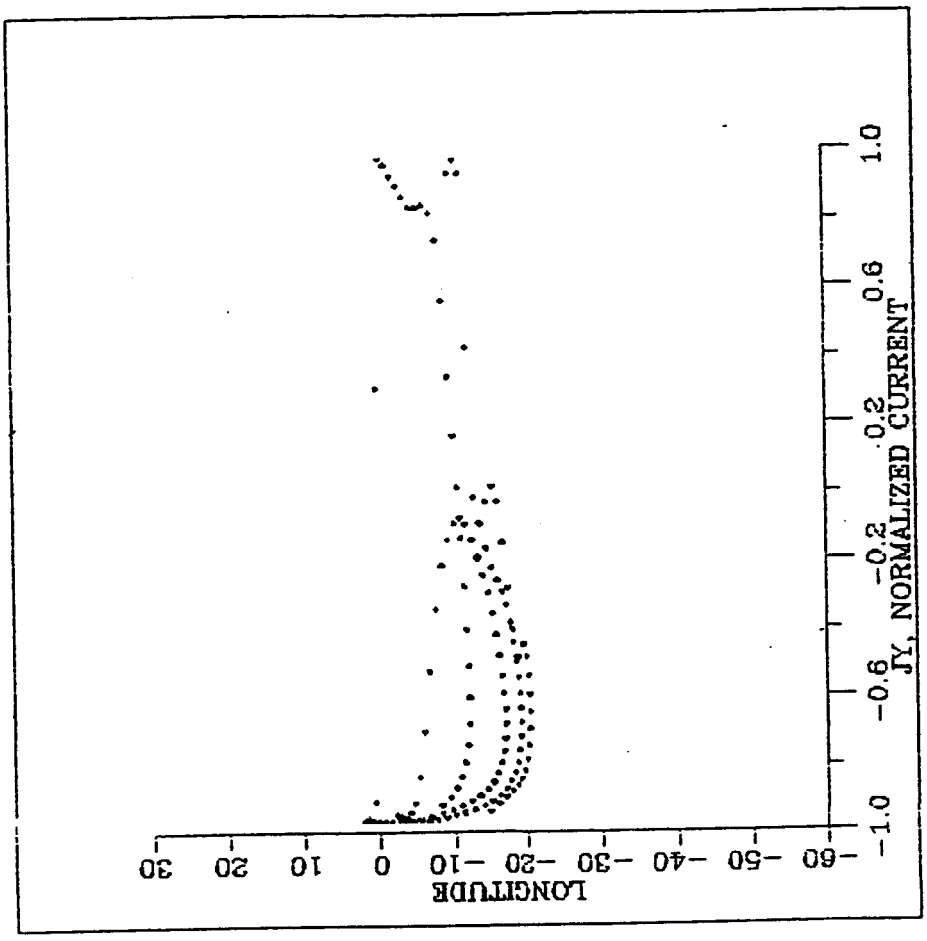

Figure 21b

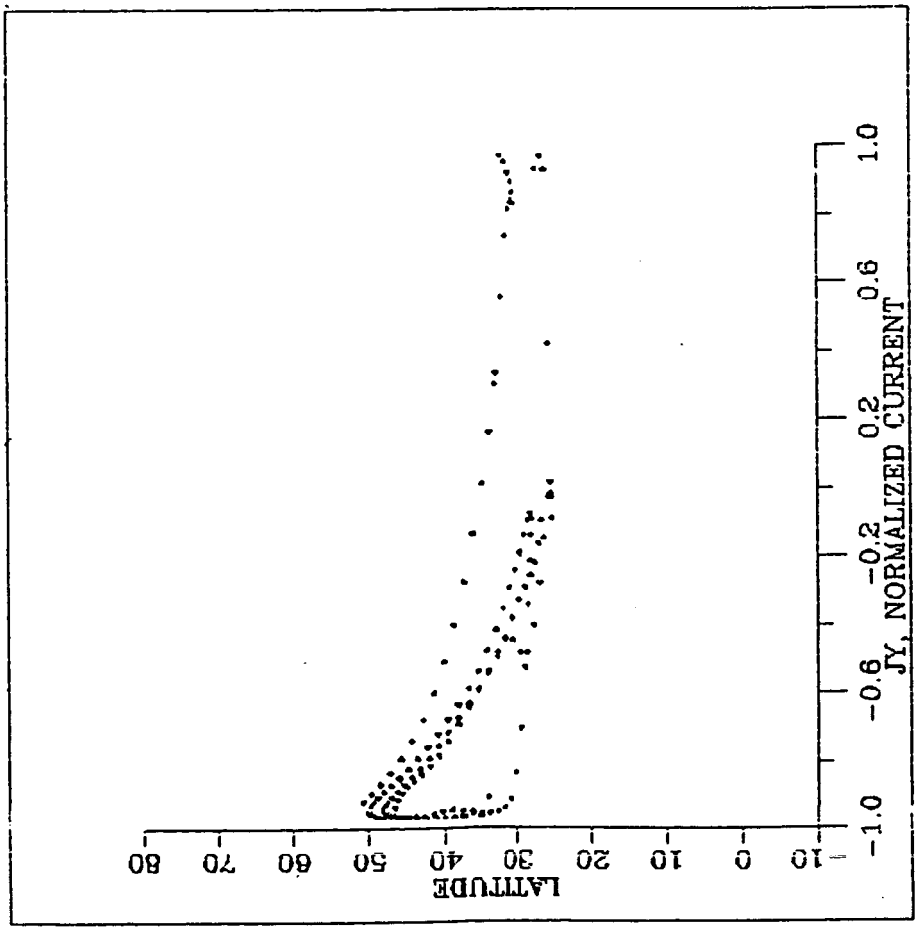

Figure 21a

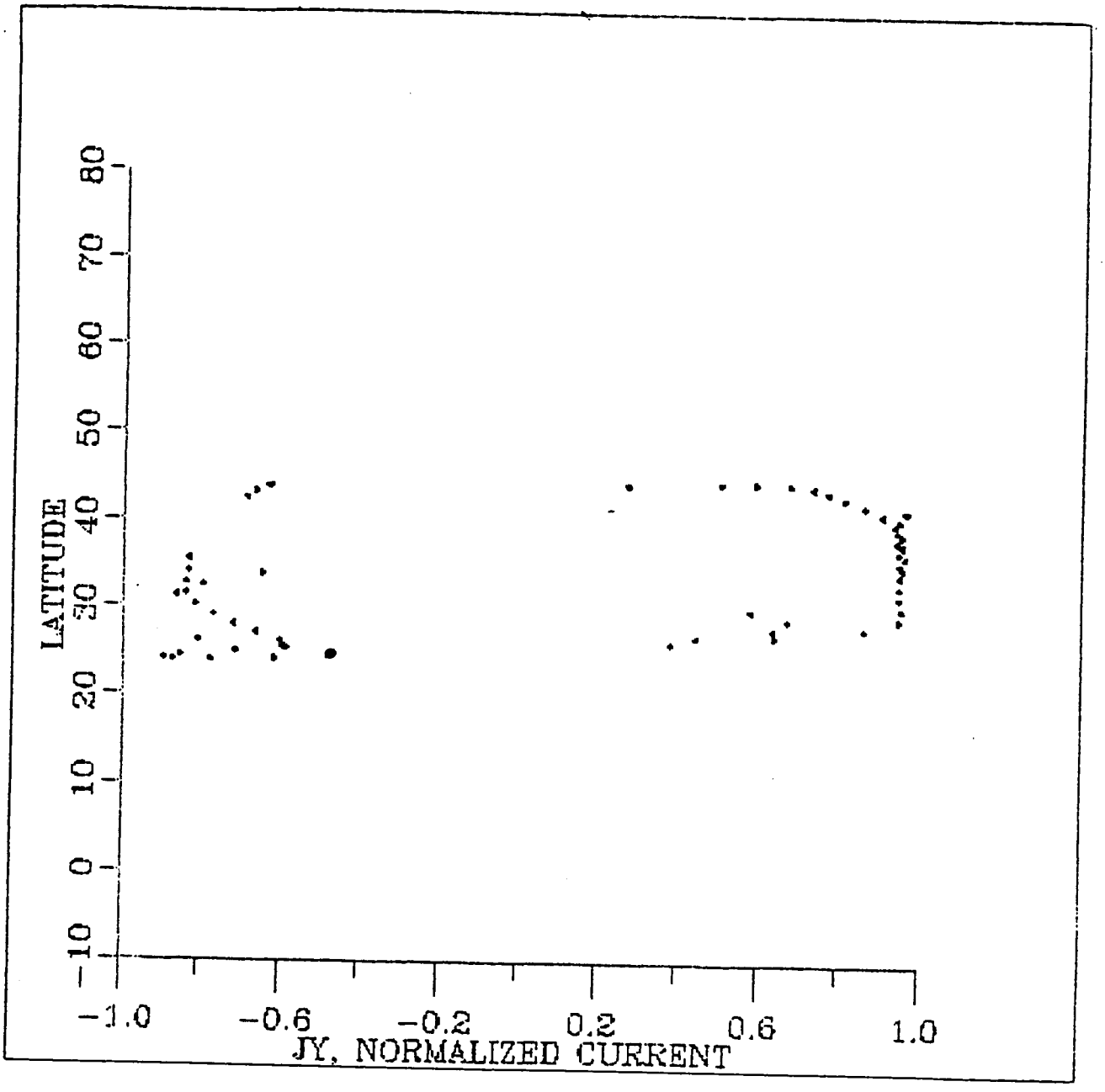
LATITUDE
80
70
60
50
40
30
20
10
0
-10
-1.0
-0.6
-0.2
0.2
0.6
1.0
JY, NORMALIZED CURRENT

Figure 22

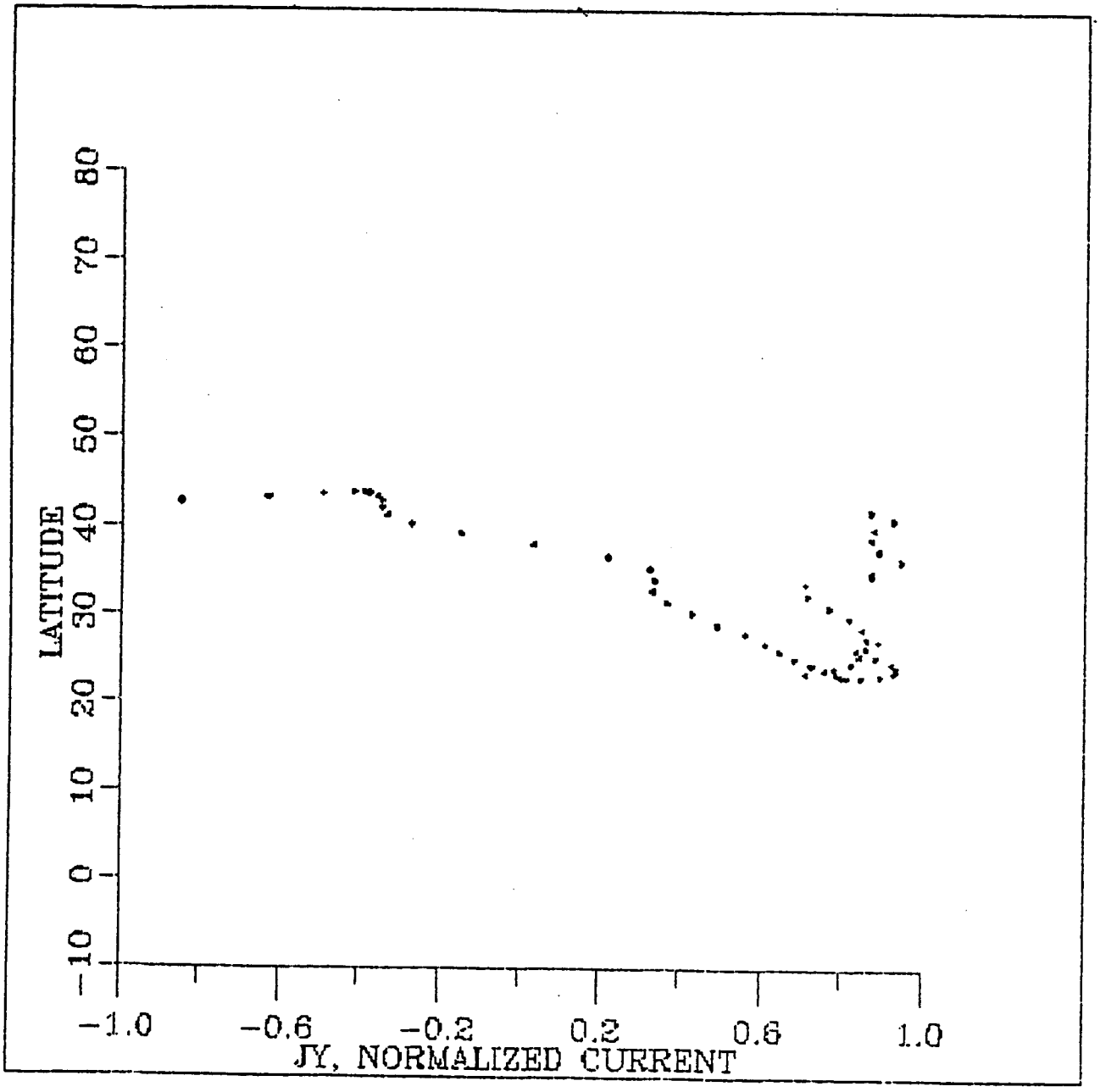
LATITUDE
80
70
60
50
40
30
20
10
0
-10
-1.0
-0.6
-0.2
0.2
0.6
1.0
JY, NORMALIZED CURRENT

Figure 23

Our studies also suggest that the inferred latitude of the cusp as deduced using this method decreases with angular distance from the MS plane in a manner which is consistent with the 10-15 degrees inferred from the values of Goertz et al. (1976). This is seen when individual points in the latitude curves (the (a) curves) are compared with the corresponding points in the longitude curve. Although none of the data points can be uniquely established as being precisely at the magnetopause, and the spacecraft moves slowly away from the planet (i.e., the curves of Figures 19-23 do not refer to simple motion of the spacecraft along a magnetopause boundary), nevertheless these results lend support to the previous interpretation of the magnetometer data in terms of a low latitude cusp.

The characteristics of Figure 24, which displays the field vectors projected into a twisted MR system (M is the primary vector, R, or spacecraft postion vector, is the secondary vector) suggest that the Jovian magnetosphere was undergoing numerous changes as Pioneer 11 proceeded outbound. For example, the magnetopause is penetrated initially at about 52 R_J (apparently moving in past the spacecraft), the spacecraft is in the magnetosheath out to 57 R_J, back in to the magnetosphere at 57 R_J, then out through the magnetopause at about 76 R_J. One notes that just prior to the 52 RJ penetration, the field lines gradually turn significantly northward. However, shortly thereafter the field is strongly southward. There is considerable dynamical evolution (spatial or temporal?) over the 57-76 interval, and again strongly southward beyond. If the cusp were simple, as suggested in the model field lines of Figures 3 and 5, etc., then just at the magnetopause, when north of the cusp, one would expect that the field lines should increase their northward trend. However, in every case, the field tends to be southward. We note the possible similarity between the increasing northward, then strong southward trend of the field that is displayed in Figure 24 with the cusp configuration resulting from the global MHD model of Wu (1983, 1984). He finds that a cusp current sheet develops which produces a field configuration that displays a strong field reversal beyond the cusp. Moving outward from the cusp, the standard diverging of the field lines is observed, and for Jupiter, the field at higher latitudes than the cusp should point northward, and southward at lower latitudes. However, radially continuing beyond the magnetopause the results of Wu (1983, 1984) suggest that after passing through the cusp current sheet the field lines should turn southward. Figure 24 strongly suggests that this may be

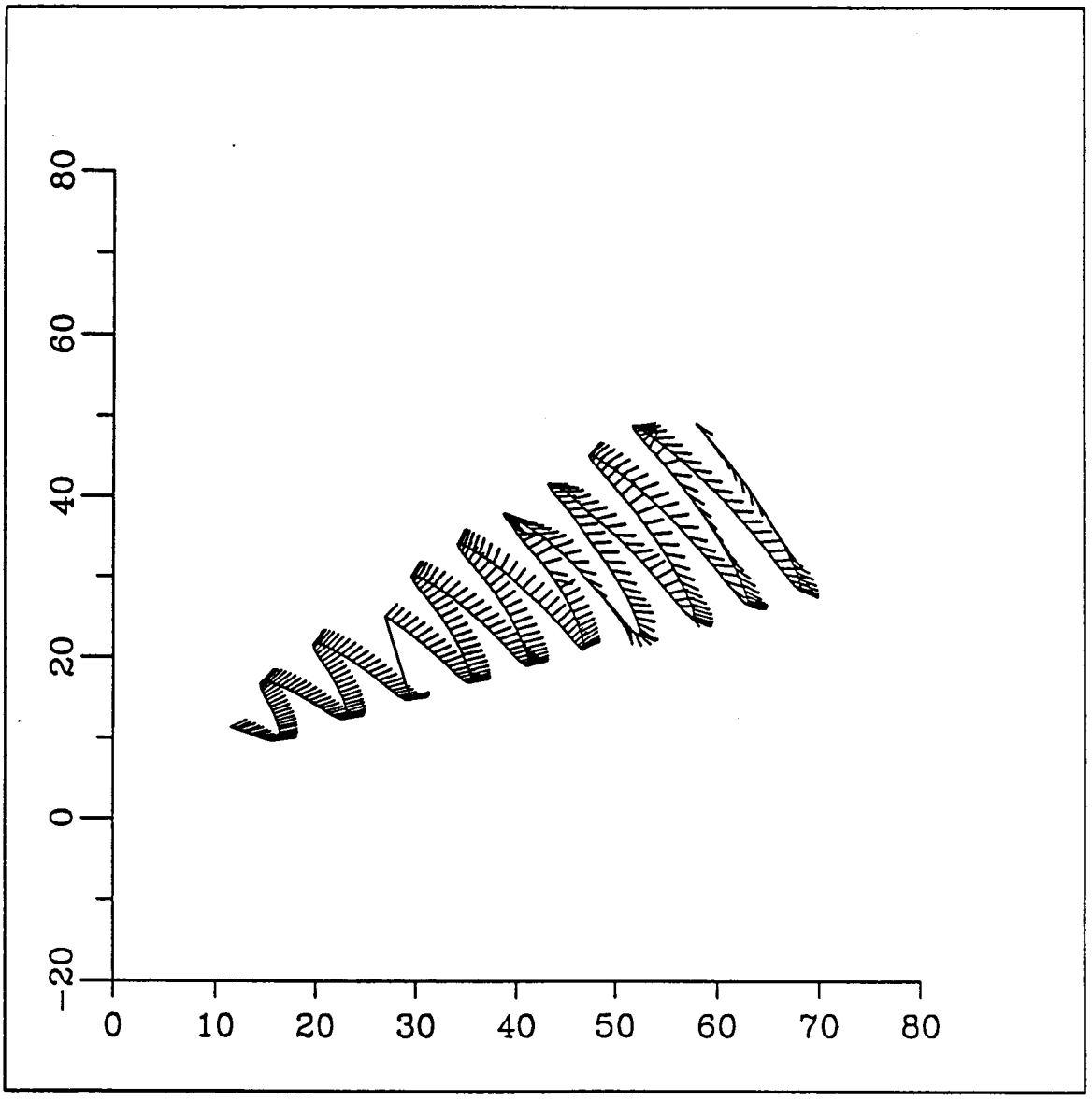

Figure 24

happening. Of course, the state of the magnetosphere has changed between the two magnetopause penetrations, and our modelling predicts that if the dayside current sheet weakens (in response to a weakening of solar wind pressure) then the magnetopause tends to be more earth-like, and the latitude of the cusp should increase. Hence, the more freqently observed southward field nature beyond 60 R_J is consistent with such a change, and does not necessarily require a cusp current sheet like that resulting from the MHD global modelling of Wu (1983, 1984). Allowing the outer interval to be a large fraction of the data set used in the modelling shows a definite trend towards a higher latitude cusp. With the cusp at a higher latitude, the likelihood of encountering southward fields near the magnetopause as the spacecraft moves radially outward is greater. While some consistency with the Wu model may exist in the Pioneer 11 outbound data, the dynamically nature of the solar wind and hence the magnetosphere suggest a simple model wherein the cusp latitude responds to the solar wind pressure.

Saturn's Variable Magnetospheric Currents and The Planetary Dipole

(Gordon R. Wilson and Douglas E. Jones)

Introduction

The ring current surrounding Saturn, first observed in the Pioneer 11 magnetic field data (Smith et al., 1980), has been modelled by Connerney et al., (1981, 1982, 1983) on the basis of the Voyager 1 and 2 data. The plane of the model ring current was assumed to coincide with the magnetic equator and, based primarily upon the V1 data, the ring current was found to extend from 8.0 to 15.5 R_S. Some differences in the V1 and V2 current ring parameters were observed although the latitude of V2 was too high to uniquely determine the ring current parameters. No time dependence in the Voyager ring current model was reported except for a transient event that occurred inbound by V1.

However, the current ring configuration was clearly different during the encounter of Saturn by Pioneer. Davis and Smith (1986) found that the best fit external uniform field (assumed to be the first order field of the ring) is not oriented parallel to the dipole axis, but tilted some 5 to 10^o degrees. Second, the inner edge of the ring is clearly less than 8 R_S at this time. This is suggested by the interior coefficient studies of Davis and Smith (1986) by the manner in which the residuals of the fit deteriorate so rapidly beyond 4.5 R_S.

In addition, there have been a number of studies of other Saturn phenomena reporting periodicities at or very near the planetary rotation period. These include spoke activity (Porco and Danielson, 1982: 621 ± 22 min) , ring electrostatic discharges (Warwick et al., 1981, 1982), Saturn kilometric radiation (SKR) (Desch and Kaiser, 1981: 10 hr 39 min 24 ±7 sec), low frequency radio emission (Carr et al., 1981), and charged particles (Carbury and Krimigis, 1982: electrons-$10^h21^m\pm48^m$; ions-$9^h49^m\pm59^m$).

On the other hand, Connerney et al (1981, 1982, 1983) find that the Saturn magnetic axis must lie within 1^o of the rotation axis, and there is no evidence in the Voyager data for a departure from axisymmetry of the planetary field at a level of ~ 2nT (0.2% of the total field measured at closest approach). Since Pioneer 11 passed much closer to the planet (1.35 R_S vs 3.07 R_S for Voyager 1

and 2.69 R_s for Voyager 2) it provided a more sensitive means of determining the higher order multipole terms than either of the two Voyagers by at least a factor of 8. However, in support of the Voyager interior models, Davis and Smith (1986) conclude that the roles of the interior coefficients g_n^m and h_n^m with $m \neq 0$ play no significant role in any model of the interior source. Hence the puzzling existence of periodic phenomena is very difficult to explain in view of the extreme symmetry of the planetary field source.

The results of two efforts to model the Saturnian magnetospheric currents will be discussed. In the first, the ring current parameters were obtained as a result of a combined interior source spherical harmonic analysis (SHA) plus exterior ring study of the Pioneer 11 data otained inside 8 R_s, in a manner similar to that used by Connerney et al. (1981, 1982, 1983) in their study of the Saturn interior field with the Voyager data. The second method models the ring current using data beyond about 5 R_s and based upon the perturbation field $(\vec{B}_{total} - \vec{B}_{interior})$ observed by Pioneer 11, in a manner similar to that reported for Jupiter (Jones and Thomas, 1983; Thomas and Jones, 1984). Since Pioneer 11 passed Saturn near the equatorial plane, the magnetic field observations were ideally suited to search for effects due to non-symmetrical characteristics of the interior field characteristics, or to other causes. In addition to modelling the Saturnian ring current under magnetospheric and solar wind conditions different from those present during the two Voyager encounters, it was our objective to determine the extent to which the perturbation field exhibited periodic characteristics. The results of a preliminary analysis and model ring current study for Saturn has already been reported (Wilson et al., 1983). A positive result has further stimulated the study of a relatively simple cylindrically symmetric representation for Saturn's magnetosphere field-plasma configuration and its response to a sudden impulse in pressure. Some features of such a model might offer an explanation to the observed magnetic field variations, which in turn might explain the observed periodicities in other phenomena. The study of a more realistic model configuration is presently underway.

Ring Current Modelling and Resultant Interior Field Source Corrections

Considerable information about the large scale characteristics of the ring current first resulted from an effort to obtain an improved model of Saturn's interior field. This program combined a spherical harmonic analysis (SHA)

representation of the interior field with a Biot-Savart representation for the field of the ring current, plus a suitable first order representation for the combined magnetopause and tail fields.

In this study fields due to exterior currents were modelled directly and then removed from the data, allowing a higher order removal of the contaminating effects of these currents in order to produce a data set from which a more accurate model of the interior source coefficients could be derived. The major difference between our method and that of Connerney et al. (1981, 1982, 1983) is that in their analysis an explicit expression for the current ring field was used in the inversion process, whereas in our study it was not. Our approach was necessary because the data showed clearly that the inbound and outbound ring current configurations differed significantly, and forcing an inversion process to use a single set of ring current parameters in this case would have resulted in inaccurated information regarding the interior source coefficients. In addition, the restricted longitudinal coverage of the planetary field by Pioneer 11 while within 8 R_s required both the inbound and outbound data be used as one data set for the SHA analysis.

The first step in modelling the exterior currents was to subtract the interior field from the data, i.e., forming a $(\vec{B}_{total} - \vec{B}_{planetary})$ data set. Since the interior field models differed, the choice of which one to use could have been a problem. This was avoided by restricting the inner edge of the fitting region to 5 R_s. Beyond this radial distance the various reliable interior models (2-2, 2-1, or axisymmetric model, 3-0,) showed little difference. The most likely candidates for the exterior currents are: a current ring, magnetopause currents, and tail currents. We modelled the current ring using the two layer concentric ring model outlined in Jones et al (1980a). To simulate the magnetopause and tail currents we included in the fitting a constant theta component of the field. In this first modelling effort no attempt was made to fit the phi component of the field. Inbound and outbound portions of the trajectory were fit separately. Actual ring parameters and theta components were determined by a function minimization algorithm which varied these quantities until a minimum residual was found.

As can be seen in the residual plots of Figures 25 and 26, and in the results displayed in Table 5, the field along the inbound and the outbound trajectories differed significantly. The model constant theta field component

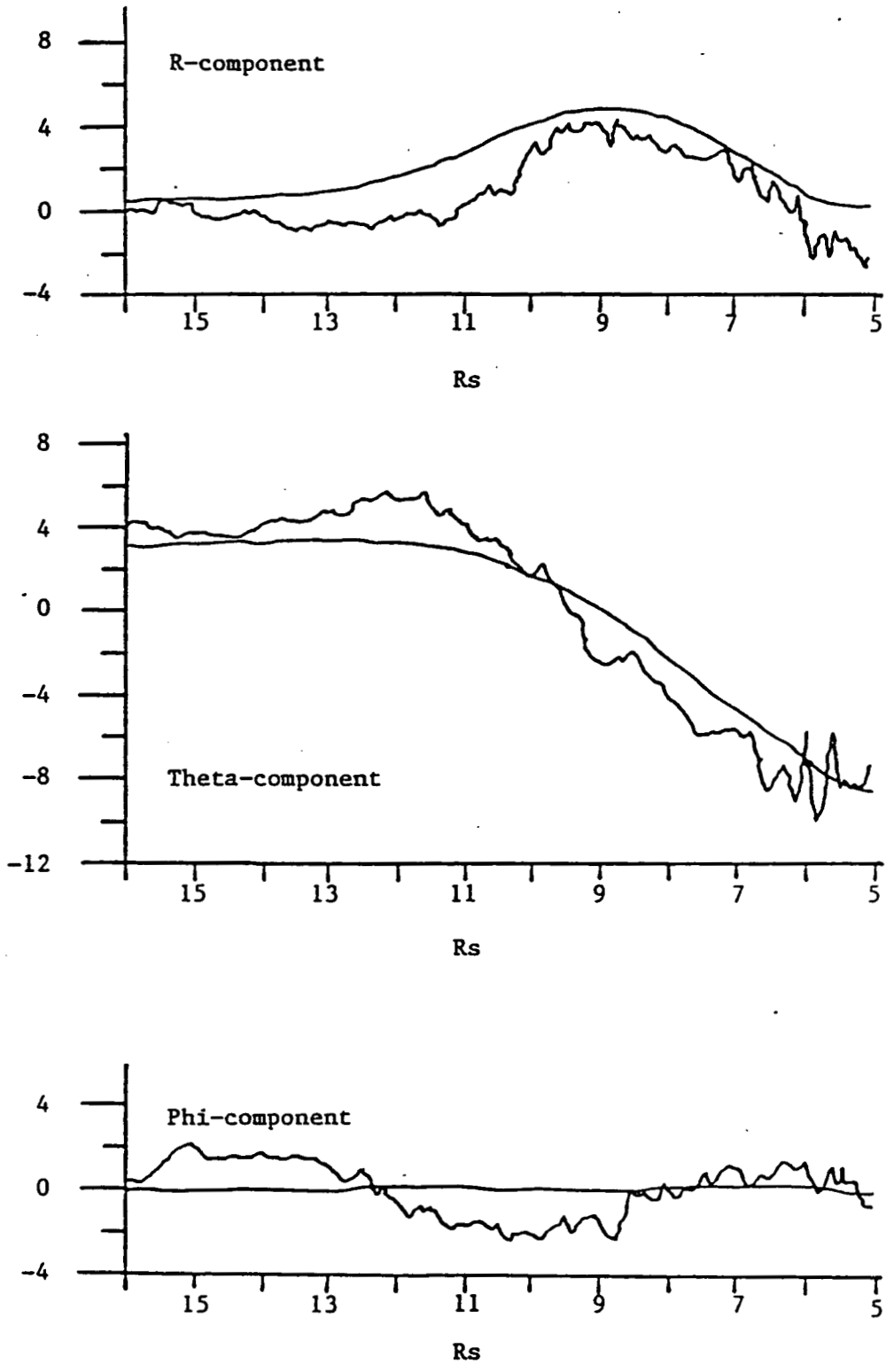
8
4
0
-4
R-component
15
13
11
9
7
5
Rs
8
4
0
-4
-8
-12
Theta-component
15
13
11
9
7
5
Rs
4
0
-4
Phi-component
15
13
11
9
7
5
Rs

Figure 25

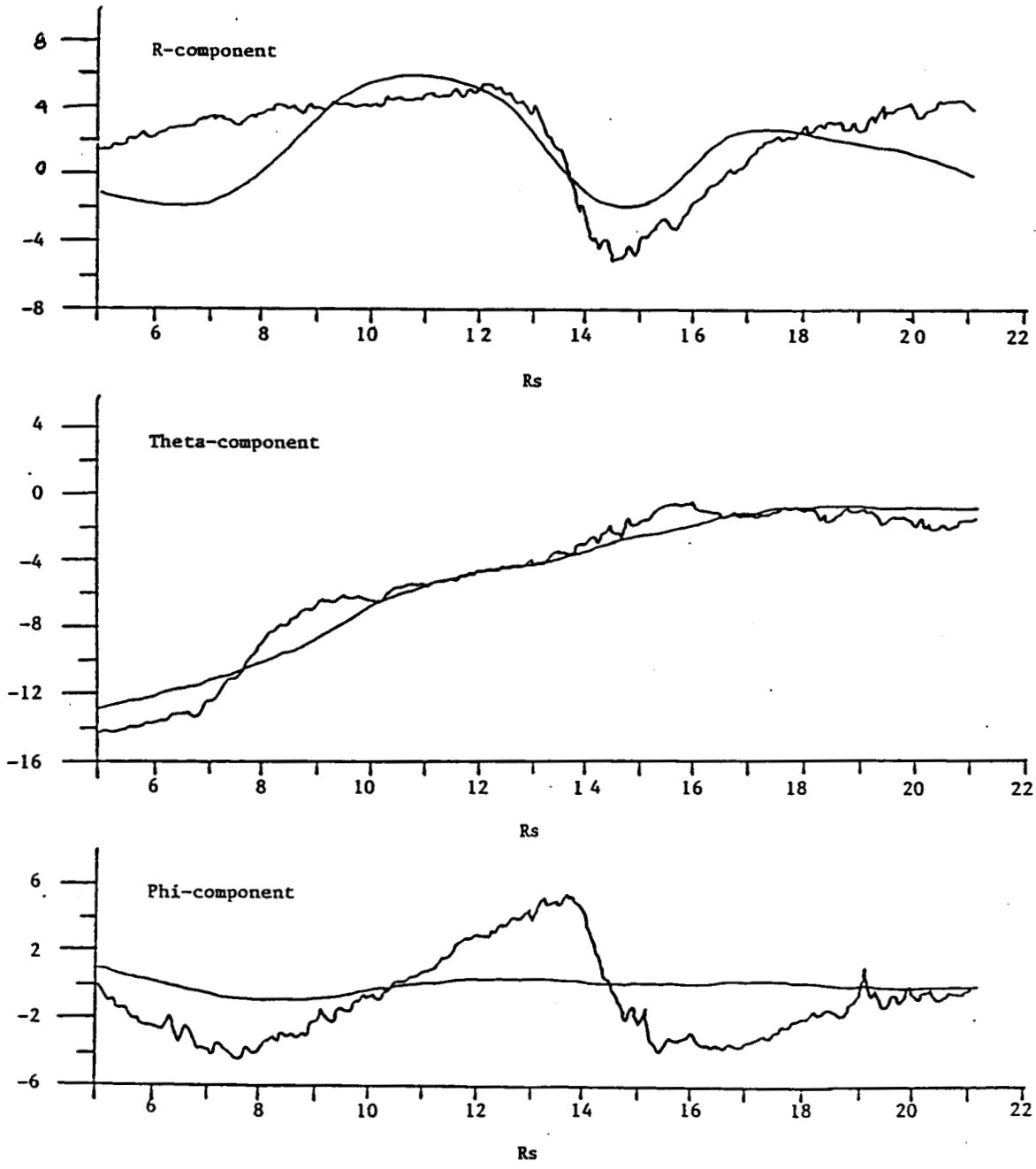
R-component
8
4
0
-4
-8
6
8
10
12
14
16
18
20
22
Rs
Theta-component
4
0
-4
-8
-12
-16
6
8
10
12
14
16
18
20
22
Rs
Phi-component
6
2
-2
-6
6
8
10
12
14
16
18
20
22
Rs

Figure 26

Table 5

	Inbound	Outbound
Ring Parameters:		
Inner Radius (R_s)	6.9	6.7
Outer Radius (R_s)	11.9	17.3
Thickness (R_s)*	1.5	2.3
Total current (10^6A)	4.3	7.0
Power Law α	0.76	0.77
Tilt angle	2.0	7.9
Longitude	100.2	337.3
Theta Field (nT)	1.6	-2.3
Residuals (nT)	2.50	3.45

shifted from +1.6 to - 2.3, suggesting a decrease in the relative contribution of magnetopause (positive theta component) versus tail currents (negative theta component). This may have been due to the expansion of the magnetosphere from its compressed stated inferred form the inbound magnetopause crossing at 17.3 R_s.

The inbound and outbound rings also differed, mainly in outer radius, tilt angle, and total current. The outer edge of the inbound ring was very distinct. During the fitting process the outer edge was varied over a large radius (6 R_s) with little change in the residual, suggesting that the outbound ring blends into some other current system which extends to the magnetopause (Smith et al., 1980). The tilts derived for the two rings are not interpreted as a tilt of the interior dipole, but as variations of the ring plane caused by changes in the solar wind. The change in total ring current from inbound to outbound may also have been caused by a changing solar wind.

Since the current ring is a variable feature it is no surprise that our results differ from those determined by Connerney et al. (1981, 1983). The current in their ring model was assumed to not vary in the axial (z) direction with a ring thickness of 5 to 6 R_s. Our model uses a Gaussian dependence on distance from the ring plane, resulting in ring half-peak thicknesses of 1.5 and 2.3 R_s. The corresponding uniform full width thickness would be about 2.3 times these valuses.

Of theoretical significance is the inner edge of the current ring. We determined a value for the inner edge by two different methods. The first was the function minimization process applied to the simple ring current configuration described above, which gave 6. 9 and 6.7 R_s for the inbound and outbound rings, respectively. The second method utilized the results of interior modelling. In doing the interior field source modelling we tried different weights (r^n, where n = 1, 2, 3, 4) and different data set sizes. When using the r^3 and r^4 weights we noted that the g_1^0 coefficient decreased sharply when the data set increased in radial extent beyond 7 R_s. Figure 27 shows a plot of the magnitude of the g_1^0 coefficient versus data set size. The point at which the sudden down turn occurs marks the inner edge of the ring (because of the degrading effects of currents in any SHA analysis) and places it at just inside of 7 R_s. Hence the results of both analysis agree very well in this regard. Hence, contrary to the results of Connerney et al (1981) and to the suggestion of Sittler et al (1981), the inner edge can at times extend inside the outer

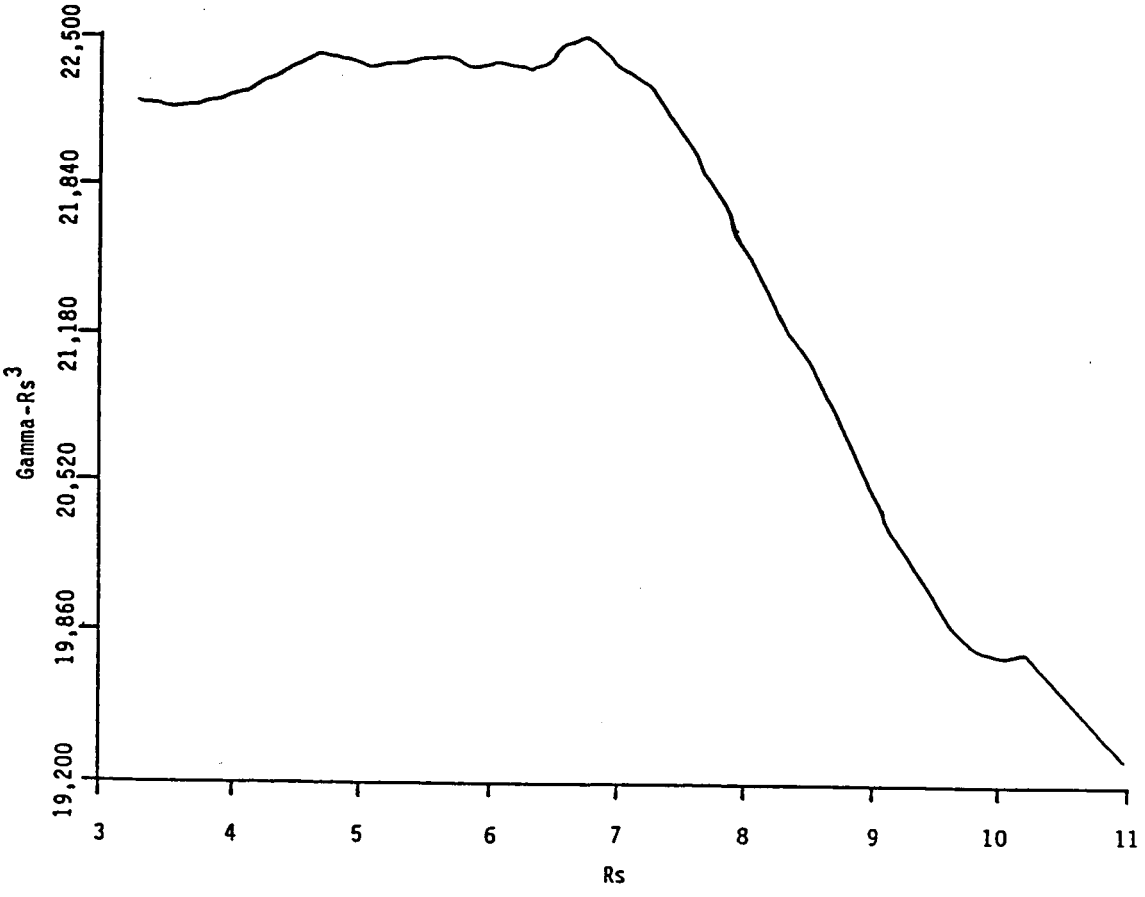
Gamma-Rs^3
22,500
21,840
21,180
20,520
19,860
19,200
3
4
5
6
7
8
9
10
11
Rs

Figure 27

edge of the E ring. For completeness we include in Table 6 the SHA (3-2) field model derived from two data sets from which the fields of the "ring current plus constant theta component model" have been removed. The dominance of the g_1^0, g_2^0, and g_3^0 terms clearly support a model consisting only of these terms. The rms residuals for these two cases are greater than those reported recently by Davis and Smith (1986) primarily because of a roll attitude error not included in our data set.

Further Saturn Magnetospheric Current Modelling Studies

A more complete modelling of the ring, tail and magnetopause current configurations was conducted using the method used previously for Jupiter (Jones etal., 1983; Thomas and Jones, 1984) in which the ρ, ϕ and z components were also modelled (Wilson et al., 1983). However, one major difference was in the use of a radial current sheet that was required in order to explain the character of the ϕ component of the inbound data. For the outbound data, models utilizing either a radial current sheet or a dayside semi-infinite tail-like current sheet configuration similar to that used for Jupiter were studied. In applying this method, various combinations of the model parameters being determined were utilized as well as various data sets. For example, one run set the inner edge of the ring current at 6.7 R_s, thereby decreasing the number of parameters required in the minimization. The varyious data sets permitted us to determine which of the parameters might be time dependent, as the current ring clearly changed between the inbound and outbound portions of the trajectory. However, based upon our analysis we suggest that this interpretation is not always correct. In view of the fact that Saturn's magnetosphere was compressed throughout most of the Pioneer 11 magnetospheric data interval, whereas during the Voyager 1 interval it was not, i.e., probably being within the Jovian magnetotail (Scarf, 1979; Scarf et al., 1981), this might offer an explanation for the differing current ring configuration. We plan to apply our model techniques to the Voyager 1 and 2 data in order to obtain an independent determinatin of the inner radius of the ring.

Table 7 lists the parameters of the model for the inbound (azimuthal and radial ring currents) data set. Figure 28 compares the inbound data and corresponding model r, ϕ, and θ components. Over the distance interval 6-12 R_s the inbound r and ϕ components are similar and apparently sinusoidal in character, but a distinct phase difference between them is observed. Inbound the required tilt for the radial current is a seemingly unrealistic 42^o, but equally of interest is the thickness of this current system, 26 R_s! The tilt

Table 6
Interior (3-2) SHA model coefficients (ring, tail and magnetopause fields removed)

Coefficient	Data Set 5 min	1 min
g01	21321	21252
g11	-106	-187
h11	97	-5
g02	2087	2116
g12	-421	-676
h12	-522	-608
g22	-78	-363
h22	392	-233
g03	3083	3374
g13	261	513
h13	-659	-576
g23	-278	-404
h23	-77	-84
g33	148	174
h33	364	-163
Condition Number:	91.2	82.3
RMS (nT)	3.87	3.72
RMS %	1.80	2.04

Table 7

Inbound (radial and azimuthal current discs, image, tail sheet)

fitting region	6-12 RS
inner radius	6.98
outer radius	12.1
BI	25.3
Power Law, α	0.74
HTHIK	4.5
TILT	2.8
TILT RATE (DEG/RS)	0.0
TWIST RATE	0.0
BO	15.06
HO	5.0
Tail sheet power law, β	0.88
IMAGE	24.1
DISTANCE	50.0
JTS	0.5
Tail Length	50.0
RMS (PER COMPONENT)	0.60

Total ring current*

Total radial current}

of the ring axis, though much smaller at 4.6°, is still at least an order of magnitude greater than the tilt inferred from the interior source coefficients alone (Connerney et al., 1982, 1984; Davis and Smith, 1986). This is to be compared to the tilt of the uniform field contribution (first term in the ring current field expansion) reported by Davis and Smith (1986).

The character of the inbound r and ϕ waveforms are consistent with a simple sinusoidal vertical movement of the current disc (perhaps caused by a finite tilt of the disc current axis relative to the Kronographic spin axis). Figure 29 displays the variation in distance from the equatorial plane of the centroids of the azimuthal and radial current discs. The considerable difference in the movement of these current systems may be an artifact caused by the large thickness parameter of the radial disc determined in the minimization procedure, and suggests that perhaps the thickness function of the model for this current may be too simple. The radial and azimuthal current systems do appear to be coupled, but apparently as a result of a complex reorientation with time of the radial and azimuthal current drivers, these currents get out of phase.

Table 8 displays the parameters for the azimuthal ring plus radial disc current model best fitting the outbound data and Figure 30 displays the corresponding outbound model and data components. For this model, although the radial component suggested relatively simple sinusoidal movement for the azimuthal ring current, the character of the ϕ component data variation suggested that for this current system was more complex, and a "ramp" type of movement for this disc was included in the model. Figure 31 displays the manner in which the centroid distances of the model azimuthal and radial disc currents vary relative to the magnetic equator during the 8-18 R_S data interval. The study and interpretation of the latter part of the second interval was complicated by the possibility that at least a portion of the perturbation field (principially the ϕ component) may have resulted from a possible extended wake of Titan (Jones et al., 1980b) possibly resulting from an interaction of the satellite with a localized heavy ion plume whose source is the satellite itself. However, although it is tempting to infer that the B_ϕ signatures in the 19-23 R_S range are caused by an interaction between the magnetospheric currents and Titan, it is important to remember that changes were occuring in all of the components, probably in response to changes in the solar wind, the variability of the components becoming more marked as the magnetopause was approached. A critical input to an interpretation in terms of the possible existence of an extended wake

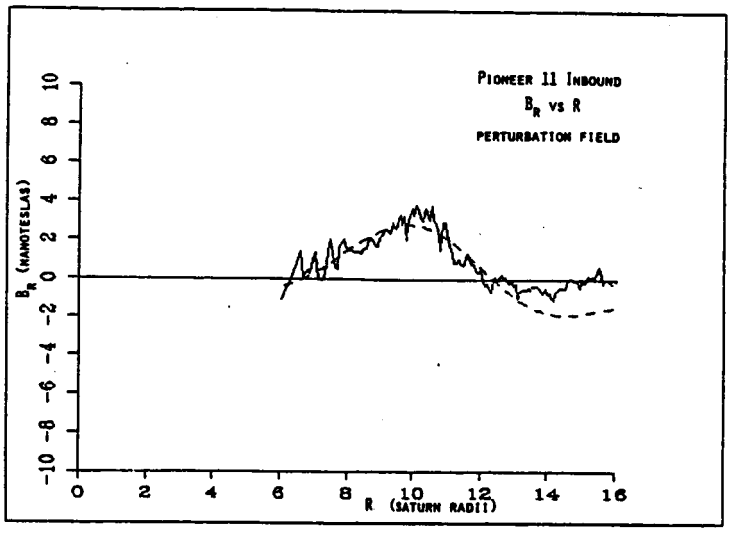
PIONEER 11 INBOUND
B_R vs R
PERTURBATION FIELD
B_R (NANOTESLAS)
R (SATURN RADII)

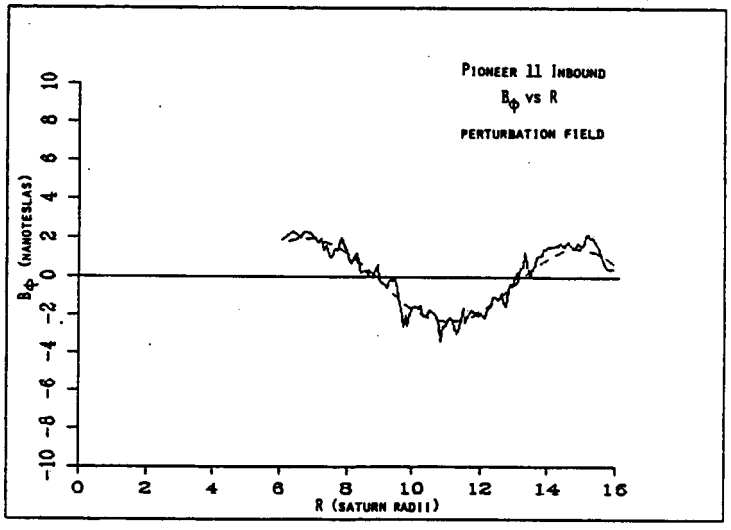
PIONEER 11 INBOUND
B_ϕ vs R
PERTURBATION FIELD
B_ϕ (NANOTESLAS)
R (SATURN RADII)

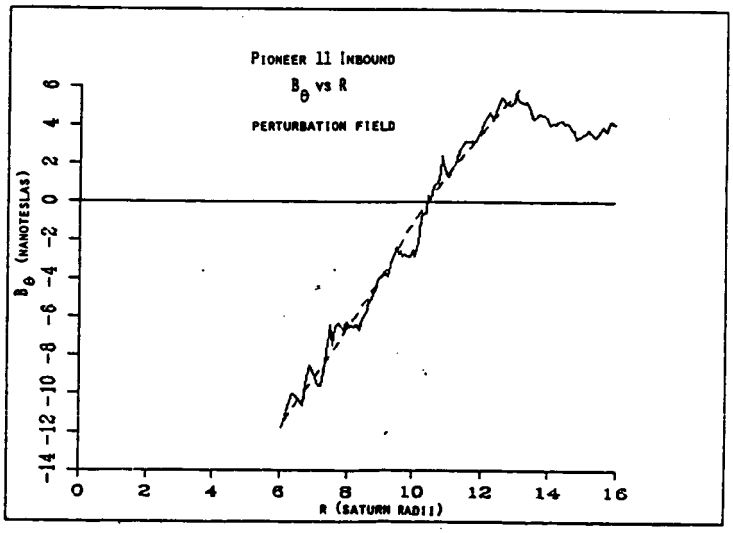
PIONEER 11 INBOUND
B_θ vs R
PERTURBATION FIELD
B_θ (NANOTESLAS)
R (SATURN RADII)

Figure 28

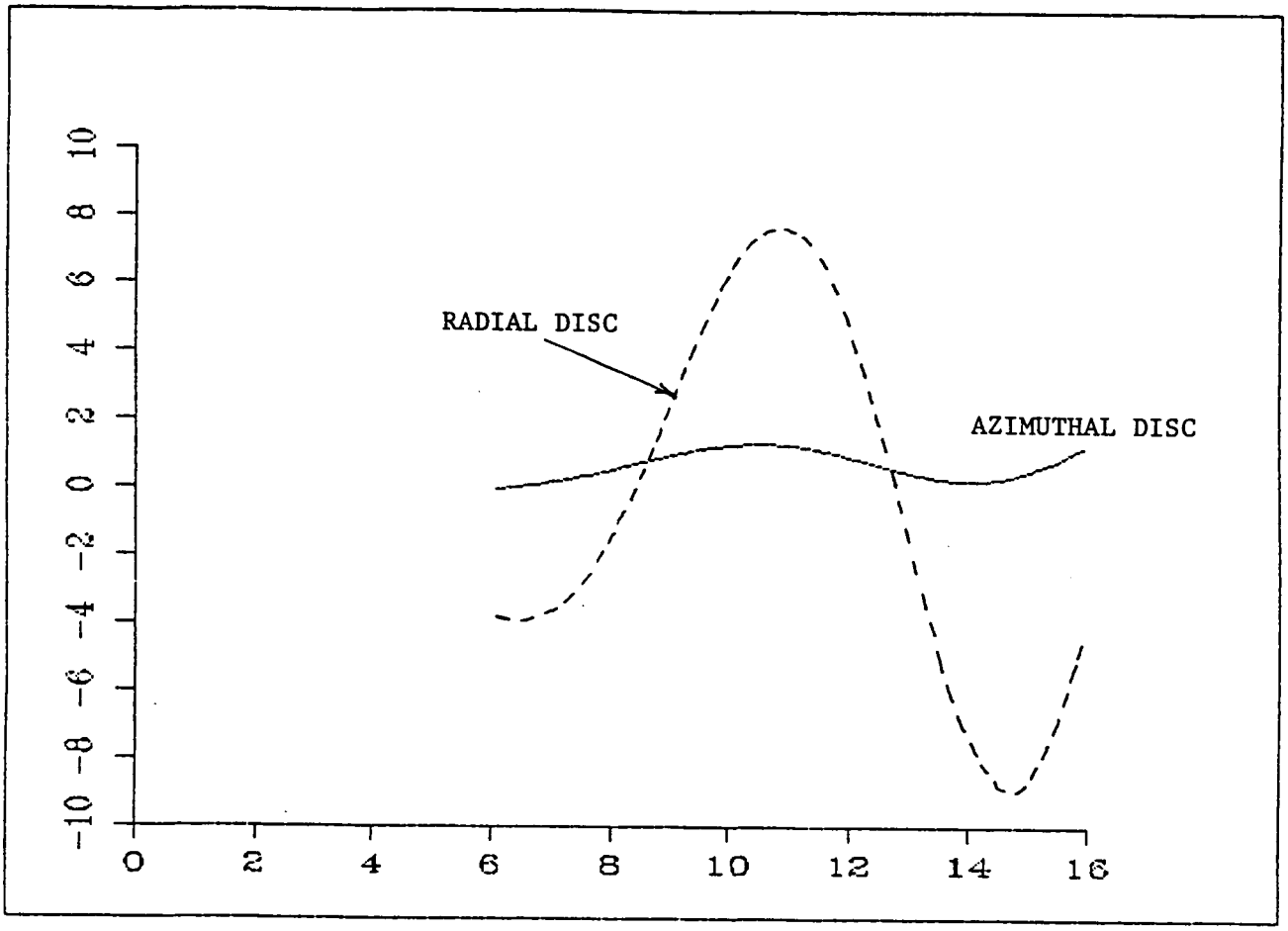

Figure 29

Table 8

Pioneer 11 Outbound

(Image, Disc, and Tail Sheet)

Fitting Region (R_s)	8-18	18-28
Image Ratio (@ 50. R_s)	-1.62	0.37
Azimuthal J_o (nT)	5.97	3.99
Lower law, α	1.52	0.95
R_{in} (R_s)*	6.74	6.74
R_{out} (R_s)	24.07	27.19
Disc Thickness (R_s)	2.34	3.52
Disc Tilt (degrees)	17.97	10.8
Tilt rate (degrees/R_s)	2.13	0.26
$Long_o$ (twist start)*	23.35	23.35
Twist rate (degrees/R_s)*	4.4	4.4
j_{radial} (nT)	7.37	14.32
Radial Thickness	2.5	8.15
Radial α	0.30	0.60
j_{tail}*	0.50	0.50
Tail Thick (R_s)*	7.8	7.8
RMS (nT)	.73	.95

(Ramp parameters: T_1 = 0.844, Period = .560, Slope = 25.124, BBB = -8.11

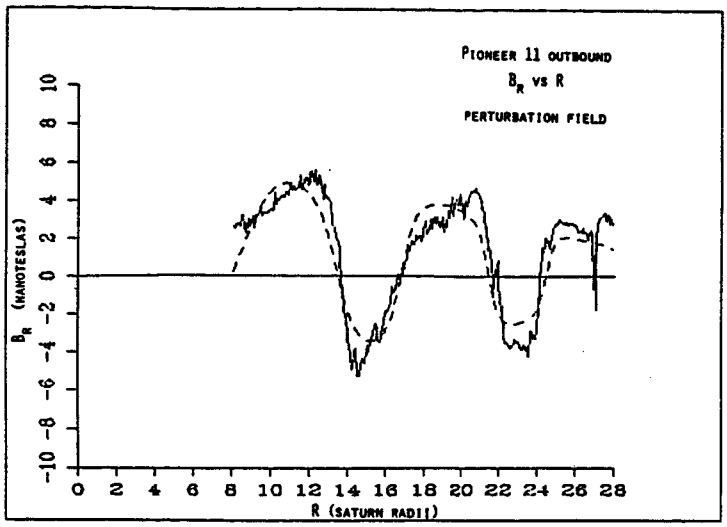
PIONEER 11 OUTBOUND
B_R vs R
PERTURBATION FIELD
B_R (NANOTESLAS)
10 8 6 4 2 0 -2 -4 -6 -8 -10
0 2 4 6 8 10 12 14 16 18 20 22 24 26 28
R (SATURN RADII)

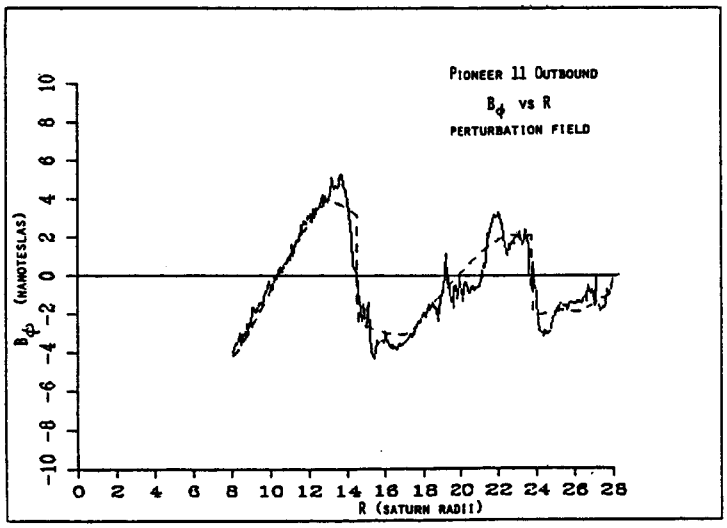
PIONEER 11 OUTBOUND
B_ϕ vs R
PERTURBATION FIELD
B_ϕ (NANOTESLAS)
10 8 6 4 2 0 -2 -4 -6 -8 -10
0 2 4 6 8 10 12 14 16 18 20 22 24 26 28
R (SATURN RADII)

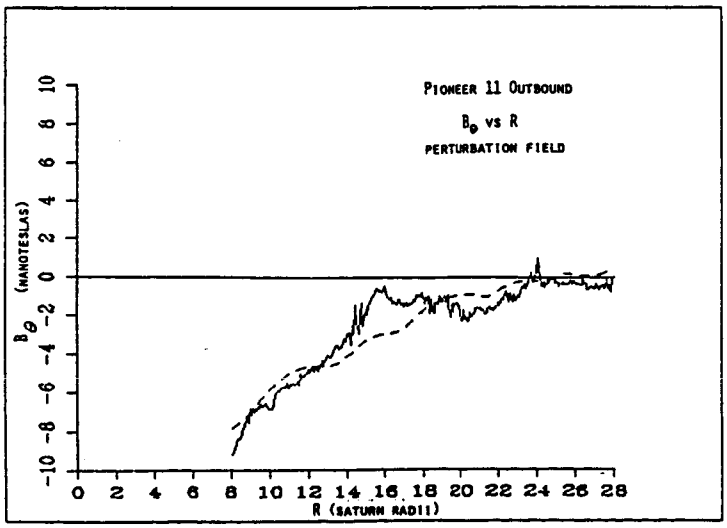
PIONEER 11 OUTBOUND
B_θ vs R
PERTURBATION FIELD
B_θ (NANOTESLAS)
10 8 6 4 2 0 -2 -4 -6 -8 -10
0 2 4 6 8 10 12 14 16 18 20 22 24 26 28
R (SATURN RADII)

Figure 30

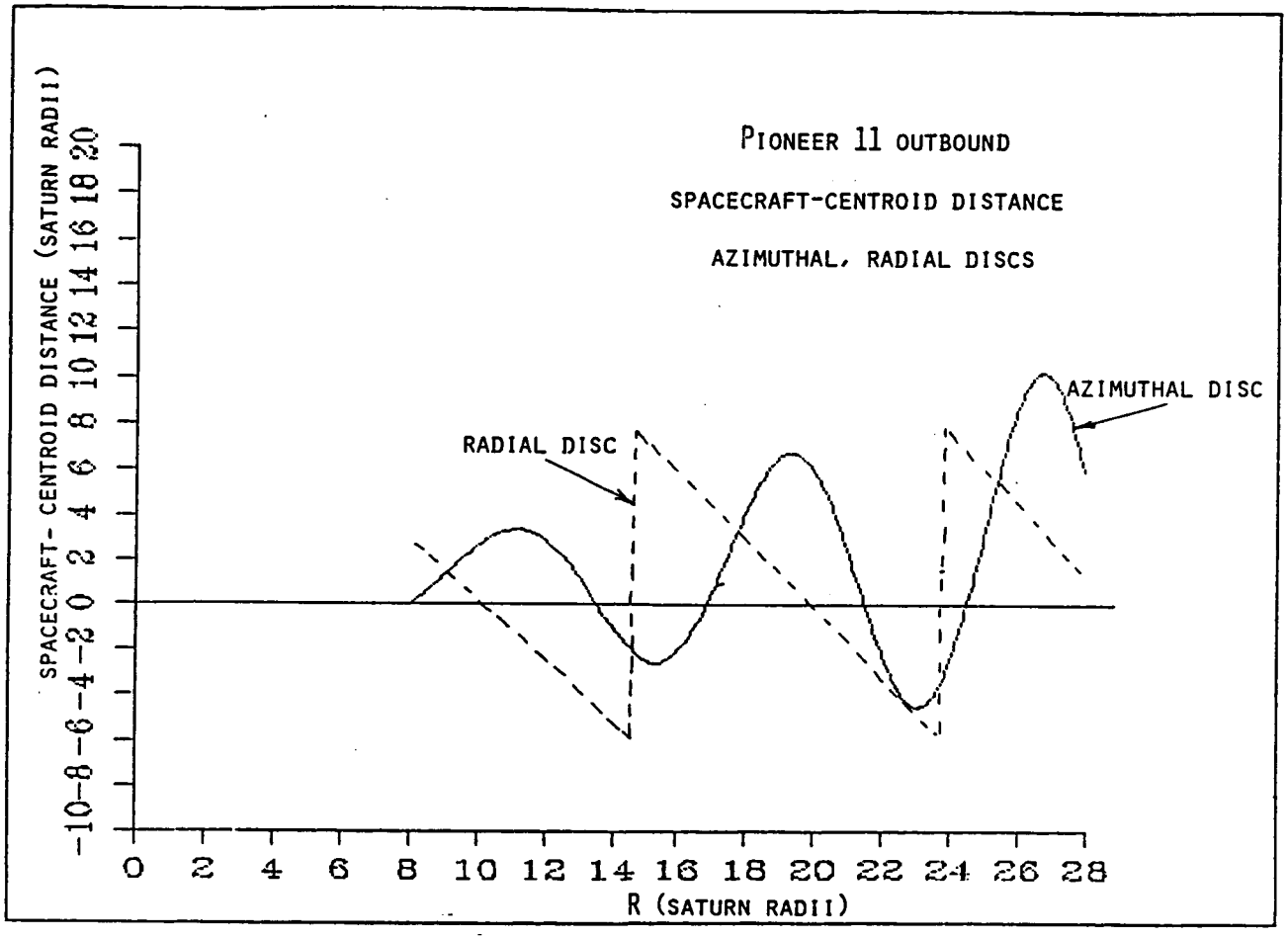
PIONEER 11 OUTBOUND
SPACECRAFT-CENTROID DISTANCE
AZIMUTHAL, RADIAL DISCS
AZIMUTHAL DISC
RADIAL DISC
SPACECRAFT- CENTROID DISTANCE (SATURN RADII)
-10 -8 -6 -4 -2 0 2 4 6 8 10 12 14 16 18 20
0 2 4 6 8 10 12 14 16 18 20 22 24 26 28
R (SATURN RADII)

Figure 31

of Titan at this time must come from studies of the interaction of heavy ion magnetospheric plasma with the satellite. Some work in this direction has been accomplished and is reported in another section of this final report.

The ramp function studied was of the form:

$$ZDIST\ (R_S) = ZO + \text{rate X } (t - TO - n \text{ X period})$$

where t is decimal day. The trapezoid function parameter values for the two outbound data sets are displayed in Table 9. Distinct differences are observed in the parameters. Of interest is the fact that the azimuthal current-equator distance varied sinusoidally at the planetary rotation period, and in a manner consistent with a simple, but unexpectedly large, tilt relative to the spin or planetary dipole axis. However, the function period for the radial (or cross sheet) z variation is much longer at $13^h\ 37 \pm 11^m$. These inferred periods are supported in subsequent spectral studies of the data discussed in a later section of this report.

Decompositon of the observed waveform to express the movement of the azimuthal and radial disc currents into complex waves/phase configuration using Fourier analysis may prove helpful in understanding the manner in which the several current systems are coupled, and how they respond individually or together to an external pressure enhancement and release. The azimuthal current system seems to be more tightly coupled to the planetary rotation, with the abmormally large tilt of this system resulting from a solar wind impulse that is not aligned parallel to the planetary equator. The presence of a small but non zero tilt, or a departure from perfect symmetry, might provide the stimulus for the growth of a perturbation at or near the planetary spin period. In a similary manner, the planetary rotation period must be important in the initial fluctuation of the radial (or cross sheet) current but its movement is far more complex, and a much looser coupling to the planetary rotation period is suggested. Other factors of the magnetosphere system must be causing a significant departure from the spin period with time.

Power Spectral Studies

We have also conducted a power spectral analysis of the inbound and outbound magnetometer data. The results are displayed in Figures 32 and 33. Several features of these plots should be pointed out. For the inbound data,

Table 9

Radial Disc Current Trapezoidal Z-distance Function Parameters

Fitting Region (R_s)	8-18	8-28
Z0 (R_s)	-3.884	-8.11
rate (R_s/day)	11.25	25.12
T0 (day)	0.834	0.844
period (day)	0.575 (13^h 26.4^m)	0.560 (13^h 48^m)

maxima for B_r and B_ϕ appear to almost coincide, and the character of the spectra are quite similar, suggesting that on the dayside, or, for several hours after the release of solar wind pressure, the variability of the two corresponding current systems was quite closely coupled. Outbound, on the other hand, it is noted that the peak in B_r is relatively sharp and occurs at a higher frequency or shorter period, whereas the B_ϕ peak is much broader, of lower amplitude, and occurs at a lower frequency, or longer period. These results are consistent with the model results. We conclude that the coupling of the radial and azimuthal current systems diminishes significantly, and the radial current (taillike for outbound?) significantly changes over the time scale of one day (several Saturn rotations (inbound start at 0.0007 day @ 16.02 and end 0.5757 day @ 5.00 Rs; outbound start 0.9667 day @ 6.02 RS and end 2.3729 day @ 29.99 Rs). In addition to suggesting that the period of the radial current is greater than that of the azimuthal or disc current, the B_ϕ outbound curve also suggests that the variability is much more complex (we interpret the br and bphi field changes primarily in terms of changing positions rather than magnitude changes). The outbound Br curve also shows some departure from simple sinusoidal nature, some first harmonic content being present. Some variation in the current magnitude might account for this. The frequency of the variation in Br is probably at the spin period (based more on the model comparisons than the spectral results because the latter are not as accurate) both inbound and outbound, whereas that of B_ϕ is only during the inbound. Any model for the response of the magnetosphere to a sharp increase in solar wind pressure, or in change in the direction of the solar wind flow, must predict the kind of changes that has been observed.

The periodicities in charged particle ratio observed on Voyager 2 began in the vicinity of the nominal, centered dipole L-shell of Titan and persisted to the vicinity of the magnetopause, with two additional minima being observed within Titan's L-shell. However, as can be seen in the Pioneer 11 data, the "periodic" penetration of both the azimuthal and radial current sheets occurred thoughout the magnetosphere. They fit parabolas to the rate ratios, whereas we have fit either a sine wave or ramp type function to the br and bphi data. They extrapolated backwards in time from Voyager 2 to Voyager 1, obtaining consistent trends in the ratios observed in the Voyager 1 data using both the SKR and SED periods. We should note that although these periods are obtained in the moving spacecraft frame, the correction factor beyond 5 R_J is small enough to not significantly affect these results.

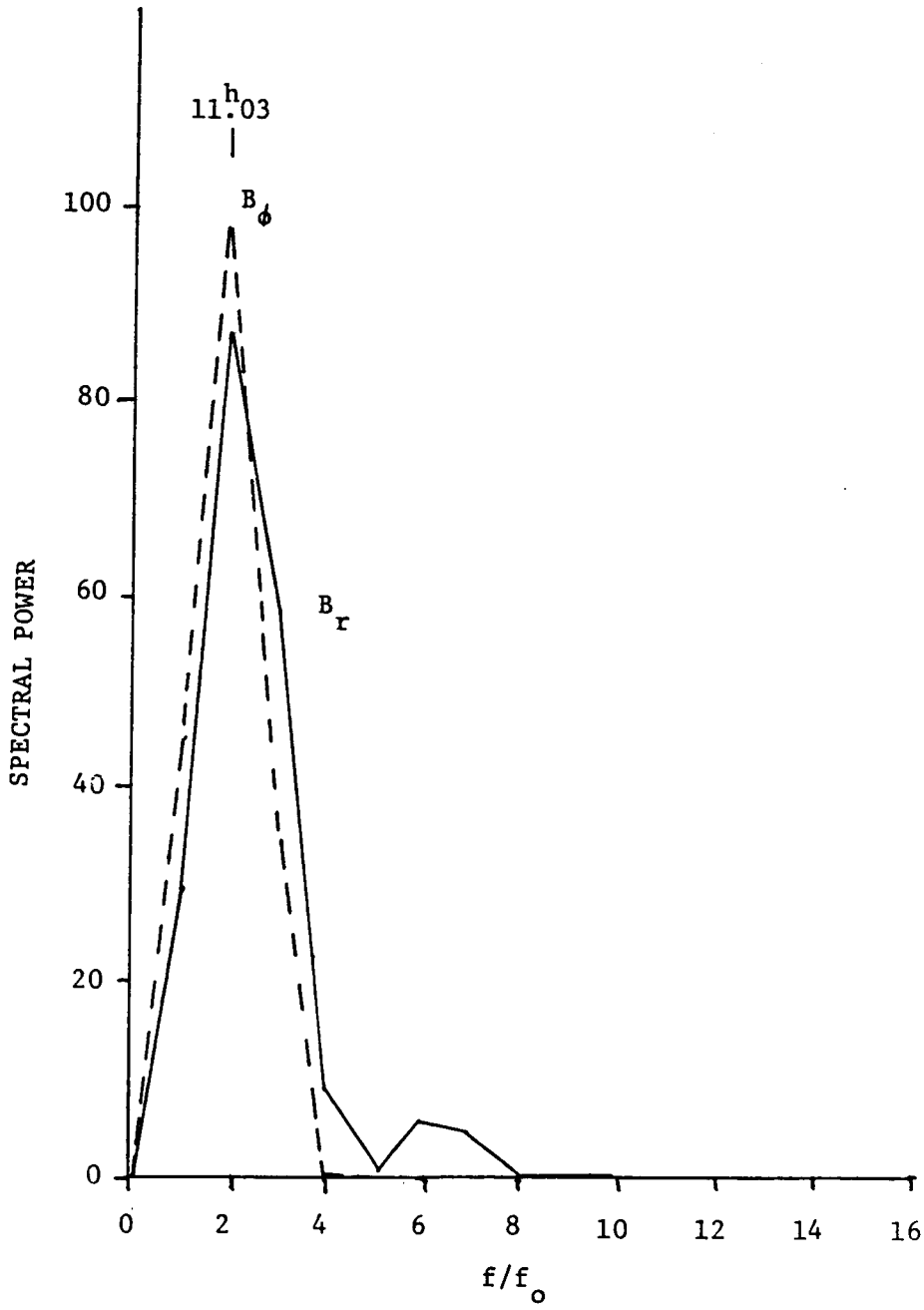
11.h03
100
80
60
40
20
0
B_ϕ
B_r
SPECTRAL POWER
0
2
4
6
8
10
12
14
16
f/f_o

Figure 32

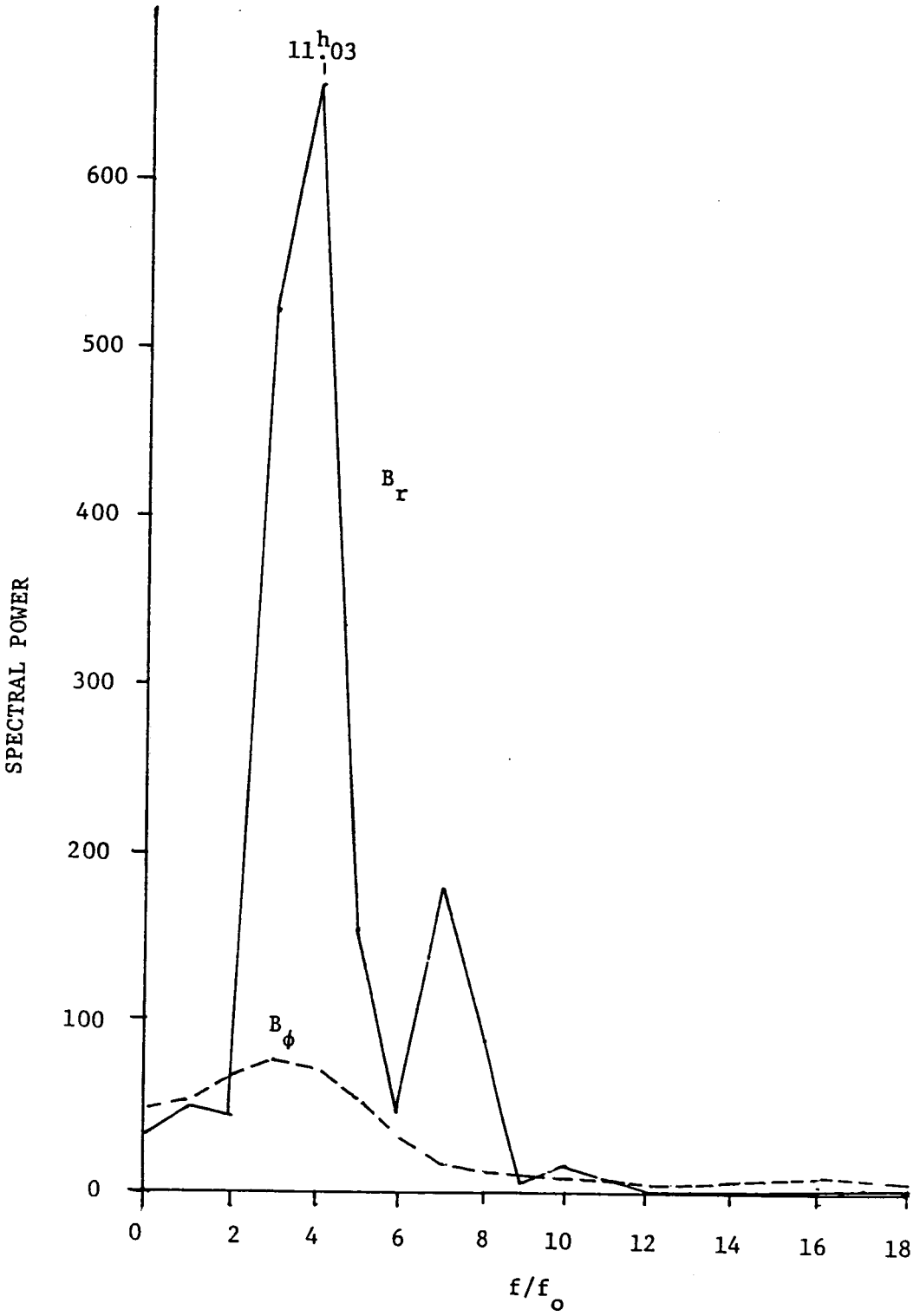
11h03
600
500
400
300
200
100
0
SPECTRAL POWER
B_r
B_ϕ
0
2
4
6
8
10
12
14
16
18
f/f_o

Figure 33

Saturn Periodicities

(Douglas E. Jones)

Natural period of the Saturnian magnetosphere

If a sudden solar wind pressure enhancement were to impinge on the magnetosphere, how might it respond? Most likely like a damped oscillator, the damping constants depending upon resistivity or inverse conductivity, self inductance, capacitance, etc. The study of the stability of a rotating cylindrical plasma might also prove fruitful as to obtaining an understanding of the manner in which the periodicities observed in the J_r and J_ϕ currents vary. What is needed is some dependence of the period on changing dimensions of the magnetosphere.

We consider first a simple L, C model for the magnetosphere (Smith, Filius and Wolfe, 1978) we have

$$L = \pi \mu b$$

where b is the radius of the ring current, and

$$C \simeq \pi \varepsilon_0 \eta a$$

estimates the capacitance (here a is the planetary radius, or some other radius [outer edge of visible rings?]). Since $\eta = (c/V_a)^2$, then the period of such a "device," is approximately $T \simeq 4\pi^2 R_s \sqrt{(b/a)} / V_a$. Periods in the ball park of the Saturnian spin period are easy to obtain, and the $\sqrt{(b/a)}$ factor can be used to associate the increaseing period of current wobble with time as the ring radius increases when the solar wind pressure decreases.

The differing nature of the movement of the radial and azimuthal equatorial currents can be interpreted either in terms of spatial or temporal variations. The wobbly motion of both the azimuthal and radial currents during the inbound passage is seen to be more nearly sinusoidally, i.e., describable in terms of a tilt of the symmetry axis in both cases relative to the spin axis. However, inspection of the B_r and B_ϕ waveforms during the outbound passage suggests that the motions are no longer simply sinusoidal, describable in terms of a tilt of the respective axes relativie to the spin axis, but are

clearly more complex. In fact, the motion of the radial (or cross tail-like) current system is more trapazoidal in nature. The changing pattern of the wobble appears to be qualitatively consistent with that predicted on the basis of a simple rotating cylindrical plasma column, which develops an instability (Rosenbluth et al., 1961; Taylor, 1962). The changing wobble period of the currents to the variations is also qualtitaively consistent with this type of configurations. Assuming an inner boundary to which the plasma is attached, there results the expression for the wobble frequency in terms of the rotation frequency the form (Spencer, 1985)

$$\frac{\omega}{\Omega} = \frac{1}{1 - \frac{b^2}{a^2}} \left[\pm 2\frac{b}{a} \quad 1 + \frac{b^2}{a^2} + 2\frac{b^2}{a^2} \right]$$

vHere, b is the radius of Saturn, or the inner boundary of the plasma, which by definition is a "hard" boundary, and a is the magnetopause boundary. If the inner boundary is the planet, then use of likely magnetopause boundaries results in ω/Ω values that are far too small. If the outer edge of the visible ring (which one?) is used to define the inner radius, then reasonable values are obtained. The results above are for the lowest, or $m = 1$, modes. Higher modes are possible at the same time for the same b/a ratio. These will have different phases. As a result, complex wave forms such as those observed may be possibly related to this mechanism. A puzzling feature of the time dependence of the currents is the fact that the ring wobble seems to remain at the spin period, while the up/down motion of the radial or front side sheet current is the one that changes with time. Although this result definitely is consistent with the possible suggestion that the system is rotationally unstable ala Taylor. One also notes that the ring current thickness decreases, which is consistent with the manner in which the earth's tail current sheet changes during a substorm, and that the image dipole strength is much stronger inbound (requiring the ring current to also be much stronger). This is consistent with the manner in which magnetopause currents increase in reponse to a solar wind pressure increase.

Preliminary Studies of the Titan Plasma Interaction

(Gordon R. Wilson and Michael T. Johnson)

At 0540:20 UT, on 12 November 1980, the Voyager 1 interplanetary probe passed within 6969 Km of the center of Titan, the largest satellite of Saturn. At that time, the plasma and magnetic field signatures suggested that the type interaction between the corotating magnetized plasma in the Saturnian magnetosphere could be best described as sub-Alfvenic. Pioneer 11 had previously crossed just above the Titan's orbit some 140 R_T downstream (Jones et al., 1980b). At that time, anomalous field and energetic particle signatures were observed. However, the critical plasma observations were not made, primarily because the detector sensor axis was oriented approximately 180° relative to the corotating flow. If the observed anomalous signatures were due to a plasma-Titan interaction, then a super-Alvfenic interaction is required. Eviatar et al (1982) have suggested that at times long-lived plumes of heavy atom/molecules from Titan exist such that Titan interacts with some of the atmosphereic molecules that escape during the plasma-Titan interaction. Heavier ions would lower the Alfven velocity making the interaction super-Alfvenic. For purposes of placing the Voyager 1 and Pioneer 11 observations relative to Titan in proper context, a theoretical program to study the plasma-Titan problem was started (see also Titan review paper to be published in Encyclia attached as Appendix A).

Titan is essentially a planet in its own right, having mass and physical dimensions larger than the planet Mercury and a more extensive atmosphere than Earth. Voyager discovered that Titan's atmosphere is mostly (82%) N_2 gas. The atmosphere is very much extended and forms a unique type of obstacle to the plasma flow about it. The study of how the upper atmosphere and the ionosphere effect the plasma flow has subsequently become of great interest to planetary and plasma physicists. The Titan plasma interaction is substantially different from the four other main classes of space plasma interaction, and is substantially different from the four other main classes of space plasma interactions which are typified by the cases of Earth, Venus, comets, and the Earth's Moon.

In the case of the Earth, and other magnetized planets such as Jupiter, Saturn, Uranus, and possibly Neptune, the planetary magnetic field is the primary source of distortions to the plasma flow. Secondly, because the solar

wind is super-Alfvaic (M_A=8) the interplanetary magnetic field is essentially frozen into the ions and moves with them (i.e., most of the energy is kinetic energy in the plasma and not magnetic energy stored in the interplanetary magnetic field.) Therefore, a kinetic plasma simulation of the ion flow in a planetary magnetic field is what is needed to obtain a working model of this class of interaction.

The next class of interaction, epitomized by Venus and Mars, is somewhat similar. These planets have no measurable magnetic fields, but the ionospheres are sufficiently well developed form currents strong enough to divert the flow before it enters the region where collsions with the neutrals in the atmosphere become important. The main difference between this class and the former is that it is the plasma flow itself that is responsible for the creation of the ionopheric currents which in turn diverts the flow. Again, most of the energy is kinetic and not magnetic so that the interplanetary magnetic field remains frozen in the flow.

The third class is that of comets. Large outward flows of neutrals from the comet serve as the means in which the flow is diverted. The interaction is therefore collision-dominated and not field-dominated. Since comets inhabit interplanetary space the plasma flow envolved is the super-Alfvenic solar wind and thus it is more important to model how the ions react than the interplanetary magnetic field, as this will still be frozen to the charged particles.

The fourth class is perhaps the simplest to model. Large solid objects, with no atmospheres, simply block the flow, which will eventually recombine behind the impediment. The particles aren't diverted by the fields or scattered by collisions, but are simply absorbed. Virtually every asteroid or satellite in the solar system is a member of this class. Only Titan, and possibly Jupiter's moon, Io, and Neptune's moon, Triton, should be excluded.

Titan is a very unique situation because of the variability of the conditions of the plasma flow around it. Part of the time it is in the solar wind, part inside the Saturnian magnetosphere, and part in transition. Voyager 1 encountered Titan inside the magnetosphere. At Titan's position (about 20 Saturn radii) the Alfven mach number of the Saturnian magnetospheric flow is close to 1 and is therefore trans-Alfvenic. This signifies that the energy in the flow is divided roughly evenly between kinetic and magnetic and the effect

of Titan on the magnetic field (of Saturn) must also be considered. Secondly, the currents in Titan's ionosphere are not sufficiently strong enough to prevent the flow from entering the collision-dominated regions and thus mixing of the ionosphere and the flow plasma occurs. This is significant for two reasons. First, the reaction is neither field-dominated nor collision-dominated, but both are important. Secondly, heavy ions (charge=e+, mass=28 amu) from the atmosphere enter the flow and have an effect on it. Voyager detected such particles in the tail, which are most likely N_2+ or H_2CN+. All these factors combine to make the Titan problem a more interesting and difficult one to model.

The adopted model utilizes a two-dimensional region of interaction roughly centered on Titan, but elongated behind (ie. in the direction of the flow) it so that the development of the tail can be seen. The standard unit of length adopted is 4000 km which is approximately the radius of the exobase (Re). The interaction region is divided into an 45 by 40 array of cells, with each cell having length and width equal to 400km. The region thus extends 25 cells behind Titan and 20 cells in front and to each side. The x-axis points in the direction anti-parallel to the plasma flow while the y-axis points directly away from Saturn. The Saturnian magnetic field points in the negative Z-direction and at Titan's orbital radius has a magnitude of roughly 5 nano-Tesla. Away from Titan, the magnetic field moves with the flow as if it were frozen into it. The moving magnetic field thus creates (in the rest frame of Titan) an apparant electric field in the Y-direction having a magnitude of 600 microvolts/meter. The fields change significantly close to Titan and how they change is an anticipated result of this project.

The plasma flow consists primarily of protons and electron. At Titan's orbital distance it has a density of roughly .2 cm^{-3}. Its average velocity is 120 km/sec and it has a temperature of about 200 ev. Away from Titan these protons and electrons essentially carry the Saturnian magnetic field with them. Heavier ions, originating from Titan on a previous pass, could also be in the flow, but are believed to be insignificant in this study and therefore not included in the model. When the model is extended to study "deep tail" interactions such as suggested by the Pioneer 11 measurements, such will need to be included.

The ions are divided into two groups based on mass. First, single protons

are considered. These primarily originate in the co-rotating plasma flow, but some also come from ionization in the upper atmosphere. Their gyroradii are on the same order as a cell size and so must be moved as individual particles. The other group is that of heavy 28 amu ions, which Voyager found in the tail behind Titan. Since the atmosphere is about 82% N_2 gas, most of these would be N_2+, but could also be other combinations of nitrogen, hydrogen, and carbon. These come mainly from ionization in the upper atmosphere. These heavy ions have gyroradii many times the size of a cell so that they must also be treated as individual ions. Electrons, having gyroradii many orders of magnitude smaller than a cell size, can then be treated with the fluid equations.

One of the first steps of this projects was to obtain or develop a working model of Titan's upper atmosphere and ionosphere. The upper atmosphere and ionosphere is considered to have two main elements, N_2 and H. The nitrogens were found to have a scale height of roughly 100 km and a density at 1 Re of 1 x 10^8 cm^{-3}, and the atomic hydrogen had a scale height of about 2500 km and a density at Re of 4 x 10^4 cm^{-3}. The density distribution for both was assumed to have the following form:

$$N = noe^{-r/H}$$

where H is the scale height and no is determined by the given density at r=4000 km (at r=Re) [Hartle, 1981]. Although other gases are present in the upper atmosphere, such as CH_4, more complex hydrocarbons, and H_2, they are considered to be in insignificant densities to have an important effect on the model.

After obtaining a model upper atmosphere, the next step was to model the ionosphere. Nitrogen gas is ionized primarily by electromagnetic radiation in the 500 to 800 Å range, while hydrogen is ionized by wavelengths in the 500 to 912 Å region. The intensity of solar radiation at Titan in this range is 7.9 x 10^7 photons-cm^{-3}-sec^{-1}. The ion production rate is given by

$$q = \psi \nu \Psi$$

and

$$\partial \Psi / \partial z = n \sigma \Psi$$

where Ψ is the solar flux, q is the ion production rate, c is the absorption and ionization cross-sections each about 2×10^{-17} cm^2, n is the neutral density and z is the linear distance of the light [Bauer, 1973 pp. 46, 53]. Radiation from the sun is essentially parallel and the ionization rate at each point in the reaction region was found by numerically integrating from infinity along a line parallel with the sun line (ie. the line containing the sun and center of Titan) and determined by an impact parameter b away from that line.

Several interesting results were obtained. First, the atomic hydrogen does not effectively absorb the light. This was found by using nothing but a cloud of atomic hydrogen with the above parameters and ignoring everthing else including the planet. Even along the sun line itself the ionization rate was found to be the same, to two significant figures, at the same radial distance. Therefore, light travelling through such a hydrogen cloud would still have effectively 99.8% of its initial intensity after leaving the cloud. The nitrogen and the solid planet itself were then determined to be what effectively reduces the solar radiation for ionization. Since the scale height of the hydrogen is about 6 cell lengths high, the cells as used above were considered adequate for use with the ionized hydrogen. The number of ions that should be produced during each timestep in each cell was determined from the ionization rate and then each such ion would then be given an initial random location in its particular cell. Assuming a Maxwellian velocity distribution for the atmospheric molecules, the temperature of 160°K of the upper atmosphere was used to randomly determine the initial velocity of the newly ionized particles.

Since the adopted cell size is about four nitrogen scale heights, significantly smaller cell sizes were used to generate the new nitrogen ions. Due to the rapid reduction in the density of nitrogen gas, no important ionization occurs outside of about 1.6 Re. Like the hydrogen, the temperature of 160°K was used to find the initial velocity of the ionized nitrogen. During each timestep each newly created ion was moved immediately after creation through a random fraction of the timestep to simulate continuous ion creation.

Another important element of the Titan problem is the greatly extended atmosphere. The incoming ions have a large probability of colliding with the neutrals in the atmosphere before the altered fields can completely deflect them. And therefore a mechanism for handling these collisions was developed.

the probability of collision is calculated from a comparison of the ions mean free path at the point in question and the distance the ion would have travelled should there be no collision. Collisions with both N_2 and H are treated, but collisions with N_2 were seen to be the more important, with collisions with atomic hydrogen being quite rare. Collisions with both were treated similarly. From the 160°K temperature of the upper atmosphere a random velocity was chosen for the neutral. Then the ion and the neutral collide elastically and a new velocity is obtained for the ion by the conservation of energy and momentum. The new velocity of the neutral is ignored. We assume that the densities of N_2 and H are unaffected by the interaction.

Perhaps the most important procedure in this project is that of efficiently and accurately moving the respective particles. The procedure adopted uses a leapfrog type approach where the position components are known at integer intervals (ie. at the beginning and end of each timestep) while the velocity components are known at half-integral intercals (ie. at the midpoint of each timestep). Using the velocity at the midpoint of each timestep to move the particels to the end of the timestep provides a second order movement technique at the same computing time as a simple first order technique. The velocities are similarly stepped from time t-1/2 to t+1/2 by using the electric and magnetic fields at the particle's position at time t. This finds an average acceleration during the timestep [Lawrence Livermore laboratory Preprint UCRL-84293 on "How to get started in particle simulation"]. Since the acceleration is partly dependent on $\mathbf{v} \times \mathbf{B}$, $\mathbf{v}$ is needed at time t, but only known at t-1/2. v(t) was replaced here by the approximately equivelent term $(\mathbf{v}(t-1/2)+\mathbf{v}(t+1/2))/2$, yielding an equation of the form.

$$\mathbf{v}(t+1/2) = f(\mathbf{v}(t-1/2), \mathbf{v}(t+1/2), \mathbf{B}(t), \mathbf{E}(t))$$

where $\mathbf{v}$, $\mathbf{B}$, and $\mathbf{E}$ are the usual velocity, magnetic field, and electric field vectors. Since only the x and y components of $\mathbf{v}$ are needed, this reduces to a set of two equations and two unknowns, which was then solved for the x and y components of $\mathbf{v}(t+1/2)$. A similar method of stepping the magnetic and electric fields is still being worked on and should be solved soon.

The simulation was accomplished in the yet uncomplete form of not stepping the fields. The fields were considered constant both spacially and temporally throughout the simulation. This then gives an idea of what the final form of

the currents and the flow should be like and should give an indication of what the final form of the fields should look like.

Figure 34 displays the interaction region with the surface of the planet as a solid circle and the exobase as a dashed circle. The directions to the sun and Saturn at the time of encounter are shown. Also, the path of Voyager 1 path through the tail is depicted. The solid line shows the spacecraft trajectory when it was abo e the equatorial plane, and the dashed line when it was below this plane. Figure 35 shows the density of heavy ions after they reached equilibrium. This is highly dependent on the direction to the sun since ionization of N_2 occurs almost entirely near the exobase and around the sub-solar point. For the configuration appropriated for Voyager 1, a wide jet of heavy ions entering the flow near the sub-solar point is seen to spiral out of the interaction region. Each printed dot represents 4.8×10^{22} real ions and is equivalent to 32 dots in the hydrogen plot. Near Titan the fields change significantly in the region where most of the ionization of nitrogen occurs, and the actual structure of the nitrogen flow is expected to be quite different from that depicted.

Figure 36 shows the heavy ion flow vectors. It can be seen that the ions are created with little velocity near the exobase on the sunward side, and subsequently experience many collisions which tend to keep their velocities low in this region. The density in this region builds up to a few orders of magnitude above that of the co-rotating plasma flow away from Titan. When the ions escape, they gradually accelerate in the y and eventually the -x directions,- and eventually spiral out with a radius of 3 or 4 Re.

Figure 37 displays the density of hydrogen ions that primarily originate from the co-rotating plasma, but also ionized protons from the ionosphere are also included. A large density build-up can be seen along the leading edge of the atmosphere that spreads toward the sunward side of Titan and thence towards the back, creating a plasma jet behind the sunward side and not the other. A near vacuum of protons forms behind the planet, filled only with occasional, recently ionized hydrogen.

Figure 38 provides additional information about the proton interaction picture by showing the proton flow directions. The line from the dot in the center of each cell shows both the magnitude and direction of the averge velocity of the particles in the respective cell these clearly show a great

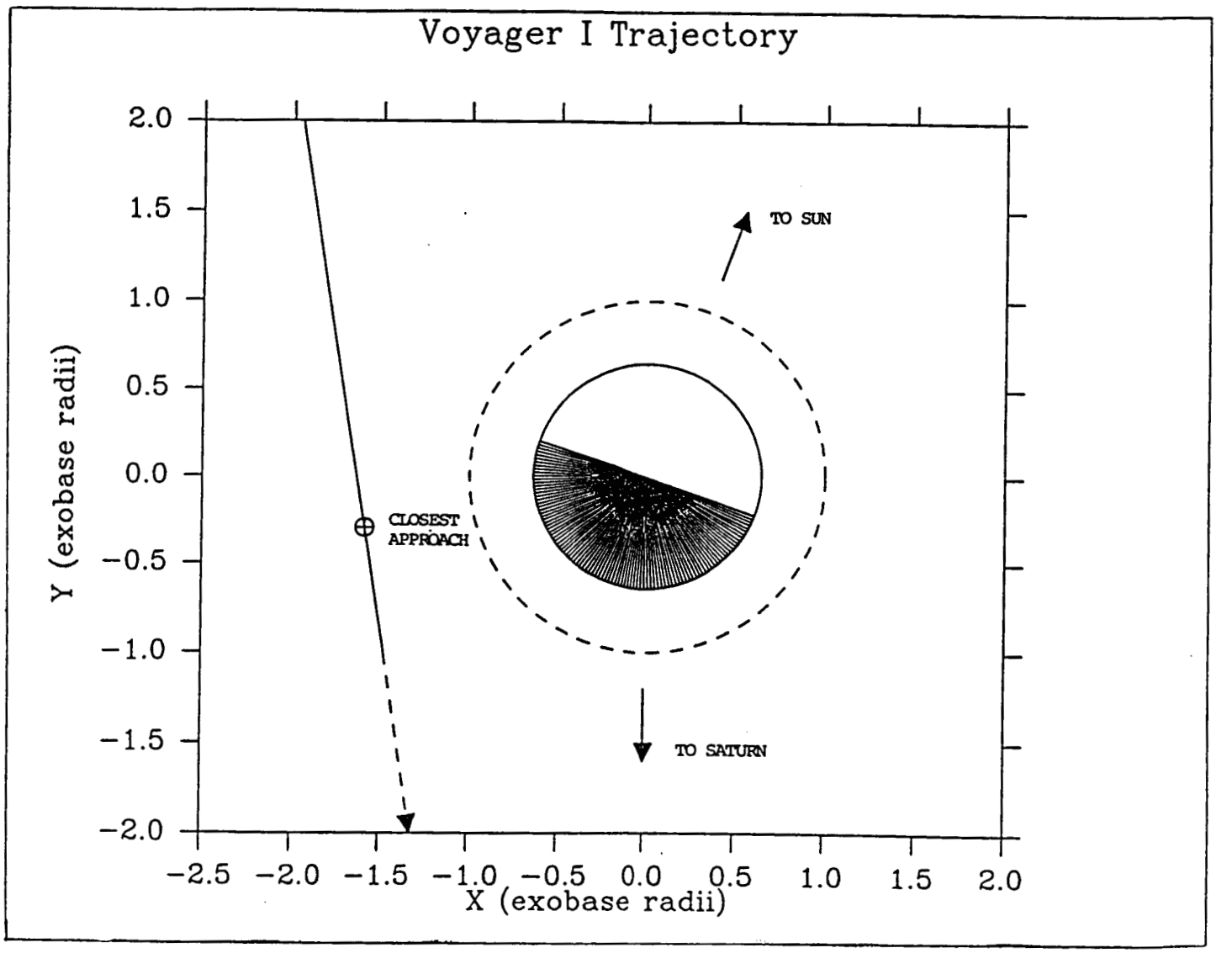
Voyager I Trajectory
2.0
1.5
1.0
0.5
0.0
−0.5
−1.0
−1.5
−2.0
Y (exobase radii)
TO SUN
CLOSEST
APPROACH
TO SATURN
−2.5 −2.0 −1.5 −1.0 −0.5 0.0 0.5 1.0 1.5 2.0
X (exobase radii)

Figure 34

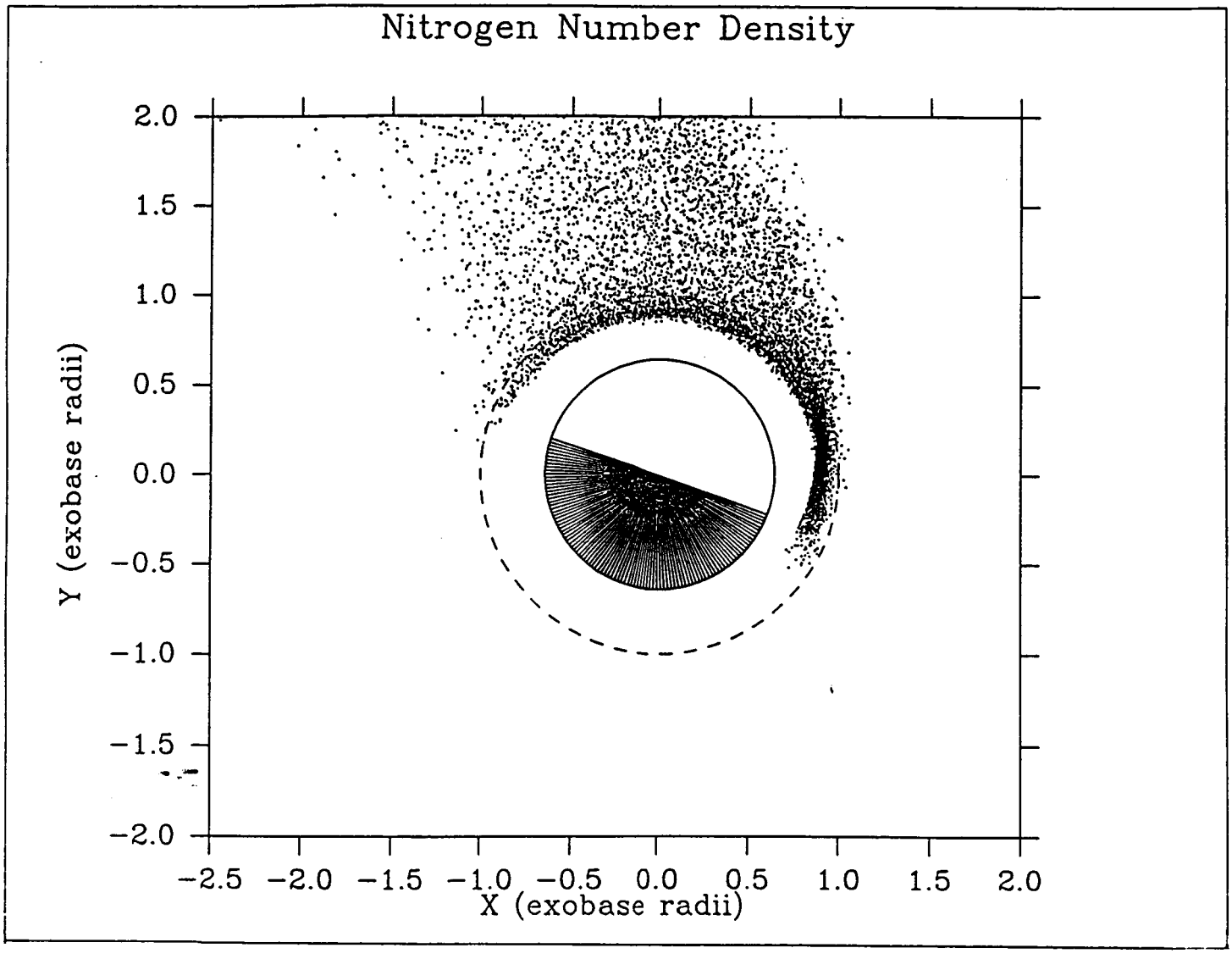
Nitrogen Number Density
2.0
1.5
1.0
0.5
0.0
−0.5
−1.0
−1.5
−2.0
Y (exobase radii)
−2.5 −2.0 −1.5 −1.0 −0.5 0.0 0.5 1.0 1.5 2.0
X (exobase radii)

Figure 35

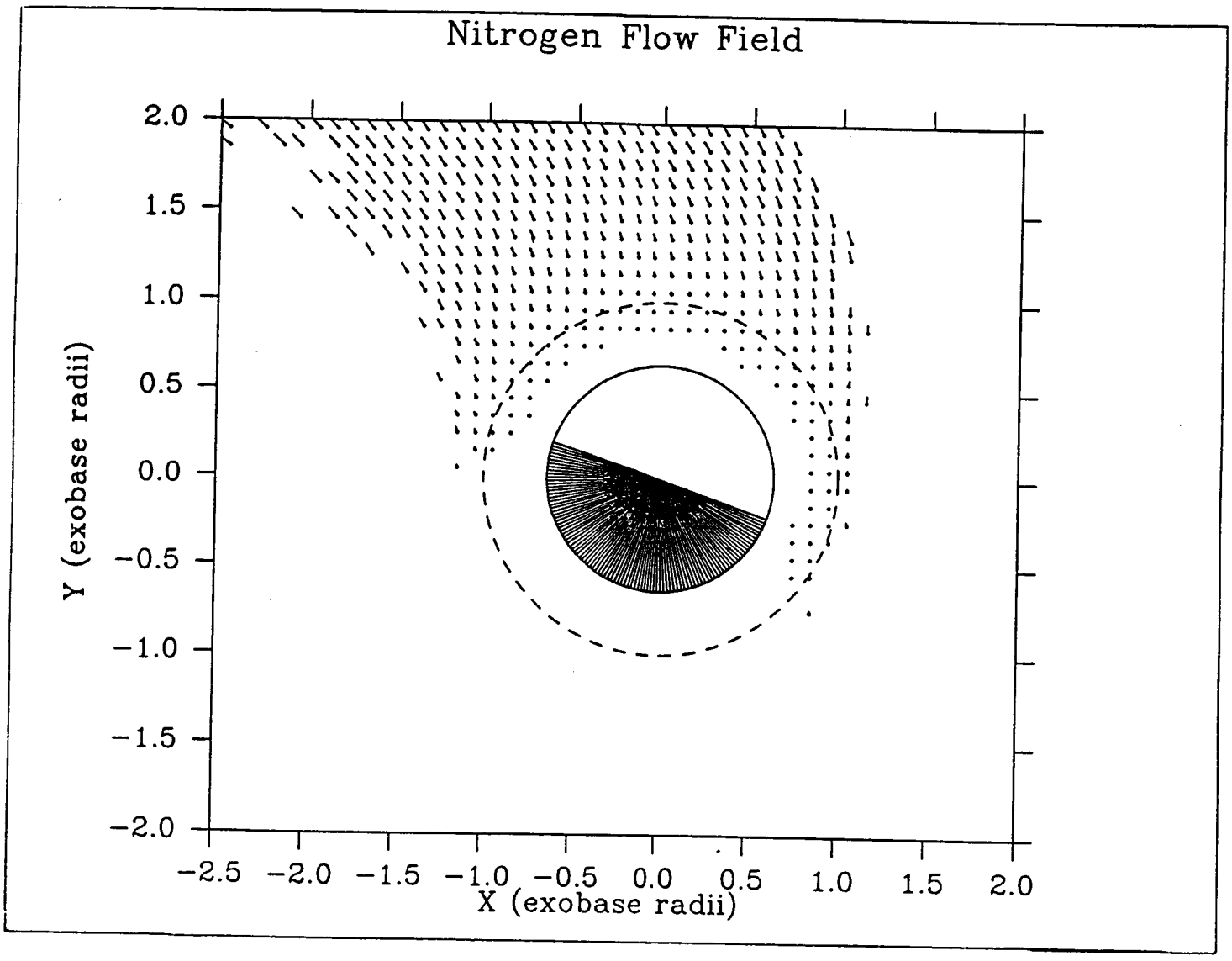
Nitrogen Flow Field
2.0
1.5
1.0
0.5
0.0
−0.5
−1.0
−1.5
−2.0
Y (exobase radii)
−2.5 −2.0 −1.5 −1.0 −0.5 0.0 0.5 1.0 1.5 2.0
X (exobase radii)

Figure 36

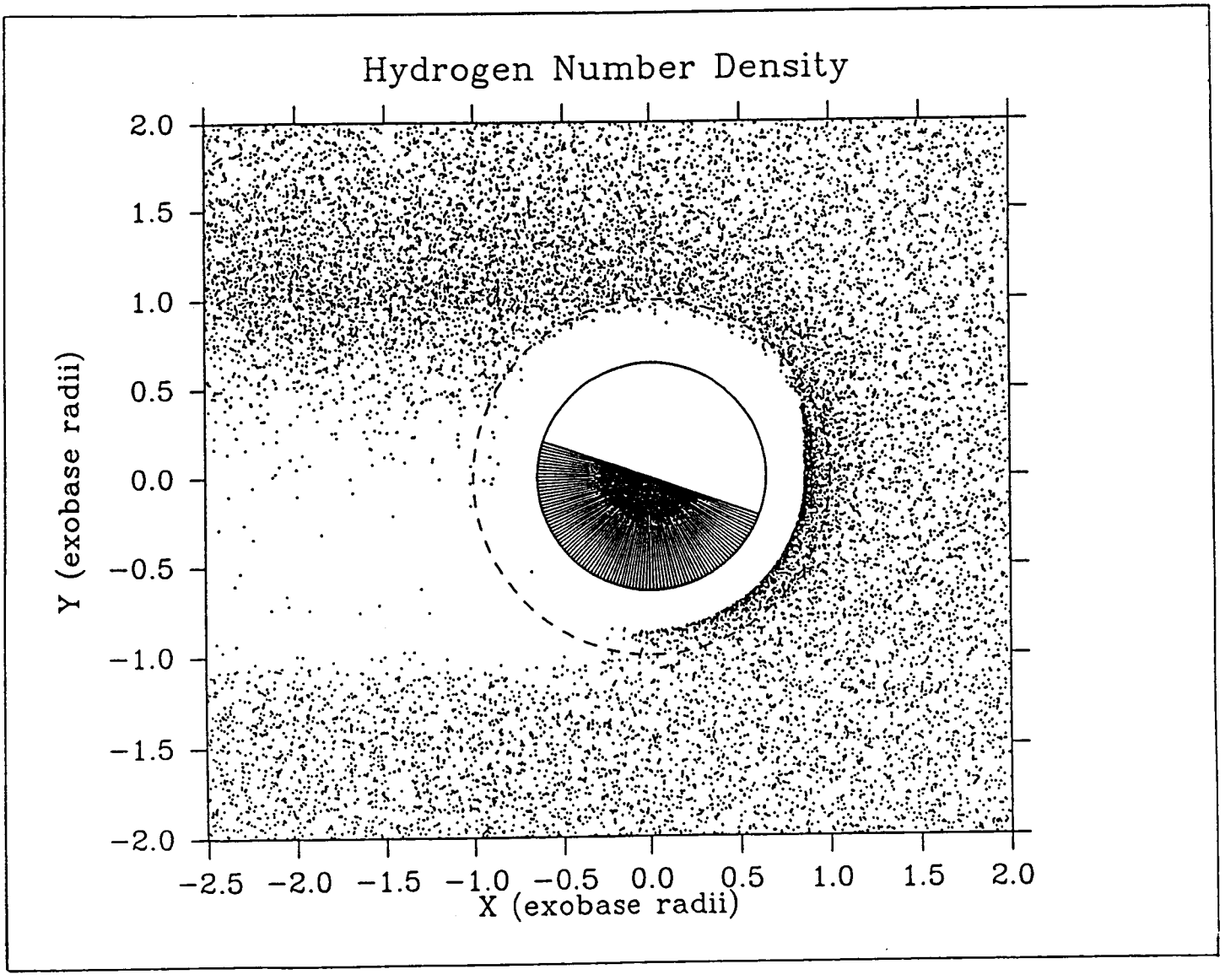
Hydrogen Number Density
2.0
1.5
1.0
0.5
0.0
−0.5
−1.0
−1.5
−2.0
Y (exobase radii)
−2.5 −2.0 −1.5 −1.0 −0.5 0.0 0.5 1.0 1.5 2.0
X (exobase radii)

Figure 37

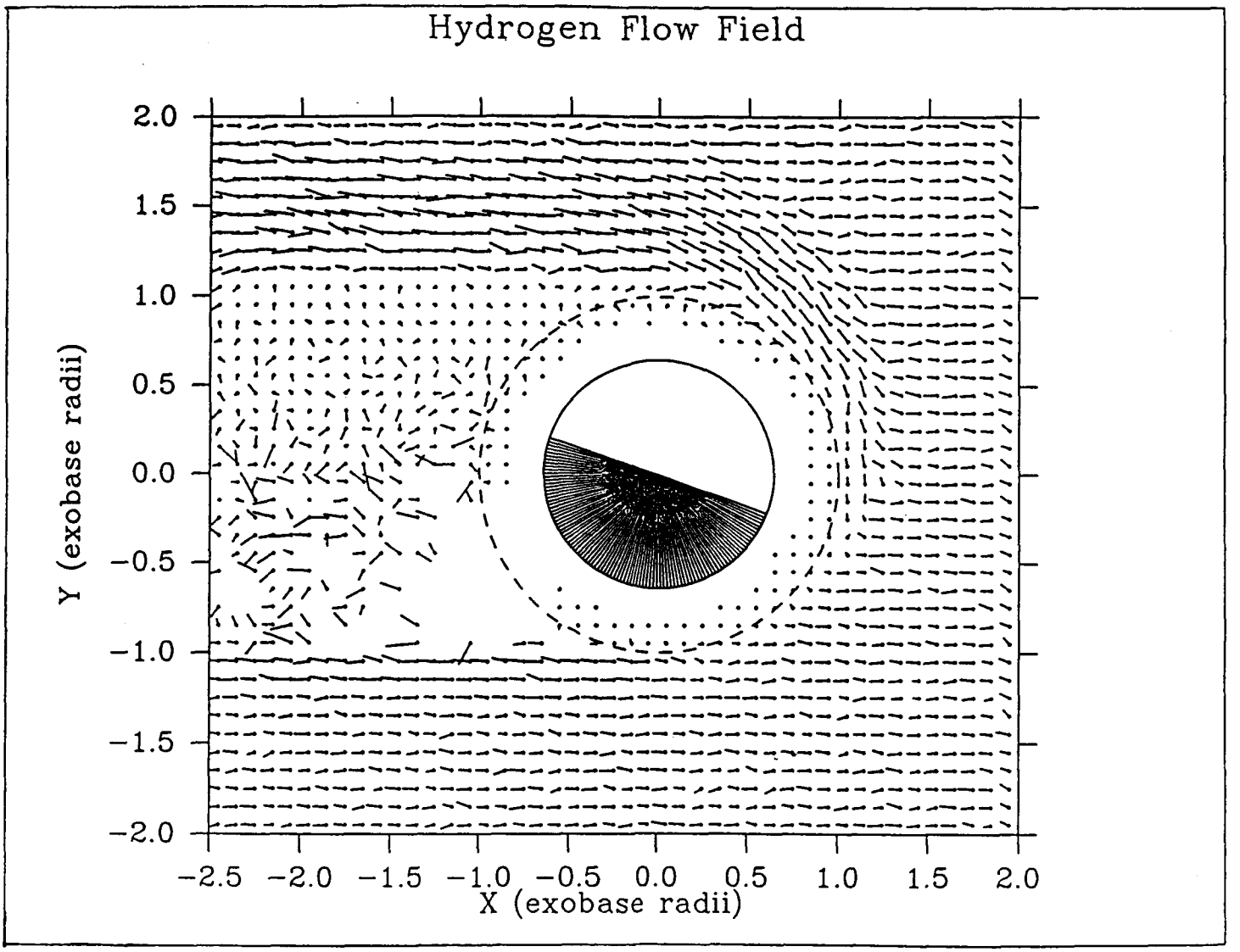
Hydrogen Flow Field
2.0
1.5
1.0
0.5
0.0
−0.5
−1.0
−1.5
−2.0
Y (exobase radii)
−2.5 −2.0 −1.5 −1.0 −0.5 0.0 0.5 1.0 1.5 2.0
X (exobase radii)

Figure 38

slowing down of the flow protons as they collide with the atmosphere. They then slowly begin to move around toward the sunward side and eventually move in a concentrated jet on that side behind the planet, in confirmation of what appeared in Figure 34

The results displayed in Figures 34-38 are preliminary since the ions in each plot will effect the magnetic and electric fields around themselves, and the altered fields could then significantly change the results given above. Allowing the fields to change, both spacially and temporally, is one of the most important parts of this project. A hybrid model for moving ions as particles and electrons as fluids which would then allow the fields to be stepped at each timestep and in each cell based on work by M. M. Leroy, et. al., [Leroy, 1982] is being worked on. One of the major difficulties is keeping the number of particles in the simulation manageable, while having a sufficient number to yield smooth enough ion densities and flow velocities to obtain the numerical derivatives required to find the electron and magnetic fields, and therefore to step the fields.

From the results obtained to date a number of predictions about the final form of the fields are possible. First, a strong current buildup on the front face of Titan should yield an increased magnetic field in front and a decreased field behind. The heavy ions may not be pulled off in the positive y-direction as quickly as indicated and more may end up in the part of the tail located in the interaction region. Also, in the tail the electic field which normally points in the y-direction may be greatly reduced, and in some places, particularly near the main proton jet, may even be reversed, and thus the main proton jet may be pulled in the y-direction and spread out in the tail. Continued studies of this problem should establish precisely what happens.

The longer term study will involve determining as completely as possible the characteristics of the trans-Alfvenic,transonic interaction. When this is sufficiently solved, the possible trans-, super- interactions will be studied. This will be in preparation for determining that type of interaction that would have been required to explain the anomalous data observed as Pioneer 11 crossed above Titan's orbit.

References

Bauer, Siegfried J., The Physics of Planetary Ionospheres, vol. 6 of series "Physics and Chemistry in Space," Springer-Verlag, 1973.

Beard, D. B., The interaction of the terrestrial magnetic field with the solar corpuscular radiation, J. Geophys. Res., 65, 3559, 1960.

Burch, J. L., Effects of the interplanetary magnetic field on the auroroal oval and plasmasphere, Space Sci. Rev., 23, 449, 1979.

Carbury, J. F., and S. M. Krimigis, Charged particle periodicity in the Saturninan magnetosphere, Geophys. Res. Lett., 9, 1073, 1982.

Carbury, J. F., and C. -I. Meng, Relations between the interplanetary magnetic field B_z, AE index, and cusp latitude, J. Geophys. Res., 91, 1549, 1986a.

Carbury, J. F., and C. -I. Meng, Correlation of cusp latitude with B_z and AE (12) using nearly one year's data, J. Geophys. Res., 91, 10047, 1986b.

Carr, T. D., J. J. Schauble, C. C. Shauble, Pre-encounter distributions of Saturn's low frequency radio emission, Nature, 292, 745, 1981.

Connerney, J. E. P., Comment on 'Azimuthal Magnetic Field at Jupiter' by J.L. Parish, C. K. Goertz, and M. F. Thomsen, J. Geophys. Res., 86, 7796, 1981.

Connerney, J. E. P., M. H. Acuna, and N. F. Ness, Saturn's ring current and inner magnetosphere, Nature, 292, 74, 1981.

Connerney, J. E. P., N. F. Ness, and M. H. Acuna, Zonal harmonic model of Saturn's magnetic field from Voyager 1 and 2 observations, Nature, 298, 44, 1982.

Connerney, J. E. P., M. H. Acuna, and N. F. Ness, Currents in Saturn's magnetosphere, J. Geophys. Res., 88, 8879, 1983.

Connerney, J. E. P., L. Davis Jr., and D. L. Chenette, Magnetic field models Saturn,, p. 354, ed. T. Gehrels, U of Arizona Press, Tucson, Arizona, 1984.

Davis, L. Jr., and E. J. Smith, New models of Saturn's magnetic field using Pioneer 11 vector helium magnetometer data, J. Geophys. Res., 91, 1373, 1986.

Desch, M.D., and M.L Kaiser, Voyager measurement of the rotation period of Saturn's magnetic field, Geophys. Res. Lett., 8, 253, 1981.

Engle, I. M., and D. B. Beard, Idealized Jovian magnetosphere shape and field, J. Geophys. Res., 85, 579, 1980.

Eviatar, A., G. L. Siscoe, J. D. Scudder, E. C. Sittler, and J. D. Sullivan, The plumes of Titan, J. Geophys. Res., 87, 8091, 1982.

Fillius, W., The trapped radiation belts of Jupiter, in Jupiter, edited by T. Gehrels, p. 896, University of Arizona Press, Tucson, 1976.

Goertz, C. K., D. E. Jones, B. A. Randall, E. J. Smith, and M. F. Thomsen, Evidence for open field lines in the magnetosphere of Jupiter, J. Geophys. Res., 81, 3393, 1976.

Hartle, R. E., et. al., Titan's Ion Exosphere Observed From Voyager 1, J. Geophys. Res., 87, 1383, 1982.

Hones, E. W. Jr., Motions of charged particles trapped in the earth's magnetosphere, JGR, 68, 1209, 1963.

Jones, D. E. and J. G. Melville, Preliminary model studies of the magnetosphere of Jupiter: Pioneer 10, Proc. Utah Acad. Sci. Arts Lett., 52, 14, 1975.

Jones, D. E., J. G. Melville II, E. J. Smith, and L. Davis Jr., Modelling Jupiter's magnetospheric current disc: Pioneers 10 and 11, EOS, 57, 991, 1976.

Jones, D. E., J. G. Melville, and M. L. Blake, Modelling Jupiter's current disc: Pioneer 10 outbound, J. Geophys. Res., 85, 3329, 1980a

Jones, D. E., B. T. Tsurutani, E. J. Smith, R. J. Walker, and C. P. Sonett, A possible magnetic wake of Titan: Pioneer 11 observations, J. Geophys. Res. 85, 5835, 1980b

Jones, D. E., B.T. Thomas, and J. G. Melville II, Equatorial disc and dawndusk currents in the frontside magnetosphere of Jupiter: Pioneer 10 and 11, J. Geophys. Res., 86, 1601, 1981

Jones, D. E., and B. T. Thomas, Modelling Jupiter's magnetosphere: evidence for a low latitude cusp, EOS, 64, 796, 1983.

Kaiser, M.L., and M. D. Desch, Saturnian kilometric radiation: Source locations, J. Geophys. Res., 87, 4555, 1982.

Krimigis, S.M., T.P. Armstrong, W.I. Axford, C.O., Bostrom, G. Gloeckler, E.P. Keath, L.J. Lanzerotti, J.F. Carbary, D.C. Hamilton, E.C. Roelof, Low energy charged particles in Saturn's magnetosphere: Results from Voyager 1, Science, 212, 225, 1981.

Kurth, W. S., D. A. Gurnett and F. L. Scarf, Periodid amplitude variations in Jovian continuum radiaion, J. Geophys. Res., (submitted 2 April 1986).

Lawrence Livermore Laboratory Preprint UCRL-84293, Denavit, J., W. L. Kruer, How to Get Started in Particle Simulation, 1980.

Leroy, M. M., et al., The structure of Perpendicular Bow Shocks, J. Geophys. Res., 87, 5081, 1982.

McDonald, F. B., and J. H. Trainor, Observations of energetic Jovian electrons and protons, in Jupiter, edited by T. Gehrels, p. 961, University of Arizona Press, Tucson, 1976.

Northrop, T. G., C. K. Goertz and M. F. Thomsen, The magnetosphere of Jupiter as observed with Pioneer 10, 2, Nonrigid rotation of the magnetodisc, J. Geophys. Res., 79, 3579, 1974.

Parish, J. L., C. K. Goertz, and M. F. Thomsen, Azimuthal magnetic field at Jupiter, J. Geophys. Res., 85, 4152, 1980.

Porco, C.C., and G.E. Danielson, The periodic variation of spokes in Saturn's rings, Astron. J., May, 1982.

Rosenbluth, M. N., Krall, N.A., and Rostoker, N., Salzburg paper CN-10-70, Conference on Plasma Physics and Controlled Fusion Research, Salzburg Austria 1961; Nucl. Fusion.

Scarf, F. L., Possible traversals of Jupiter's distant magnetic tail by Voyager and by Saturn, J. Geophys. Res., 84, 4422, 1979.

Scarf, F. L., W. S. Kurth, D. A. Gurnett, H. S. Bridge, and J. D. Sullivan, Jupiter tail phenomena upstream from Saturn, Nature, 292, 585, 1981.

Sentman, D. D., J. A. Van Allen, and C. K. Goertz, Recirculation of energetic particles in Jupiter's magnetosphere, Geophys. Res. Lett., 2, 465, 1975.

Sentman, D. D., J. A. Van Allen, and C. K. Geortz, Correction to "Recirculation of energetic particle in Jupiter's magnetosphere, Geophys. Res. Lett., 5, 1978.

Shepherd, G. G., Dayside cleft aurora and its ionospheric effects, Rev. Geophys. Space Phys., 17, 2017, 1979.

Simpson, J. A., and R. B. McKibben, Dynamics of the Jovian magnetosphere and energetic particle radiation, in Jupiter, edited by T. Gehrels, p. 738 p. 738, University of Arizona Press, Tucson, 1976.

Sittler, E. C. Jr., J. D. Scudder, and H. S. Bridge, Distribution of neutral gas and dust near Saturn, Nature, 292, 711, 1981.

Smith, E. J., R. W. Filius, and J. H. Wolfe, Compression of Jupiter's Magnetosphere by the solar wind, J. Geophys. Res., 83, 4733, 1978.

Smith, E. J., L. Davis Jr., D. E. Jones, P. J. Coleman Jr., D. S. Coleburn P. Dyal, and C. P. Sonett, Saturn's magnetosphere and its interaction with the solar wind, J. Geophys. Res., 85, 5655, 1980.

Spencer, R. Personal communication 1985

Stern, D. P., The motion of magnetic field lines, Space Sci. Rev., 6, 147, 1966.

Taylor, J.B., Rotation and instability of plasma in fast B_z compression experiments, Plasma Physics, 4, 401, 1962.

Thomas, B. T., and D. E. Jones, Modelling Jupiter's magnetospheric currents using Pioneer data: Evidence for a low-latitude cusp, J. Geophys. Res., 89, 6663, 1984.

Thomas, B. T., M. Rigler and D. E. Jones, Further model studies related to Jupiter's cusp location based upon Pioneer 11 data, EOS, 65, 1038, 1984.

Thomsen, M. F., and C. K. Goertz, Reply to "Comment on 'Azimuthal Magnetic Field at Jupiter' by J. L. Parish, C. K. Goertz, and M. F. Thomsen," J. Geophys. Res., 86, 7798, 1981.

Warwick, J.W., J.B. Pearce, D.R. Evans, T.D. Carr, J.J. Schauble, J.K. Alexander, M.L. Kaiser, M.D. Desch, M. Pedersen, A Lecacheux, G. Daigne, A. Boischot, C.H. Barrow, Planetary radio astronomy observations from Voyager 1 near Saturn, Science, 212, 239, 1981.

Warwick, J.W., D.R. Evans, J.H. Romig, J.K. Alexander, M.D. Desch, M.L. Kaiser, M. Aubier, Y. Leblanc, A. Lecacheux, B.M. Pedersen, Planetary radio astronomy observations from Voyager 2 near Saturn, Science, 215, 582, 1982.

Wilson, G. R., D. E. Jones and B. T. Thomas, Modelling Saturn's magnetosphere and planetary magnetic field: Pioneer 11, EOS, 64, 796, 1983.

Van Allen, J.A., High energy particles in the Jovian magnetosphere, in Jupiter, edited by T. Gehrels, p. 928, University of Arizona Press, Tucson, 1976.

Wu, C. C., Shape of the magnetosphere, Geophys. Res. Lett, 10, 545, 1983.

Wu, C. C., The effects of dipole tilt on the structure of the magnetosphere, J. Geophs. Res., 89, 11048, 1984.

List of Publications and Papers Presented

1. D. E. Jones, The solar wind interaction with Titan, EOS, 64, 827, 1983. (Abstract of invited paper presented at Fall Meeting of the AGU)

2. D. E. Jones and B. T. Thomas, Modelling Jupiter's magnetosphere: evidence for a low-latitude cusp," EOS, 64, 796, 1983. (Abstract of paper presented at Fall Meeting of the AGU)

3. G. R. Wilson, D. E. Jones, and B. T. Thomas, "Modelling Saturn's magnetosphere and planetary magnetic field: Pioneer 11," EOS, 64, 796, 1983. (Abstract of paper presented at Fall Meeting of the AGU).

4. B. T. Thomas and D. E. Jones, "Modelling Jupiter's magnetospheric currents using Pioneer data: evidence for a low laitude cusp, J. Geophys. Res., 88, 3404, 1984.

5. B. T. Thomas, M. Rigler, and D. E. Jones, Further model studies related to Jupiter's cusp location based upon Pioneer 11 data, EOS, 65, 1038, 1984. (Abstract of paper presented at Fall Meeting of AGU)

6. D. E. Jones, Titan's interaction with the solar wind and Saturn's magnetosphere, Encyclia (in press, 1986).

Appendix A

Titan's Interaction with the Solar Wind and Saturn's Magnetospheric Plasma

by

Douglas E. Jones

Dept. of Physics and Astronomy,
Brigham Young University
Provo, Utah

(accepted for publication in Encyclia*, 1985)

* publication of the Utah Academy of Science, Arts and Letters

Introduction

As a result of a number of factors, the flowing plasma-satellite interaction at Titan is expected to be the most varied of any object in the solar system. This is primarily due to the fact that for a little over half of the time its orbit lies outside Saturn's subsolar magnetopause, exposing it to either the free streaming solar wind, where the interaction is usually described as being both supersonic and superalfvenic, or to the thermalized solar wind or magnetosheath plasma, where the interaction is usually subsonic and superalfvenic. During the remainder of the time, Titan is located within Saturn's magnetosphere and is subsequently exposed to the nearly corotating magnetospheric plasma. The temperature, composition and density of the latter undergoes both temporal and spatial variations and as a result, the interaction can be any combination of the sub/trans/supersonic and sub/trans/superalfvenic possibilities.

In this paper we will review a number of aspects of the interaction of Titan with the solar wind and Saturn's magnetospheric plasma and report the results of a number of relevant studies. We will first consider the likelihood of Titan being exposed to the free streaming solar wind, the shocked solar wind or magnetosheath plasma, and the corotating magnetospheric plasma. We then report the results of calculations of the charge exchange absorption and mass loading of both the solar wind and magnetospheric plasma by two model Titan atmospheres that have been proposed, and discuss the implications of these results in terms of a Titan bow shock and a possible cometary type of interaction. We then discuss the Voyager 1 and Pioneer 11 magnetic field results in terms of Titan's magnetic tail and wake.

Solar Wind Pressure Variations and the Plasma Environment at Titan.

Acuna and Ness (1980) first noted that Titan's orbit (20.2 R_S; R_S = Saturn radius) is near the nominal location of the subsolar magnetopause of Saturn. Wolf and Neubauer (1982) subsequently outlined the variable magnetoplasma conditions that Titan could be exposed to while in it's orbit,

considering varying solar wind conditions and the resulting configurations of Saturns magnetosphere. Figure 1 [Slavin et al., (1983)] displays a histogram of the number of hours out of a total of 1275 that Saturn's sub-solar magnetopause was at any given distance. The mean is observed to be 18.8 R_S, or within Titan's orbit. Hence, when near the noon meridian plane, Titan will be beyond Saturn's magnetopause more than 50% of the time. Using 1.33 as the ratio of the subsolar shock-to-magnetopause distance ratio, a 20.2 R_S shock distance corresponds to a magnetopause distance of 15.2 R_S. Referring to Figure 1, we see that Titan will be at or beyond the shock location about 10% of the time. The solar wind pressure corresponding to Titan at or beyond Saturn's magnetopause is about 2.3 X 10^{-10} dynes/cm^2, and to be beyond the bow shock requires a pressure greater than about 1 X 10^{-9} dynes/cm^2. Inspection of Figure 1 suggests that while in the terminator plane, there is even a small (2 - 3%) chance of Titan being in the supersonic portion of the magnetosheath.

Based upon an earlier estimate of Titan's magnetic moment by Neubauer (1978), the existance of a Mercury-like magnetic field standoff configuration was considered possible because the estimated surface field of 100 nT provided sufficient pressure to hold off a solar wind pressure of 4 X 10^{-9} dynes/cm^2, i.e., such a field would be able to withstand the > 1 X 10^{-9} dyne/cm^2 pressure needed to push the bow shock to within the orbit of Titan. However, using Voyager 1 magnetic field data obtained very near Titan and downstream of the nearly corotating magnetospheric plasma, Ness et al. (1982) have shown that the observed magnetic field is primarily induced, resulting from the piling up and subsequent draping of Saturn's magnetospheric field.

As a result of the foregoing discussion it is possible to exclude a terrestial-like, or planetary magnetic field dominated type of interaction. Also, Titan has been known for some time to have an extensive atmosphere (Kuiper 1944), and therefore a lunar type of interaction can also be excluded. It is therefore only necessary to consider the three types of atmospheric interactions outlined in Figure 2 due to Michel (1971a). In the first (2a) the flowing plasma has a shallow component that sweeps into the ionosphere and modifies the vertical profile of the photoionization electron density. This figure would be modified for Titan to include the significantly larger collisionally induced ionization component that results when interacting with the milllion degree electrons in Saturn's magnetosphere. In

this "soft" type of interaction there will be charge exchange absorption as well as mass loading of the impinging solar wind or magnetospheric plasma. The effects of these two processes on the strength and configuration of the Titan bow shock will be discussed.

In the second (2b) the ionospheric pressure is great enough to stand off the impinging plasma high in the ionosphere, and the resulting tangential disontinuity excludes any interaction with the ionosphere, causing negligible absorption and mass loading. In the third type of interaction (2c), in which a magnetized plasma is assumed, the highly conducting ionosphere excludes the magnetic field resulting in a pileup of magnetic field lines and formation of an induced tail field. Based upon the results of Ness et al. (1982), the interaction at Titan must have at least some of the characteristics similar to that displayed in Figure 2c. However, when the observed effects of mass loading, etc., are included it is clear that while in Saturn's magnetosphere, and probably in Saturn's magnetosheath and in the solar wind as well, the characteristics of all three types of ionosphere-atmoshere interactions can occur. (For a discussion of Titan's interaction with Saturn's magnetospheric plasma at the time of Voyager 1 see Neubauer et al., 1984).

Another important feature of the solar wind interaction with Titan occurs when the latter is within Saturn's magnetosheath and concerns the relative sizes of Titan and the proton Larmor radius. Frequently the magnetic field magnitude in the sheath can be as low as 0.1 nT. Because of a higher temperature plasma there, and therefore high velocity component perpendicular to the field, the proton Larmor radius can be larger than Titan's radius, the resulting interaction configuration differing considerably from the nominal.

Atmospheric Absorption and Mass Loading

When a plasma impinges on an atmosphere, absorption of the plasma occurs through charge exchange, and that portion that flows past is "mass loaded" through the pickup of cool, heavy ions. The degree with which the impinging plasma suffers absorption has a direct effect on the strength and sub-solar distance to the shock that is likely formed. Mass loading primarily affects the shape of the shock, greater mass pickup causing a blunter shock surface. Wallis (1971) has pointed out that charge excange and photoionization, together with the resulting mass loading of the flow, may smoothly decelerate

the solar wind from supersonic to subsonic velocities either without a generating a shock at all, or creating just a weak shock ($M \simeq 2$).

Computation of both the minimum ionopause distance and the 100% absorption flow line, below which no solar wind can penetrate as a result of charge exchange, requires a knowledge of the composition and structure of Titan's upper atmosphere. The atmosphere has been found to be composed primarily of molecular nitrogen plus either atomic or molecular hydrogen. Using the exospheric distribution for N_2 reported by Broadfoot et al. (1981), Hartle et al. (1982) have estimated the minimum ionopause distance to be about 4400 km, at which level the N_2 density is 4.5×10^{5} /cm^3. For this they assumed the ionopause to be the altitude where the ion-neutral mean free path, $1/\sigma n$, equals the scale length for horizontal flow ($\cong$ 1 Titan radius, or R_T), and a value for the ion-neutral cross section, σ, of 5×10^{-15} cm^2. The neutral density, n, is assumed to be primarily N_2 below 5000 km (see Figure 3a).

In order to estimate the maximum depth of penetration of the impinging plasma, we have computed the radius of that flow line at which the plasma is totally absorbed. Following the method outlined by Gombosi et al. (1980, 1981) applied previously to Venus, and by Russel et al. (1983) applied to Mars and Venus, we have

$$\varepsilon(h) = \sum_i n_i(h)\ \sigma_i$$

where $\varepsilon(h)$ is the probability per unit length along a flow line of a charge exchange interaction at an altitude h, $n_i(h)$ is the density of the i-th neutral species, and σ_i is the charge transfer cross section between a proton and the i-th neutral species. The number per unit area of fast solar wind ions participating in a charge exchange process while moving a distance Δs, is

$$\Delta N = - \varepsilon(h(s)) \cdot N \cdot \Delta s$$

The total fractional absorption along a flow line is then

$$L = 1 - e^{- \int_{path} \varepsilon(h(s))\ ds}$$

L is plotted in Figures 4 and 6. The total dayside absorption above a given flow line, normalized to the amount of unperturbed solar wind flow that the planet of obstacle radius R_n would absorb, can be written as:

$$\mathcal{L}_{n(h_o)} = \frac{\int_{r(h_o)}^{\infty} 2\pi\, r(h)\, L(h)\, dr}{\pi R_n^2}$$

$\mathcal{L}(h_o)$ is plotted in Figures 5 and 7. In these calculations the simple circular geometric configuration similar to that of Gombosi et al. (1980) has been used. The more accurate results obtained using flow lines derived from the work of Spreiter et al. (1978) is currently in progress, but these results are not expected to change significantly, as is apparent when the Gombosi et al. (1980) and (1981) results are compared. Figures 4 (percent absorption along a flow line versus flow line radius) and 5 (total percent absorpion versus R_{min}) display the results obtained using the 165° K molecular nitrogen and atomic hydrogen atmospheric model of Strobel and Shemansky (1982) with solar wind conditions, and Figures 6 and 7 display the results for the same atmospheric model assuming magnetospheric plasma compositions and nearly corotational velocities, etc., consistent with Voyager observations. The 100% absorption flow lines are seen to occur at a radial distance of 4240 km under solar wind conditions and 4100 under magnetospheric plasma conditions. The corresponding absorption percentages are, respectively 20% and 25%. The velocity dependent charge exchange cross sections have been obtained from Rose and Clark (1961). For purposes of comparison, we also show as inserts in these figures the corresponding results from the two papers of Gombosi et al. (1980, 1981). The effects of magnetic fluctuations [See Gombosi et al., (1980)] have not been included. If the ionosphere has an electron-ion density of sufficient temperature to stand off the solar wind at a greater radius, the net plasma absorption will decrease accordingly.

Recently, Bertaux and Kockarts (1983) have proposed a model exosphere consisting of both molecular nitrogen and molecular hydrogen in which the density of molecular hydrogen is much greater than that in the Strobel and Shemansky model, i.e., more than a factor of 10^4 at the 4000 km level (see Figures 3b). However, although there is significantly more molecular hydrogen in the region above the 100% absorption flow line, when account is taken of

the fact that atomic hydrogen undergoes a resonant charge exchange with protons whereas molecular hydrogen does not, and the effects of the velocity dependence of the cross-sections are included, the increase in absorption of the (N_2,H_2) model is not as great as one might expect. Using their model atmosphere (including a two step temperature profile of 165°K and 186°K), the 100% absorption radii and net absorpion under solar wind and magnetospheric conditions have been computed as before, resulting in the values (4140 km, 37%) and (4000 km, 19%) respectively. Hence, under all conditions we find that solar wind and magnetospheric plasma absorption at Titan are greater than at Venus.

In order to determine the conditions under which the ionosphere pressure standoff radius is greater than the 100% absorption flow line radius as well as the corresponding mass loading, we have used the method of Hartle et al. (1982) and computed the density of ions and electrons produced by photoionization and by collisions between atmospheric neutrals and the impinging plasma. This has been done under varying conditions of pressure in terms of both the density and velocity appropriate for the solar wind (including the shocked solar wind or magnetosheath plasma) and the magnetospheric plasma. A determination of the degree of mass loading is necessary in order to determine the type (if any) of shock that will likely result. Using the velocity dependent ionization cross-sections (protons or electrons) for molecular nitrogen and for either atomic or molecular hydrogen (Rose and Clark, 1961); Banks and Kockarts, 1973) we have determined the ionopause radius assuming either 186°K or 8600°K electrons and ions, the corresponding Saturn magnetopause distance, and the degree of mass loading. The maximum values of $S/\rho v$ below which there should be no shock have been computed from Michel, (1971b), i.e.,

$$S = [\, N_e\, V_e\, \sigma_e \;+\; N_i\, V_i\, \sigma_i \;+\; J\,]\, N_o H\, m_o$$

and

$$S = k\, \rho_1\, V_1$$

where N_e, V_e, σ_e, and N_i, V_i, σ_i are the number density velocity and collisional ionization cross sections for electrons and ions, respectively, J

respresents the photoionizing flux from the sun, N_o, H, m_o are the number density, scale height and mass of the atmospheric atom or molecule in question at the exobase, k is a proportionality constant, and ρ_1, V_1 are the mass density and velocity of the plasma. If k_{max}, defined by (Cloutier et al., 1978)

$$k_{max} = \frac{S_{max}}{\rho_1 V_1} = \frac{(1 - M^2)^2}{(\gamma + 1) M^2 [2 + (\gamma-1)M^2]}$$

is exceeded a shock must form. Here M is the Mach number of the flow, and γ is the ratio of specific heats. For $\gamma = 5/3$ and $M \to \infty$, then $k_{max} = 0.56$ and for $M = 2$, $k_{max} = 0.18$.

The ionopause standoff distance and $S/\rho v$ ratio have been computed for different solar wind densities and speeds with the constraint that the bow shock be located within Titan's orbital radius, or $R_{bow\ shock} < 20.2\ R_S$, and for magnetospheric plasma conditions. The results for the former are displayed in Figures 8a and b for (N_2,H) and (N_2,H_2) atmospheres, respectively. Also shown are the regions where $S/\rho v \geq .56$, the high Mach number minumum value of the mass loading ratio for which a shock will form. For low Mach number (a major portion of the time in the magnetosphere), the corresponding value of $S/\rho v$ is 0.18 ($M = 2$). Recalling the 100% absorption flow line results, we see that only over a very limited range of solar wind density and velocity will there be an ionopause above the critical absorption radius, and that the (N_2,H) and (N_2,H_2) models differ as to whether a shock will form,- shock formation more likely occurring only for the latter model.

In like manner we have computed the same quantities corresponding to Titan interacting with magnetospheric plasma and thereby being influenced by the 200 ev electron gas and (almost) rigid corotating protons (heavy ions neglected). Both the (N_2,H) and (N_2,H_2) models predict, at most, a very weak shock. Figures 9a and b display the variation in ionopause distance with proton density corresponding to different plasma velocities for the (N_2,H) and (N_2,H_2) models. For comparison with the Voyager 1 measurements near Titan, Figures 10a and b display the electron density-plasma proton density-ionopause radius results for 186 and 8600°K electron-ion temperatures.

In the foregoing analysis, the considerable variability in the characteristics of the magnetospheric plasma (Goertz, 1983) has been

neglected. The magnetoplasma conditions while Titan is in the tail region should differ considerably from those anywhere else since outflow down the tail of Saturn's magnetospheric plasma should occur here, and the field direction may undergo relatively rapid directional changes there as the tail current sheet flaps up and down in response to solar wind pressure and direction changes.

Titan Observations

There have been three opportunities to observe Titan plasma interactions, but of these, only Voyager 1 and Pioneer 11 were either near Titan or at least passed near its orbit. In both of these cases Titan was in Saturn's magnetosphere. On the other hand, occurring while Titan was in Saturn's magnetosheath, Voyager 2's flyby was at a much greater distance and occurred well out of Titan's orbital plane. Only Voyager 1 passed close enough to Titan to conduct direct measurements of the interaction. The next best opportunity was afforded Pioneer 11, which passed roughly 20 R_T (Titan radius = 2575 km) above Titan's orbit some 145 R_T downstream.

Figure 11, from Ness et al. (1982), displays two views of the Voyager 1 trajectory near Titan along with magnetically important event intervals and a corresponding field magnitude plot. Figure 12 [from Hartle et al., (1982)] displays the sun, Saturn, and corotation directions, a Titan orbital plane projection of the plasma steamlines, and important plasma and field event intervals (compare Figures 11 and 12). Figure 12 suggests either that the flow around Titan is dissimilar on either side of the plasma flow axis, or else the flow direction changed during the short time that Voyager 1 passed through Titan's wake.

In their studies of the solar wind interaction with planets having atmospheres, Spreiter et al. (1980) describe the bow shock and magnetopause contours in terms of the parameter H/r_o, where H is the ionization scale height and r_o is the ionopause distance. Figure 13 displays scaled magnetopause and bow wave curves based upon their results that have been scaled for Titan. Their studies, however, assume a tangential discontinuity (see Figure 2b) which may not exist because of the considerable absorption noted above. It should be possible to obtain an estimate of the value of the H/r_o parameter from data related to the size of the obstacle presented by

Titan to the flow. The relevant data are the energetic particle observations as well as those of the magnetic field by Ness et al. (1982). Figures 15a (from Vogt et al., 1981) and b (from MacLennan et al., 1982) display two energetic particle profiles. The obstacle radius due to Titan is seen to average about 3830 km, which is roughly 5-10% less than the computed 100% absorption radius, is consistent with a small value of H/R_o (see Figure 13), and suggests that the ionopause radius is not greater than the 100% absorption radius.

Kivelson and Russell (1983) have extrapolated the field vector directions obtained in the tail lobes by Voyager 1 back to a plane oriented perpendicular to the flow direction, and found that the plasma flow needed to be aberrated an average of 27^o toward Saturn at the time. Figure 14, which is a modification of their Figure 7, shows the exobase circle (3800 km radius), a 4240 km 100% absorption radius circle due to charge exchange, and an $H/r_o=0.02$ flow-normal plane circle radius assuming the method of Spreiter et al (1980) can be applied. Although the extrapolated lobe field lines (X's contained in the contours) in the figure should lie outside the ionopause circle, one finds that most of them can be found between this boundary and that of the exobase. This suggests that the flow and field lines are not excluded from Titan's ionosphere, and that the interaction likely is quite "soft." Certainly, (refering to Figures 2b and c) there appears to be no evidence for either a tangential discontinuity or strong exclusion of the magnetic field embedded in the impinging plasma by the ionospheric conductity. The plasma atmsophere interaction at Titan in existence during the Voyager 1 flybe would appear to be one combining the characteristics displayed in Figures 2a and c, although if the plasma flow direction was changing at the time all three types of interactions could occur.

The implied small value of H/r_o (assuming the existence of the required tangential discontinuity) suggests that H must be small and therefore, with low mass density due to ionized hydrogen above the exobase, a low temperature ionosphere at the interaction region is required. If the electrons are in equilibrium with the cool neutrals, use of the computed collisional and photoionization induced electron-ion density suggests that there will be no ionopause. A higher temperature electron component, that is not in equilibrium with the neutrals, is required in order for the ionopause to be located outside the 100% absorption radius. However, this is not consistent

with the data unless variations in the flow direction of the plasma are assumed to have led to incorrect estimates of the obstacle size, i.e., H/ro.

Analysis of the EUV emission by Strobel and Shemansky (1982) requires the existence of hot (2 X 10^5 ^oK) secondary electrons in the atmosphere at and below the exobase, i.e., characteristic of auroral electrons. In addition, some of the emission features appear to come from narrow altitude regions (i.e., 250 km at 5000 km) and from both high and low temperature regions. They conclude that the energy deposition requirements needed to explain the EUV emission exceeds the EUV deposition rate by about a factor of 10, i.e., photoelectrons alone cannot provide the required amount of energy. The EUV results would tend to strongly favor the porous interaction model instead of a tangential discontinuity type of boundary. They also estimate that if collisional ionization occurs over the altitude range 3600-4000 km, the

estimated production of N_2^+ and N^+ of 9 X 10^8 and 1.8 X 10^8 /cm^2 yields an average electron density of about 3 X 10^3/cm^3 for an assumed recombination coefficient of 3 X 10^{-6} cm^3/sec. This value for the electron density is consistent with the upper limit suggested by the radio occultation data of Lindal et al. (1983).

It is instructive to compare the preceding electron density with that obtained using the formula suggested by Hartle et al. (1982), where the production rate, P, is given by

$$P = (N_e V_e \sigma_1 + J) n$$

where N_e, V_e are the number density and speed, respectively, of the magnetospheric or solar wind electrons, σ = 1-2 X 10^{-16} cm^2 is the collisional ionization cross-section, J is the photoionization flux nominally about 5 X 10^{-9} sec^{-1}, and n is the number density of the neutral atom or molecule participating in the charge exchange reaction. In this calculation we are neglecting secondary electron or magnetic field effects. For a magnetospheric configuration, and neglecting the much slower protons or ions (the several million degree electrons have V_e about 9000 km/sec), use of this formula results in an average electron density over the 3800-4000 km height interval of about 1.8 X 10^3 cm^{-3}. Substitution of typical magnetosphere plasma values suggests that roughly 80% of the ionization is a result of collisions, i.e.,

collisional ionization dominates over photionization, essentially reverse the situation at Venus. Comparison of this with the electron density estimate of Strobel and Shemansky (1982) suggests that about 40% of the electrons may have been deposited near the exobase directly from the magnetospheric plasma electron component rather than resulting from any ionization process. Strobel and Shemansky (1982) have interpreted some of the features of the EUV emission in terms of very hot electrons that exist intermitantly in the exosphere, and it is perhaps curious, then that estimates of Titan's energetic particle obstacle radius, etc., suggest a value of H/r_o that is consistent with very low temperatures. Perhaps electrons produced by collisional impact ionization with cold (160^oK) molecules of nitrogen are able to cool very rapidly. Referring again to Figures 10a and b, it is seen that the smaller inferred obstacle size is consistent with a low temperature, several X $10^3/cm^3$ density, ionosphere. A high temperature, $10^3/cm^3$ ionosphere should have resulted in a larger obstacle for Titan. If the direction of flow of the magnetoplasma changed during the Voyager 1 flyby of Titan such as to cause the effective obstacle size to be underestimated, and the ionopause radius was actually greater than the 100% absorption flow line radius, then a higher temperature ionosphere is implied. We will return to this point when discussing measurements of Titan's magnetic tail.

Assuming the higher temperature ionosphere and therefore an ionopause that lies outside the 100% absorption radius, and neglecting any draped magnetic field, we have followed the method outlined in Wolff et al. (1979) and found the variability in the Titan ionopause altitude due to changes in solar EUV flux to be only of the order of 1 - 2%. Variations in the magnetospheric plasma will be the dominant factor controlling the altitude of Titan's ionopause because photoionization is only about 25% that due to collisions. The relative importance of both changes in the solar wind plasma and the solar photoionization flux at Titan should be only about 1% what they are Venus, although significant enhancements in the former can occur when stream-stream interactions persists all the way to 10 AU (Burlaga et al., 1983). We should note, however, that under circumstances where the magnetic field piled up near the ionopause is great enough to significantly decrease the ability of the solar wind or magnetospheric plasma to collisionally ionize Titan's upper atomsphere, then ionopause distance variations may be controlled more greatly by variations in the solar EUV.

Speculations on Titan's Bow Shock

It has been suggested above that both the solar wind and magnetospheric plasma undergo significantly more charge exchange absorption in the atmosphere of Titan than in that of Venus. As a result, the shock should be weaker and the nose of the shock closer to Titan than at Venus. There may have been occasions at Venus when a weak subsolar shock surface may have moved inside the planet (Russell, 1977) and with a greater absorption predicted for Titan, one would expect such a phenomenon to occur more frequently there. Another modification of the shock shape occurs when mass loading of the field lines by cold ions occurs, which results in a displacement of the shock surface away from the object in the flow-normal plane. Figure 8 suggests that under the usual high Mach number solar wind conditions, for which $S/\rho v$ must be > 0.56 in order for a shock to form, even if the solar wind pressure is great enough to push Saturn's bow shock inside Titan's orbit, the Titan shock may still be very weak or even non-existent at times of relatively high density [i.e., $>0.3/cm^3$ for the (N_2,H) model]. Under the typically low Mach number conditions occurring in the magnetosphere, the minimum value of $S/\rho v$ for a shock to form is only 0.18 ($M = 2$), and reference to Figure 9 suggests that under high density conditions (i.e., .6 - $1./cm^3$) the shock may not form even if the value of M would normally suggest that it should. That is, a shock may form at the lower values of $M > 1$ only if the density is low enough. For purposes of comparison, Figure 16 displays both the Titan and Saturn bow shock (neglecting mass loading in the case of the former, including the magnetopause in the case of the latter) that are consistent with a particularly energetic solar wind event [Burlaga et al., 1983].

Possible Comet-Like Titan-Solar Wind Interaction

Some of the characteristics of comets that produce a significantly different type of interaction with the solar wind than that of a typical planet include the considerably larger scale height and therefore slower rate of absorption of the solar wind, and outflow velocities that are high enough to produce an internal shock (partly because the sound speed decreases with distance in response to decreasing temperature). Hence, both an external and

internal shock surface can develop, either or both being fairly weak. As noted previously, high velocity plasma absorption in Titan's atmosphere is likely significantly greater than that predicted for Venus, and the weak gravity-light molecule exosphere configuration will allow for a greater gas outflow at Titan as well. Bertaux and Kockarts (1983) have computed the outflow rate for their (N_2,H_2) model and suggest a value of 5.22×10^{27} molecules/sec at 4100 km, i.e., about an order of magnitude greater than the upper limit estimate for Venus by Brace et al. (1982), but still about 40 times less than that for Comet West at 0.7 AU by Feldman and Brune (1976). The Titan value corresponds to a velocity of about 80 m/sec at 4100 km. In general,

$$v(r) = \frac{K}{4\pi r^2 n_o} e^{\frac{m g r_o}{k T}\left(1 - \frac{r_o}{r}\right)}$$

where K is the outflow rate. For molecular hydrogen at 186°K, using a value for r_o of 4100 km, we find $v(r_o) \simeq 80$ m/sec. The corresponding sound speed is about 1.13 km/sec. Since the outflow velocity should basically decrease as $1/r^2$, the only way supersonic conditions could occur is for the upper atmospheric temperature above 4100 km to rapidly decrease with altitude to an unrealistically low value or 1 or 2°K. In some comet models, it has been proposed that the temperature decreases some two orders of magnitude over 100 km (Mendis and Houpis, 1982). A similar type of temperature decrease with altitude in the upper atmosphere of Titan is required for an internal shock to occur.

We have considered other parameters (the inner and outer radii of the contact zone, the ionization radius, etc.) useful in discussing the solar wind-Titan interaction in cometary terms and also find that these parameters differ considerably from those of typical comets. We conclude that only in terms of solar wind absorption and mass loading (including the formation of a magnetic tail) will some degree of similarity be observed.

Titan's Magnetic Tail and Wake

Titan's intrinsic magnetic moment has been found to be so small that only an induced bi-lobe tail configuration has been observed (Ness et al., 1982).

While beyond Saturn's bow shock, Titan will usually be exposed to a solar wind in which is frozen a spiral magnetic field that is usually confined to the orbital plane of Saturn. On the average, the tight spiral angle of the interplanetary magnetic field plus sufficient conductivity in the ionosphere will result in the type of configuration displayed in Figure 17a that is due to Alfven (1957) (from Verigin et al., 1983) The neutral sheet separating the Titan toward and away tail field lobes is then oriented essentially normal to Saturn's orbital plane. When Titan is within Saturn's magnetosphere, the "external" field will usually be oriented perpendicular to Titan's orbital plane, and the neutral plane of the induced bi-lobe tail will lie in Titan's orbital plane, or somewhat perpendicular to the solar-wind configuration [Figures 17b and c, from Verigin et al., (1983)]. However, because of the weakened dipolar field at 20.2 R_S and relatively strong azimuthal and tail-like or radial sheet currents that are frequently observed in Saturn's magnetosphere (Wilson et al., 1983), considerable angular rotation of Titan's induced tail neutral plane about the corotational direction should occur at times when these currents move past Titan.

Some predictions can be made assuming that some of geometric features, etc., of the interaction at Venus can be scaled to Titan. For example, referring to Gombosi et al. (1980) (their Fig. 1), one might expect a magnetic field versus distance along the subsolar line for Titan that is similar to that displayed in Figure 18. That is, a nominal 0.3 nT interplanetary field, oriented predominately in the azimuthal direction because of tightening of the spiral, models to a field of about 2 nT at the bow shock, and 3 nT at the ionopause. In order to estimate the scaling factor relating the nominal lobe strength in the induced tail field to that in the magnetopause we refer to the measurements of Acuna and Ness (1982).

Ness et al. (1982) found that the inbound lobe was weaker but broader than the outbound lobe, i.e., (w = 3230 km,B = 3.25 nT) and (w = 1440 km,B = 6.7 nT), respectively. These data have been interpreted in terms of tail lobes that are much taller than they are wide (Ness et al., 1982). For example, one notes that the two w-B products agree to within 10%, and for purposes of geometric simplicity it is tempting to assume that the vertical extents of the two tail lobes are the same. Conservation of flux assuming a flux ring of radius R_o and width $\Delta R \simeq H = 0.02\ R_o$ in the flow-normal plane suggests that the vertical extent, h, of the lobes must be about 4800 km if it

is assumed that little flux is "lost" as a result of field lines closing crossing the neutral sheet within 2.6 R_T behind Titan. It is interesting to note that $\sqrt{wh} \simeq R_o$.

On the other hand, it is tempting to assume that the difference in the lobe width may, in large part, have been the result of a change in direction of the flow that occurred as Voyager 1 passed through Titan's magnetic tail. That is, if one assumes a circular tail, conservation of flux, and the field profile of Figure 20, then if R_o is 4000 km and $\Delta R \simeq H$ (= 0.02 R_o) the size of the first lobe suggests a tail field of about 3.1 nT, while the second lobe suggests a lobe field of about 15.4 nT, i.e., good agreement with measurements of the field of the first lobe but poor agreement with that of the second. If one assumes that the flow direction changed during the Voyager 1 encounter of Titan in such a way that the lobe widths were underestimated (i.e., that the radially inward component of the flow decreased during the flyby), then a 50% increase in the width of the second lobe results in the predicted tail field of both agree closely with the data. Allowance for a possible flow direction change that caused both lobe widths to appear smaller than they actually were could result in actual lobe radii more consistent with parallel lobe field lines and a large flow-normal ring thickness, ΔR. Differences in the two lobes could result entirely from the effects of differing mass loading effects caused by the interaction of the magnetized plasma with an assymetrically ionized atmosphere [Neubauer et al. (1984)]. However, while in the magnetosphere most of the ionization of Titan's atmosphere is collisional (roughly 80%) rather than electromagnetic and hence, the difference between the day and night ionospheres may not be very large. Regardless of the details of the interaction, the average tail field observed by Voyager 1 is very nearly the same strength as the field of the magnetized plasma, and therefore, under the solar wind conditions outlined above, the tail field near Titan is likely to be roughly the same as the field frozen into the solar wind, or about 0.3 nT.

Pioneer 11 passed near Titan's orbit some 145 R_T downstream at a time when relatively strong azimuthal and radial or dayside tail-like currents were flowing in the vicinity of Saturn's equatorial plane. These current systems moved somewhat independently, but both seemed to be moving up and down perpendicular to Titan's orbit and were therefore sweeping past Titan and the spacecraft prior to, during, and after Pioneer 11 crossed Titan's orbit.

Consequently, it has been difficult to separate effects that are strictly due to these current sheets from purely Titan effects, and even from possible conductance effects on these currents due to Titan's tail or some of its remanent plume material. Jones et al. (1980) have suggested that the data near the Titan orbit crossing were consistent with passage of Pioneer 11 through a possible Titan wake. This interpretation was based upon a comparison of some of the features of the Titan interval with several candidate flucutations in the field that occurred prior to and after the event in question. It was pointed out that preliminary estimates of the composition of the magnetoplasma at the time were consistent with the possible detection of a weak shock based upon changes in field directions, whereas the suggested possibiliy of passage through the wake was based on the somewhat unique character of the field variability of the interval in question. It should also be mentioned that at the time of the Pioneer 11 measurements very little photoionization was occurring in the same hemisphere as that in which most of the collisional ionization was occurring. However, the geometry was such that more photoionization and subsequent mass loading, etc. effects should have been observed before Pioneer 11 passed Titan's orbit, which is consistent with the data (Jones, 1980).

Comparison of the magnetic field observed during the Pioneer 11 Titan interval with predicted field changes due to azimuthal and tail-like currents that successfully model the remaining portion of the outbound perturbation field ($B_{total} - B_{planetary}$) also suggest that the Titan interval is unique, particularly in terms of the ϕ component of the field. Figures 19a and b (from Wilson et al., 1983) compare r and ϕ components predicted by a computer derived model current system with that of the data. The manner in which the field varies during the Titan interval is seen to be particularly anomalous when compared to the preceding interval (the following interval displays effects that may be the result of approaching the magnetopause boundary layer). Since Pioneer 11 passed above Titan's orbital plane, and the "input field" is primarily due to the planetary dipole field, (i.e., a vertical field), Pioneer 11 should observe primarily a lobe field that shows up as an azimuthal, or ϕ perturbation.

Eviatar et al., (1982) have suggested that the Voyager data are consistent with the existence of plumes containing signifant amounts of heavy ions gas from Titan that have sufficiently long lifetimes to allow for them to

wrap around the planet and thereby participate in the magnetospheric plasma-Titan interaction. However, an alternate interpretation of these data has been proposed by Goertz (1983). If such long-lived plumes do exist, then Titan could interact with this heavy ion materal and when account is taken of various possibilities in terms of composition, number density and temperature, it is clear that at times it is possible that the Titan-mangetospheric plasma interaction can be described in terms of Mach numbers greater than 1. Also, at times when the field is weakest (at the center of the several current sheets mentioned above) and Titan is immersed in one of its high density plumes, the flow could also be described as superalfvenic. Under such conditions, the observation of wake phenomena at large distances downstream from Titan would appear to be a distinct possibility. Such may have occurred coincident with the passage of Pioneer 11 near Titan's orbit.

Acknowledgements

We wish to acknowledge helpful discussions with J.A. Slavin, B.T. Tsurutani, and G.L. Siscoe. This research was supported, in part, by the NASA-Ames under research grant NAG 2-145.

References

Acuna, M.H., and N.F. Ness, The magnetic field of Saturn: Pioneer II observations, Science, 207, 444, 1980.

Alfven, H. On the theory of comet tails, Tellus, 9, 92, 1957.

Banks, P.M. and Kockarts, G. Aeronomy Part A, Academic Press, pp. 184-239, New York 1973.

Bertaux, J.L. and G. Kockarts, Distribution of molecular hydrogen in the atmosphere of Titan, J. Geophys. Res., 88, 8716-8720, 1983.

Brace, L.H., R.F. Theis and W.R. Hogey, Plasma clouds above the ionopause of Venus and their implications, Planet. Space Sci., 30, 29-37, 1982.

Broadfoot, A.L., et al., Extreme ultraviolet observations from Voyager 1 encounter with Saturn, Science, 212, 206, 1981.

Burlaga, L.F., R. Schwenn and H. Rosenbauer, Dynamical evolution of interplanetary magnetic fields and flows between 0.3 AU and 8.5 AU: Entrainment, Geophys. Res. Lett., 10, 413-416, 1983.

Cloutier, P.A., M.R. McElroy and F.C. Michel, Modification of the Martian ionosphere by the solar wind, J. Geophs. Res., 74, 6215-6228, 1969.

Cloutier, P.A., R.E. Daniell, Jr., A.J. Dessler, and T.W. Hill, A cometary model for Io, Astrophys. and Space Sci., 55, 93-112, 1978.

Eviatar, A., G.L. Siscoe, J.D. Scudder, E.C. Sittler, Jr., J.D. Sullivan, The plumes of Titan, J. Geophys. Res., 87, 8091-8103, 1982.

Feldman, P.D. and W.H. Brune, Carbon production in Comet West 1975n., Astrophys. J. 209, L45-L48, 1976.

Goertz, C.K. Detached plasma in Saturn's front side magnetosphere, Geophys. Res. Lett. 10, 455-458, 1983.

Gombosi, T.I., T.E. Cravens, A.F. Nagy, R.C. Elphic and C.T. Russell, Solar wind absorption by Venus, J. Geophys. Res., 85, 7747-7753, 1980.

Gombosi, T.I., M. Horanyi, T.E. Cravens, A.F. Nagy, and C.T. Russell, The role of charge exchange in the solar wind absoprtion by Venus, Geophys. Res. Lett., 8, 1265-1268, 1981.

Hartle, R.E., E.C. Sittler, Jr., K.W. Ogilvie, J.D. Scudder, A.J. Lazarus, and S.K. Atreya, Titans ion exosphere observed from Voyager, J. Geophys. Res, 87, 1383, 1982.

Jones, D.E., B.T. Tsurutani, E.J. Smith, R.J. Walker, and C.P. Sonett, A possible magnetic wake of Titan: Pioneer II Observations, J. Geophys. Res., 85, 5835-5840, 1980.

Kuiper, G.P. Titan: A satellite with an atmosphere, Astrophys. J., 100, 378, 1944.

Kivelson, M.G., and C.T. Russell, The interaction of flowing plasmas with planetary ionospheres: A Titan-Venus comparison, J. Geophys. Res., 88, 49-57, 1983.

Lindal, G.F., G.E. Wood, H.B. Hotz, D.N. Sweetnam, V.R. Eshleman, and G.L. Tyler, The atmosphere of Titan: An analysis of the Voyager 1 radio occultation measurements, Icarus, 53, 348-363, 1983.

MacLennan, C.G., L.J. Lanzerotti, S.M. Krimigis, R.P. Lepping, and N.F. Ness, Effects of Titan on trapped particles in Saturn's magnetosphere, J. Geophys. Res., 87, 4111, 1982.

Mendis, D.A., and H.L.F. Houpis, The cometary atmosphere and its interaction with the solar wind, Rev. Geophys. Space Sci., 20, 885-928, 1982.

Michel, F.C. Solar wind interaction with planetary atmospheres, Rev. Geophys. Space Phys., 16, 427-435, 1971a.

Michel, F.C. Solar-wind-induced mass loss from magnetic field-free planets, Planet Space Sci., 24, 1580-1583, 197b.

Ness, N.F., M.H. Acuna, R.P. Lepping, J.E.P. Connerney, K.W. Behannon, L.F. Burlagh, and F.M. Neubauer, Preliminary results at Saturn from the magnetic field experiment on Voyager 1, Science, 205, 211, 1981.

Ness, N.F., M.H. Acuna, K.W. Behannon, and F.M. Neubauer, The induced magnetosphere of Titan, J. Geophys. Res., 87, 1369, 1982.

Neubauer, F.M. Possible strengths of dynamo magnetic fields of the Galilean satellites and of Titan, Geophys. Res. Lett., 5, 905, 1978.

Neubauer, F.M., D.A. Gurnett, J.D. Sudder, R.E. Hartle, Titan's magnetosphere interaction in Saturn, edited by T. Gehrels, p._____, University of Arizona press,Tucson, 1984.

Rose, D.J. and M. Clark, Jr., Plasmas and Controlled Fuscon, The M.I.T. Press, Cambridge, Mass. and John Wiley and Sons, Inc., pp. 29-53, New York, 1961.

Russell, C.T., The Venus bow shock: Detached or attached?, J. Geophys. Res., 82, 625-631, 1977.

Russell, C.T., T.I. Gombosi, M. Horyani, T.E. Cravens and A.F. Nagy, Charge-Exchange in the magnetosheaths of Venus and Mars: A comparison, Geophys. Res. Lett., 10, 163-164, 1983.

Slavin, J.A., J.R. Spreiter and E.J. Smith, A comparative study of the solar wind interaction with Jupiter and Saturn, (1984 submitted).

Spreiter, J.R. and S.S. Stahara, Solar wind flow past Venus: Theory and comparisons, J. Geophys. Res., 85, 7715, 1980.

Strobel, D.F. and D.E. Shemansky, EUV emission from Titan's upper atmosphere: Voyager 1 encounter, J. Geophys. Res., 87, 1361, 1982.

Verigin, M.I., K.I. Gringauz, and N.F. Ness, Comparison of induced magnetospheres at Venus and Titan, (1983 in preparation).

Vogt, R.E., D.L. Chenett, A.C. Cummings, T.L. Garrard, E.C. Stone, A.W. Schardt, J.H. Trainor, N. Lai, and F.B. McDonald, Energetic charged particles in Saturn's magnetosphere: Voyager 1 results, Science, 212, 231, 1981.

Wilson, G.R., D.E. Jones and B.T. Thomas, Modelling Saturn's magnetosphere and planetary magnetic field: Pioneer 11, (paper presented at the Fall AGU meeting, San Franciscio, Calif., December, 1983).

Wolf, D.F. and F.M. Neubauer, Titan's highly variable plasma environment, J. Geophys. Res., 87, 881-886, 1982.

Wolff, R.S., B.E. Goldstein, and S. Kumar, A model of the variability of the Venus ionopause altitude, Geophys. Res. Lett., 6, 353-356, 1979.

Figure Captions

Figure 1: Histogram of the frequency of occurrance of a specific value of the Saturn magnetopause distance, R_N, based upon 1275 observations of the solar wind extrapolated to the vicinity of Saturn (after Slavin et al., 1983).

Figure 2: Solar wind flow patterns in the vicinity of non-magnetic planets having atmospheres in terms of a) direct interaction; b) tangential discontinuity; and c) magnetic barrier (after Michel, 1971a).

Figure 3: a) Model atmospheric distributions of N_2 and H for Titan (after Hartle et al., 1982); b) Model atmospheric distributions of N_2 and H_2 for Titan (after Bertaux and Kockarts, 1983).

Figure 4: Absorption of solar wind plasma in the atmosphere of Titan due to charge exchange along a circular flow line as a function of flow line radius due to the (N_2,H) model used by Hartle et al. (1982). The inset figure shows the results for Venus obtained by Gombosi et al. (1981).

Figure 5: Total absorption of solar wind plasma in the atmosphere of Titan due to charge exchange absorption by the (N_2,H) model used by Hartle et al. (1982). The inset figure shows the results for Venus obtained by Gombosi et al. (1980).

Figure 6: Same as for Figure 4 except that the absorption is of magnetospheric plasma.

Figure 7: Same as for Figure 5 except that the absorption is of magnetospheric plasma.

Figure 8: a) Contours of ionopause distance versus incident proton density at constant solar wind velocity using the (N_2,H) atmosphere of Hartle et al. (1982). Also shown are the corresponding values of the mass loading ratio corresponding to a large Mach number flow. Regions where Titan is located in the free streaming solar wind (left diagonal) and where a shock must form (right diagonal) are also shown. An ionospheric temperature of 8600°K has

been assumed. Figure 8b is the same as 8a, except the (N_2,H_2) atmosphere of Bertaux and Kockarts (1983) is used.

Figure 9: Similar to Figures 8a and 8b, except magnetosphere plasma conditions and the region of shock region is not formed, although the 100% absorption radius has.

Figure 10: Ionopause electron density versus magnetospheric plasma proton density at constant flow velocity for high (8600°K) and low (186°K) ionospheres. Also shown are the corresponding ionopause radii. Voyager 1 observations near Titan would tend to favor the low temperature - high electron density model.

Figure 11: Magnitude of magnetic field observed near Titan closest approach. Upper panels display the trajectory in Titan-centered coordinates with the Y axis directed radially outward from Saturn, Z parallel to Saturn's rotation axis, and X "upstream" from the corotating magnetosphere. L_1 and L_2 refer to the northern and southern magnetic tail lobes. A may be a feature related to the dayside hydrogen corona, B and D to the inbound and outbound crossings of the tail boundaries, and C to the current sheet separating the northern and southern tail lobes.

Figure 12: Idealized plasma flow around Titan. L_1 and L_2 refer to the northern and southern magnetic tail lobes. The shaded bars refer to minima corresponding to magnetopause and neutral sheet crossings. The trajectory of a proton is approximately to scale in the observed magnetic field (after Hartle et al., 1982).

Figure 13: Scaled ionopause and bow wave contours for Titan corresponding to several values of the H/R_o parameter (based upon Spreiter et al., 1980).

FIgure 14: (Top) Projection of Voyager 1 trajectory near Titan into a plane oriented transverse to the flow (27° inward from corotational). Titan is represented by a circle, and distances are labeled in kilometers. Positions along the trajectory are assigned numbers from -55 to 39. (Bottom) Mappings of points along the Voyager 1 trajectory into the same plane as in the upper

figure along the measured magnetic field directions. Numbers given to mapped points correspond to their source location along the trajectory [from Kivelson and Russell (1983), their Figure 7]. Also shown are the exobase, ionopause radius assuming only charge exchange for an (H_2,H) atmosphere, and the corresponding ionopause circle in this flow-normal plane as inferred from Figure 13.

Figure 15: a) Counting rate versus time curves for flux of > 0.43 MeV protons measured by Voyager 1 along its trajectory as displayed in the upper curve (after Vogt et al., 1981), and b) velocity versus time contours for several ion energy ranges and the corresponding position of Voyager 1 relative to Titan (after MacLennan et al., 1982).

FIgure 16: A figure comparing the Titan and Saturn bow shocks under solar wind conditions that are sufficient to push the latter within Titan's orbit. The Titan bow shock corresponds to high Mach number conditions, and the Saturn boudaries are consistent with the bow shock and magnetopause studies of Slavin et al. (1983)

Figure 17: Sketches of magnetic lines of force and current systems associated with solar wind interaction with (a) comets (Alfven, 1957), (b) Venus (Yeroshenko, 1979) and (c) Venus (Gringauz, 1981) [after Verigin et al., 1983)].

Figure 18: Scaled magnetic field profile in the shock-ionopause, etc., region along the noon meridian for Titan as scaled from the corresponding figure for Venus by Gombosi et al., 1980.

Figure 19: a) Modelled (dashed) and measured (solid) radial and b) azimuthal perturbation field variations due to a dayside tail-like sheet current that moved up and down past Pioneer 11 as it traversed the outbound magnetosphere of Saturn near Titan. The apparently anomalous interval is contained in the several R_S region spanning 20 R_S and appears mostly in the azimuthal component.

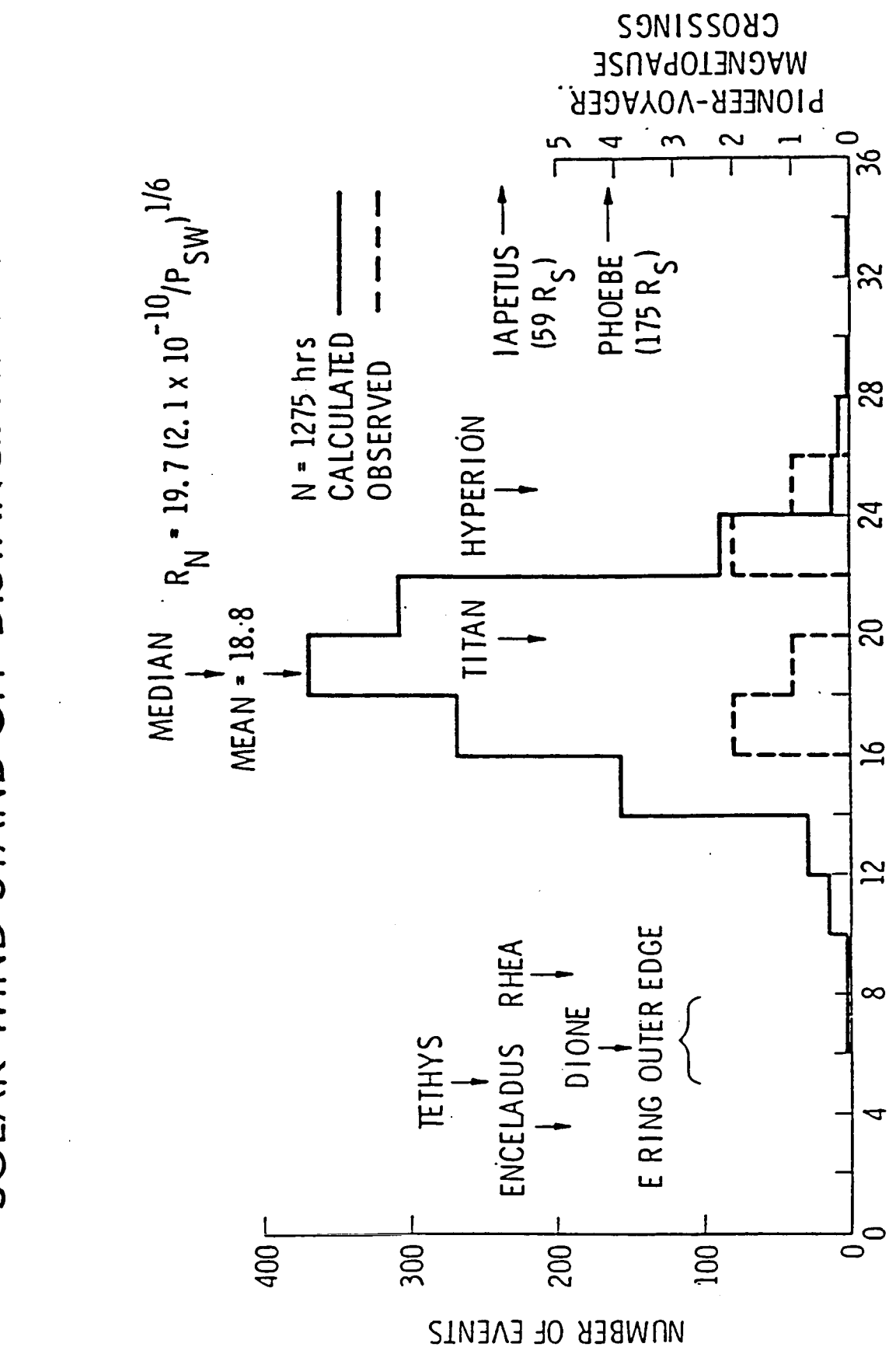

Figure 1. SLAVIN, ET AL. "A COMPARATIVE STUDY OF THE SOLAR WIND INTERACTION

SOLAR WIND INTERACTION WITH PLANETARY ATMOSPHERES

MICHEL, REV. GEOPHYS. SPACE PHYSICS, 9, 427, 1971

(A) DIRECT INTERACTION: INFLOW RESTRICTED BY PHOTOION PRODUCTION, SOLAR WIND HAS SHALLOW COMPONENT THAT SWEEPS INTO THE IONOSPHERE.

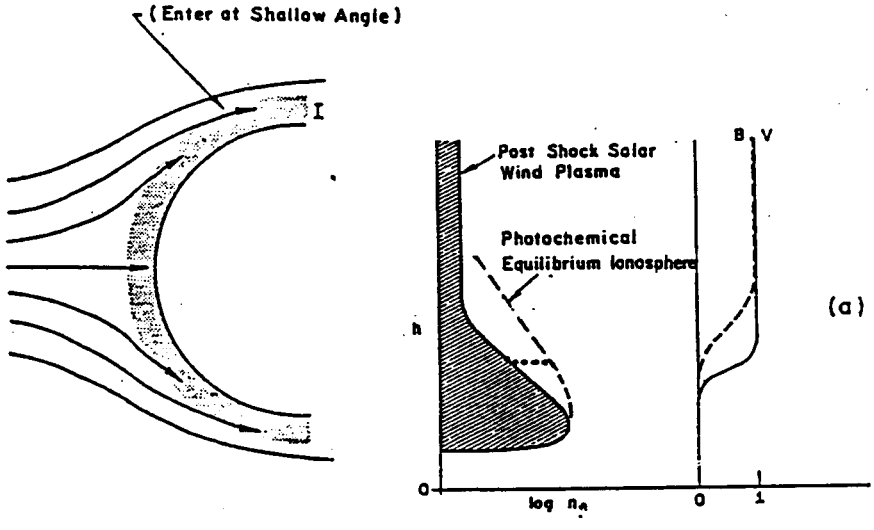

(a)

(B) TANGENTIAL DISCONTINUITY: IONOSPHERIC PLASMA EXCLUDES SOLAR WIND PLASMA, AN IMPENETRABLE INTERFACE (IONOSPHERE NKT PRESSURE EQUALS SOLAR WIND PRESSURE)

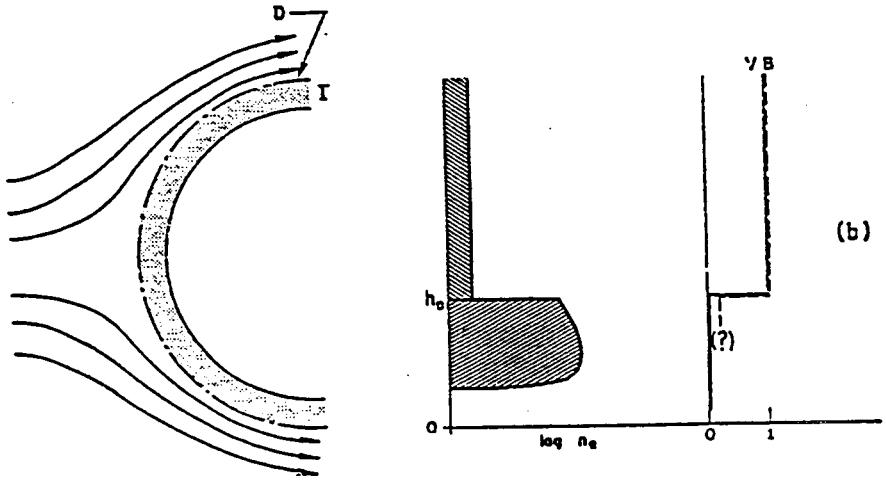

(b)

(C) MAGNETIC BARRIER: MAGNETIC FIELD LINES ACCUMULATE ABOVE HIGHLY CONDUCTING IONOSPHERE, NO DIRECT ACTION BETWEEN SOLAR WIND AND ATMOSPHERE

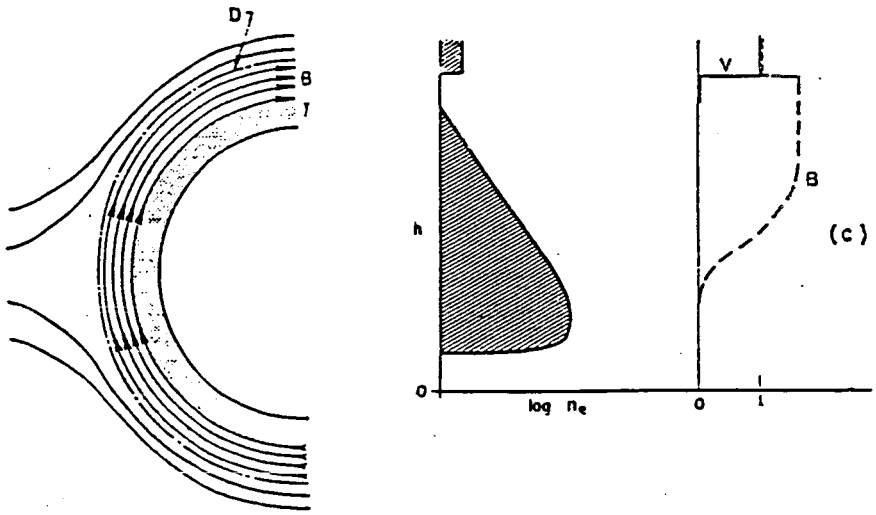

(c)

Figure 2.

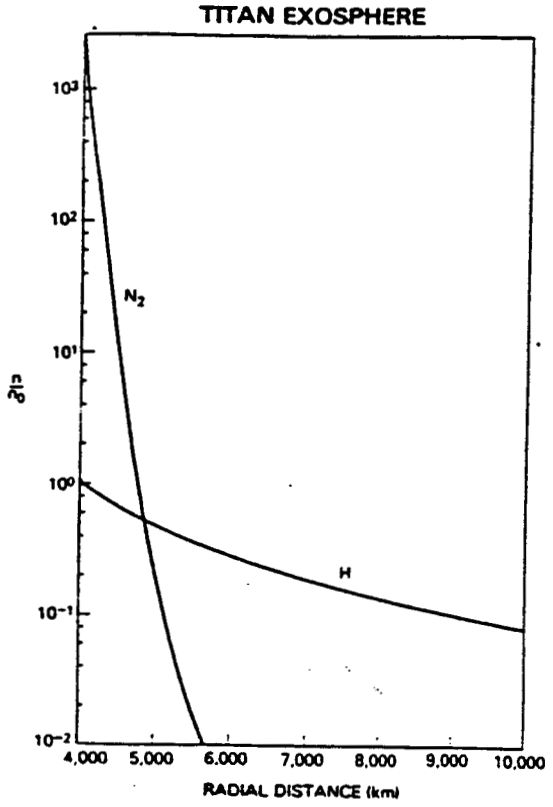

Figure 3a

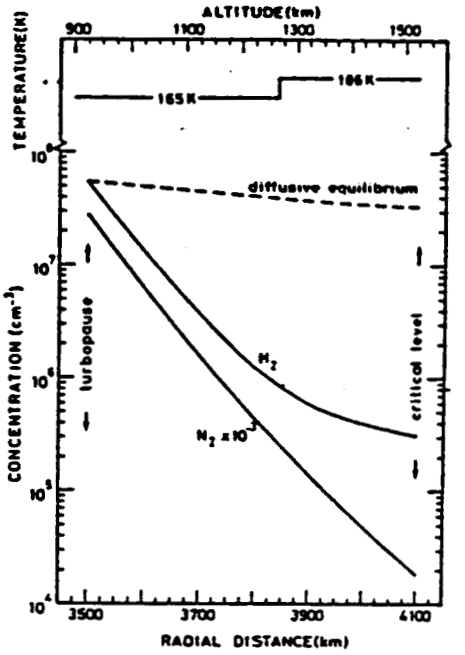

Figure 3b

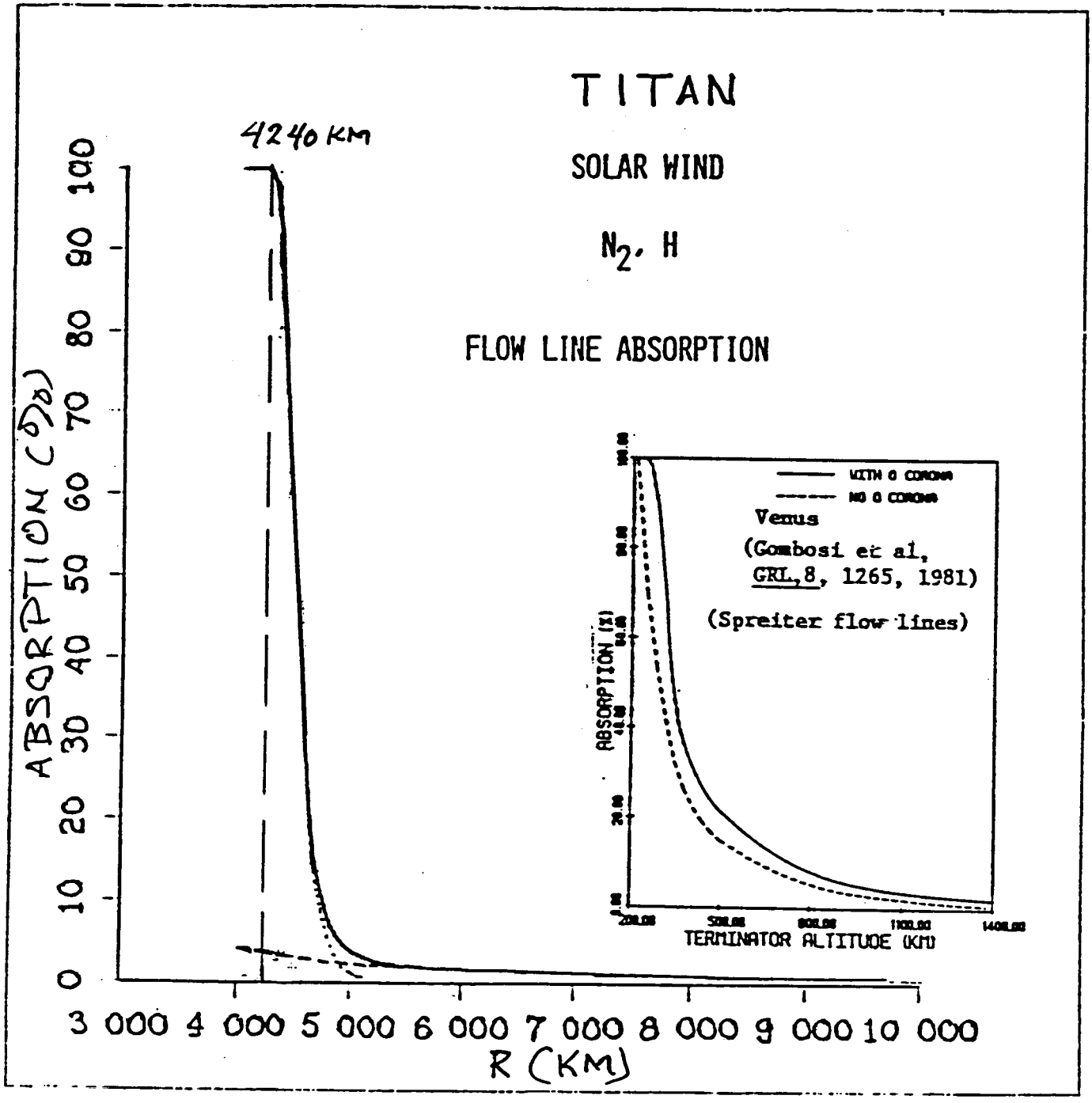
TITAN
SOLAR WIND
N_2, H
FLOW LINE ABSORPTION
4240 KM
ABSORPTION (Rb)
0 10 20 30 40 50 60 70 80 90 100
3 000 4 000 5 000 6 000 7 000 8 000 9 000 10 000
R (KM)
WITH O CORONA
NO O CORONA
Venus
(Gombosi et al,
GRL, 8, 1265, 1981)
(Spreiter flow lines)
ABSORPTION (R)
TERMINATOR ALTITUDE (KM)

Figure 4

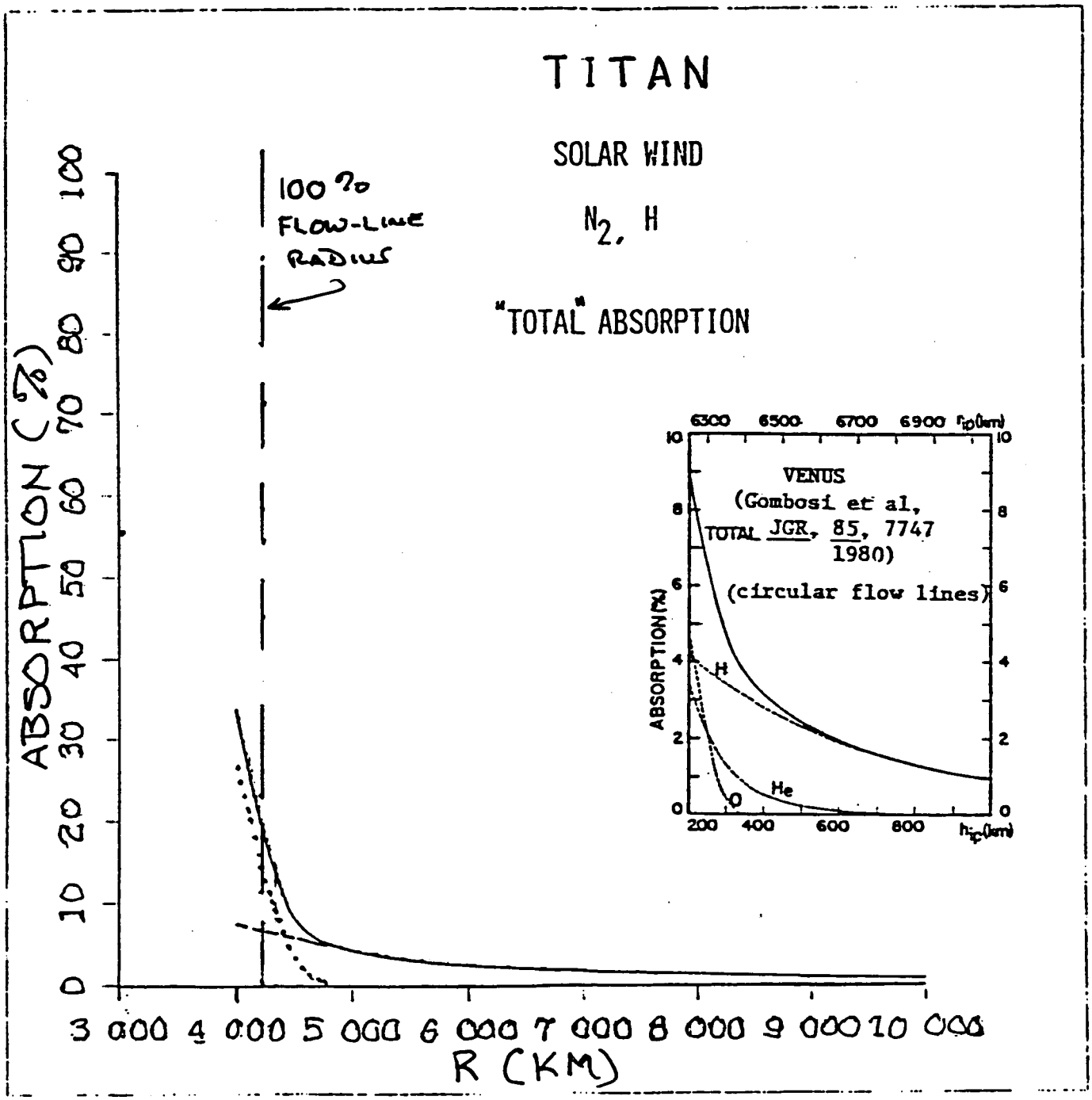
TITAN
SOLAR WIND
N_2, H
"TOTAL" ABSORPTION
100 % FLOW-LINE RADIUS
ABSORPTION (%)
0 10 20 30 40 50 60 70 80 90 100
3 000 4 000 5 000 6 000 7 000 8 000 9 000 10 000
R (KM)
VENUS
(Gombosi et al, JGR, 85, 7747 1980)
TOTAL
(circular flow lines)
H
He
O
ABSORPTION (%)
6300 6500 6700 6900 r_{ip}(km)
200 400 600 800 h_{ip}(km)

Figure 5

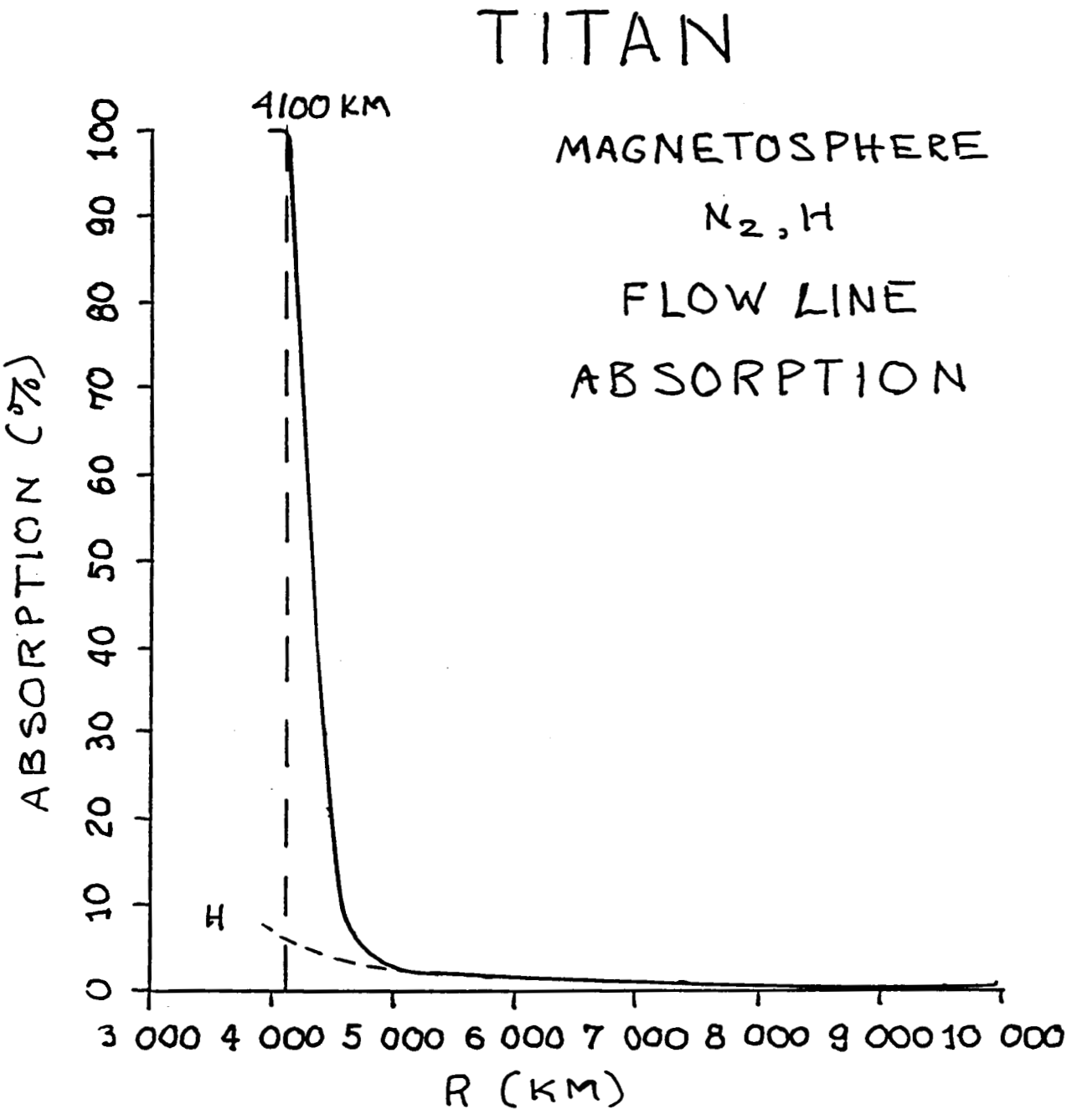
TITAN
4100 KM
MAGNETOSPHERE
N_2, H
FLOW LINE
ABSORPTION
ABSORPTION (%)
0
10
20
30
40
50
60
70
80
90
100
H
3 000
4 000
5 000
6 000
7 000
8 000
9 000
10 000
R (KM)

Figure 6

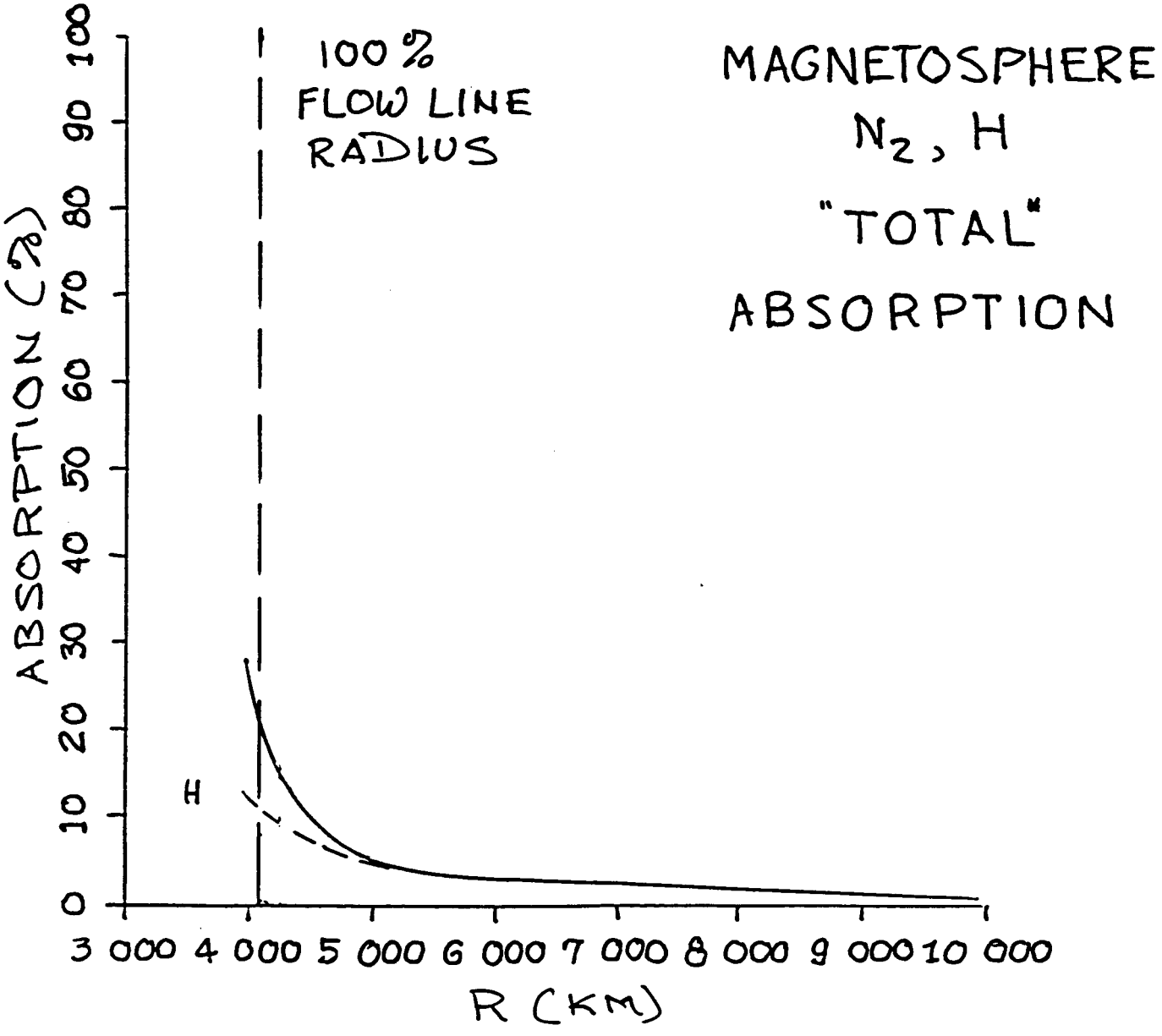
TITAN
100 %
FLOW LINE
RADIUS
MAGNETOSPHERE
N_2, H
"TOTAL"
ABSORPTION
ABSORPTION (%)
0
10
20
30
40
50
60
70
80
90
100
H
3 000
4 000
5 000
6 000
7 000
8 000
9 000
10 000
R (KM)

Figure 7

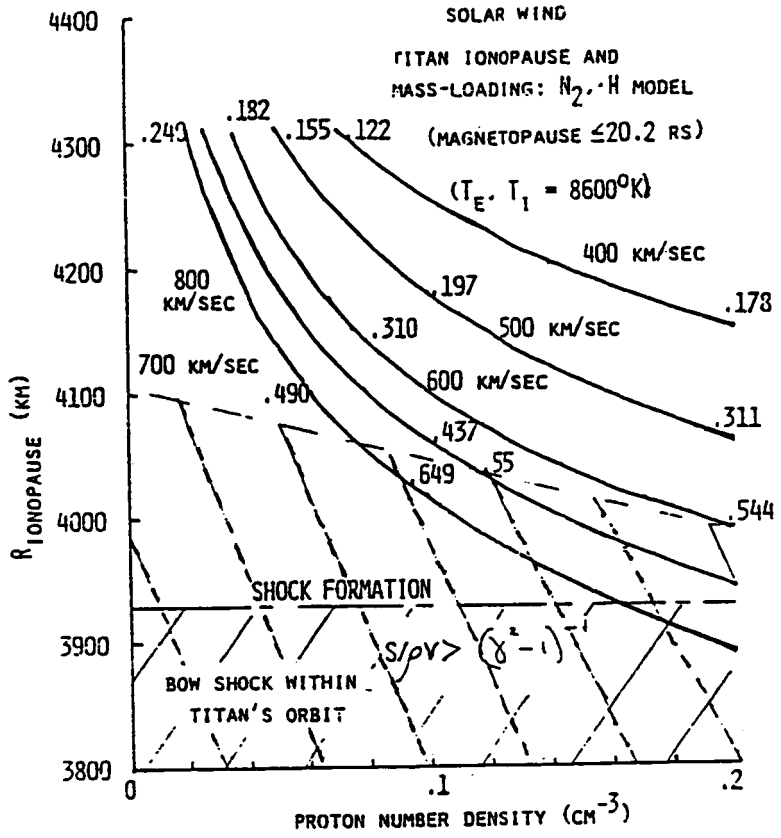

Figure 8a.

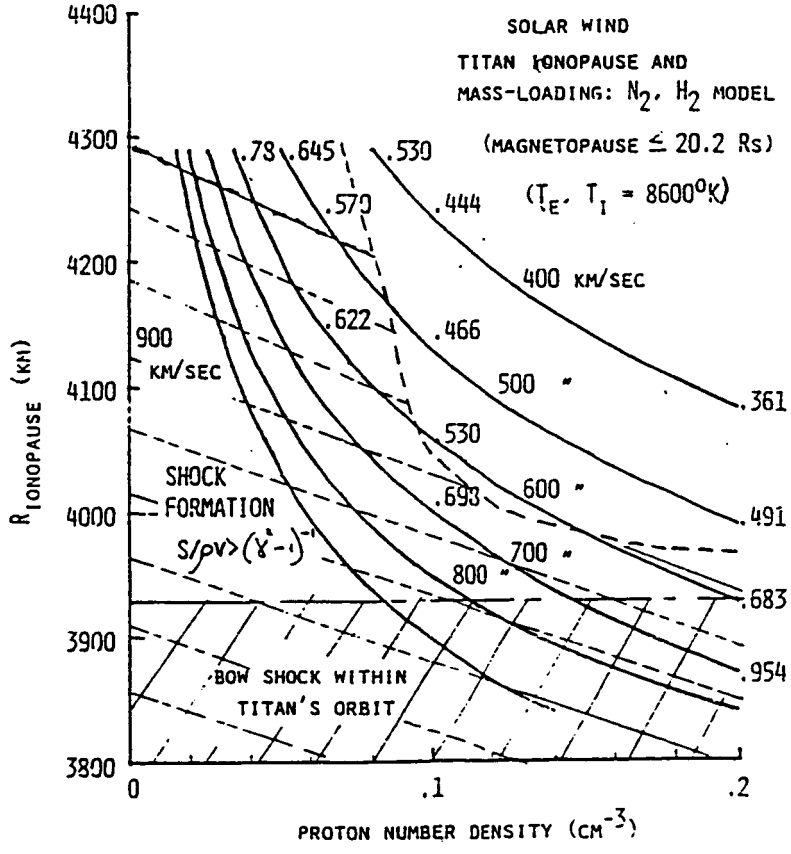

Figure 8b

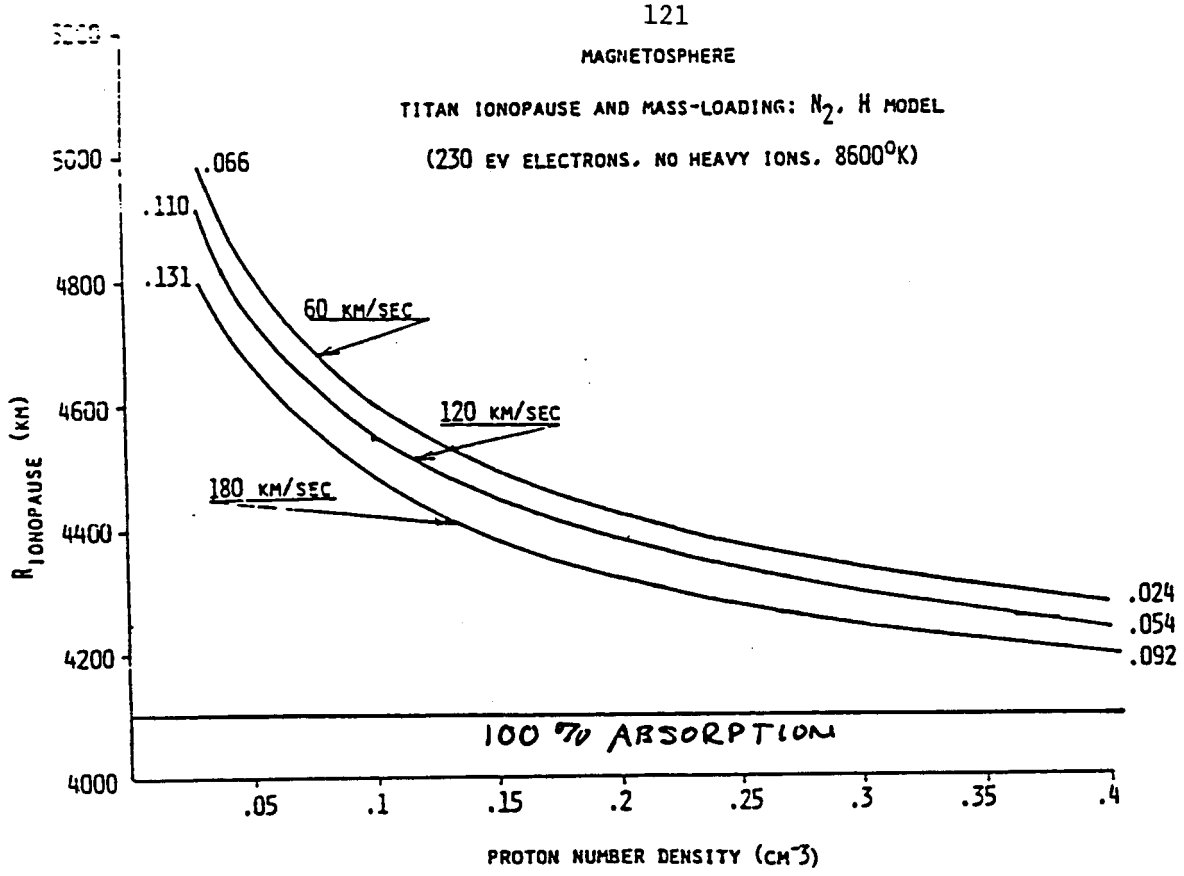

Figure 9b

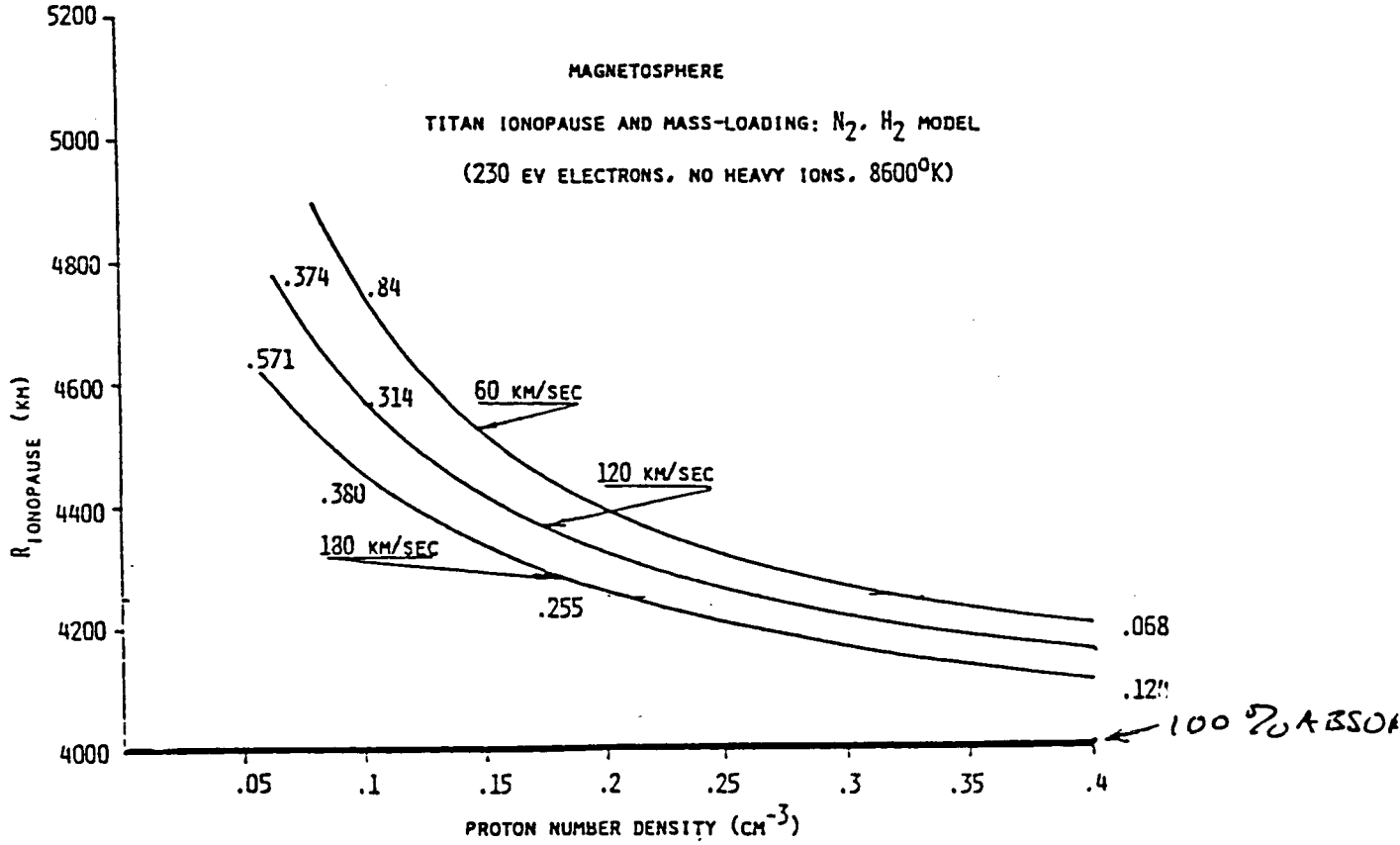

Figure 9b

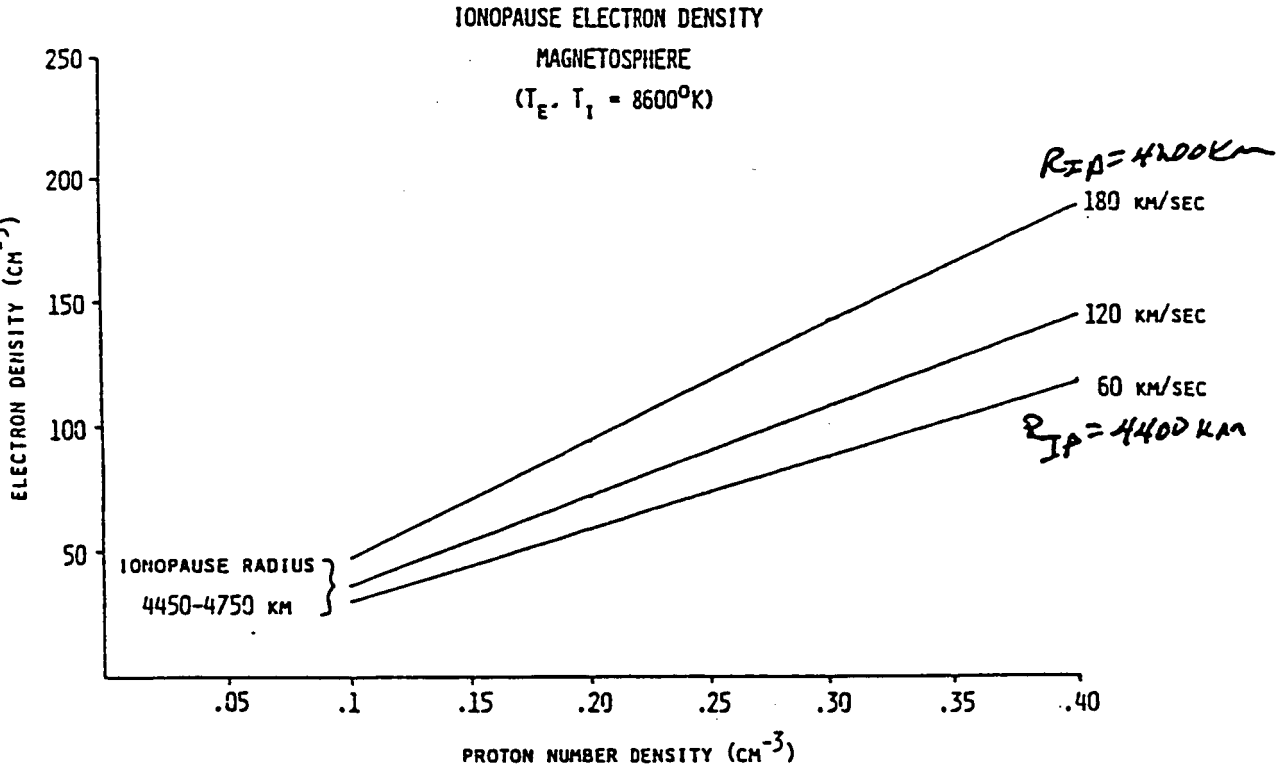

Figure 10a

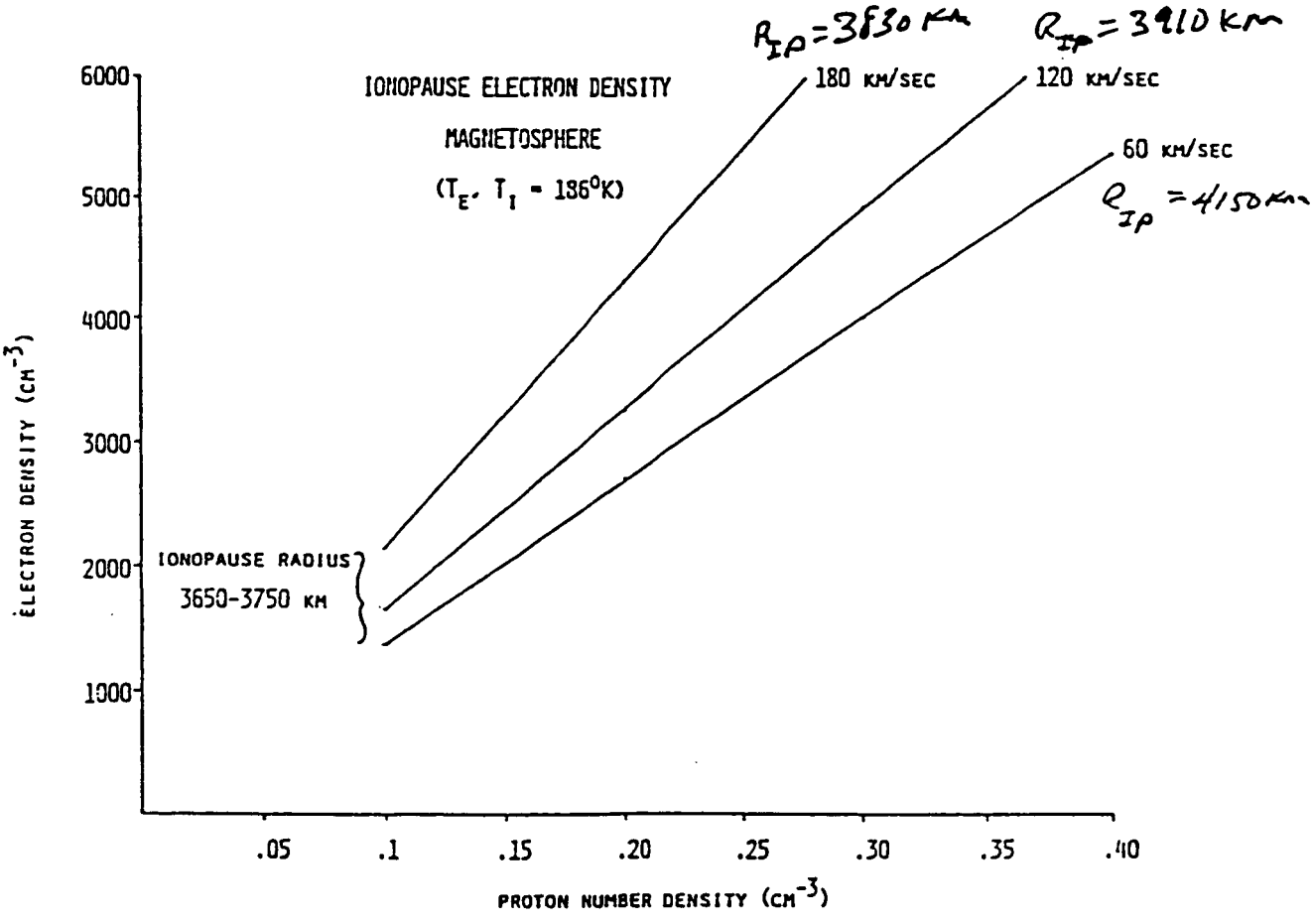

Figure 10b

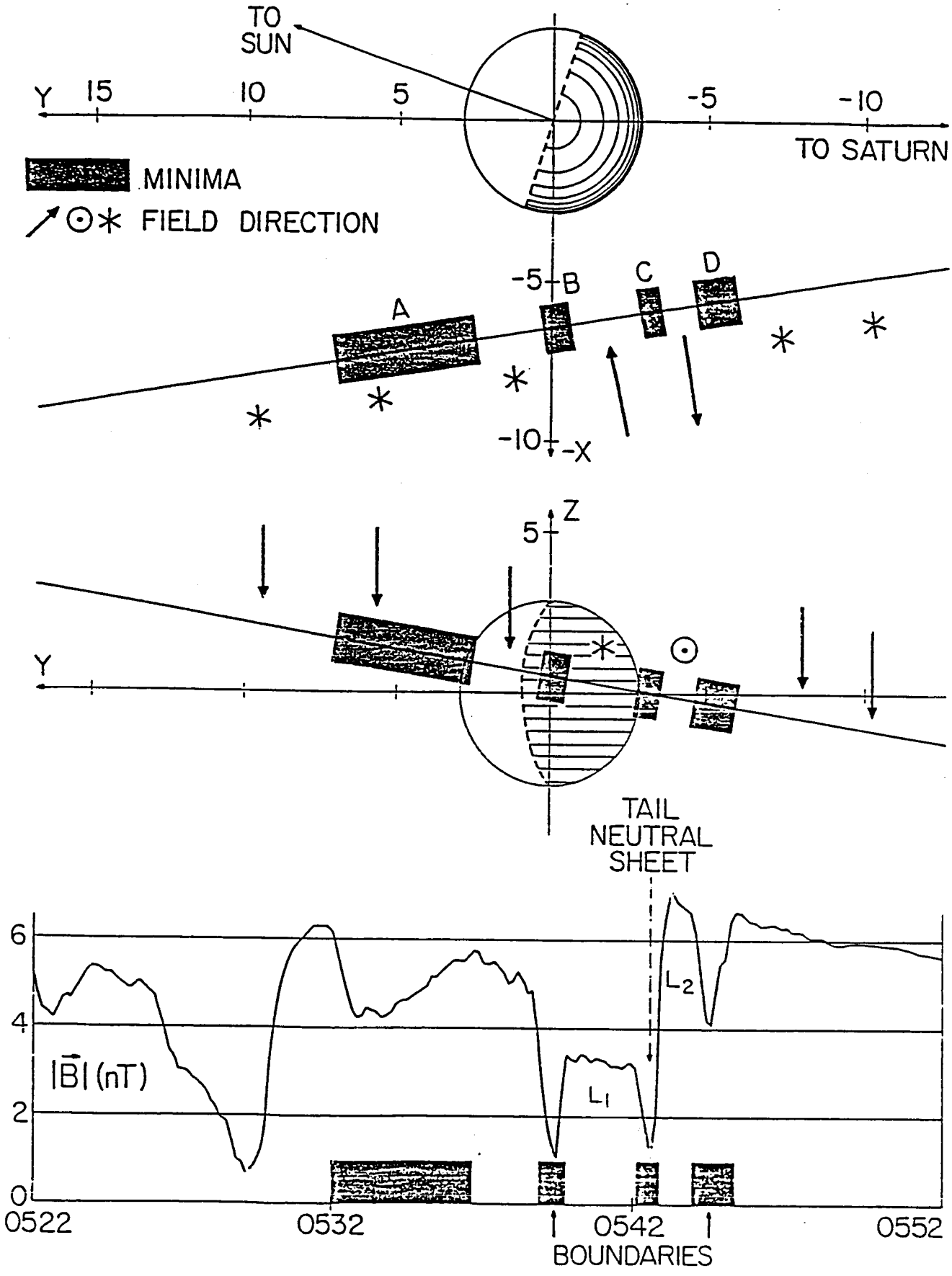

Figure 11

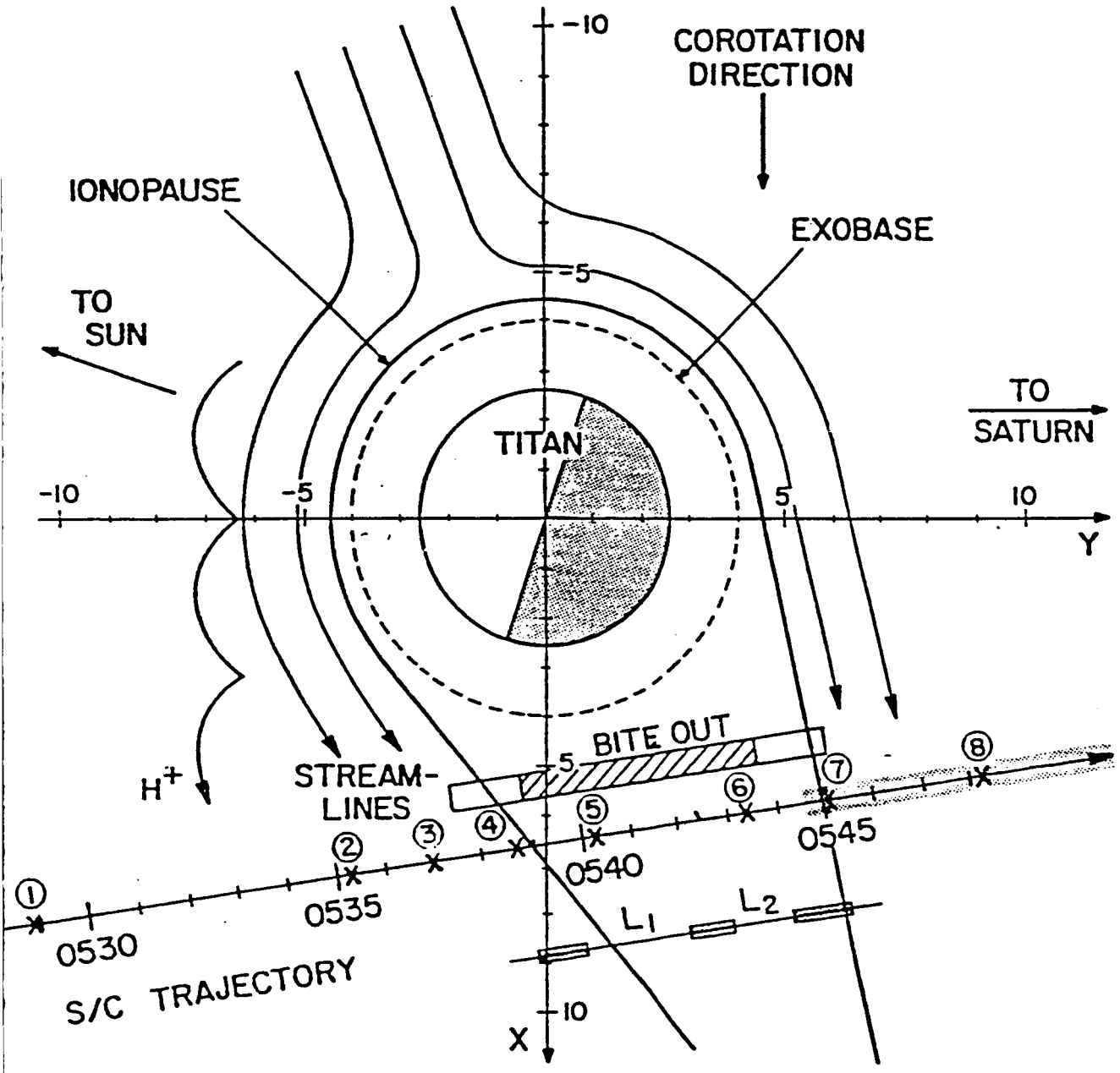

TITAN INTERACTION
NOV 12, 1980

Fig.12.

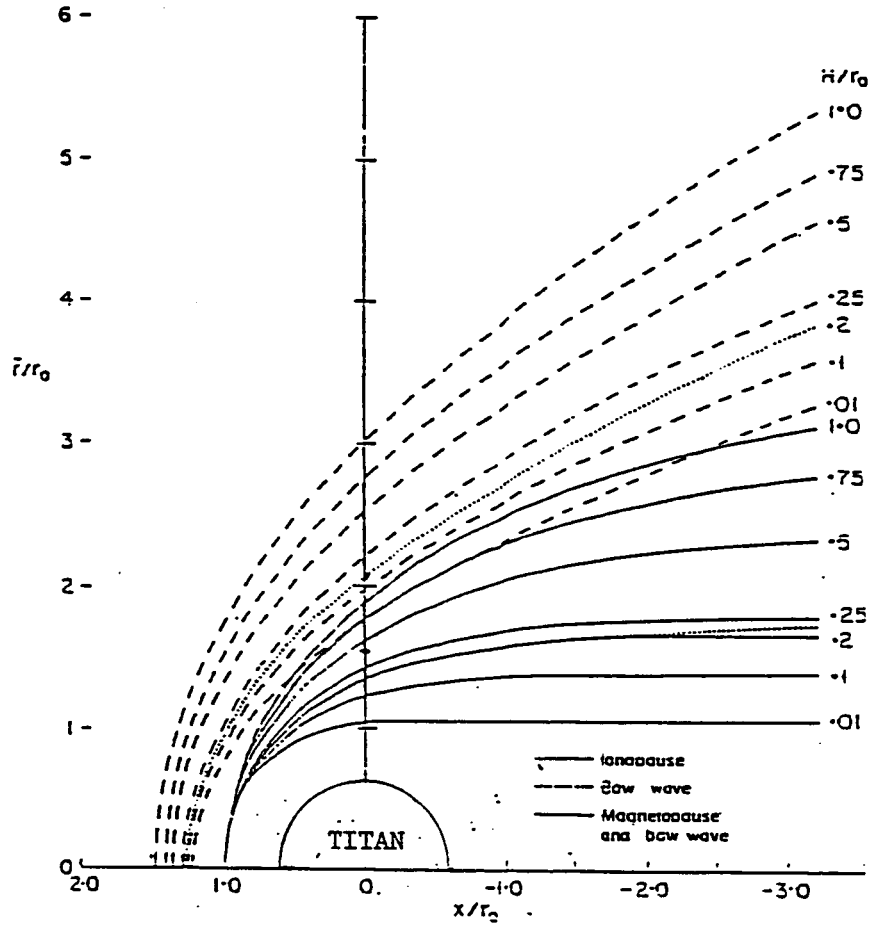

FIG. 4. CALCULATED LOCATION OF IONOPAUSE FOR VARIOUS H/r_0, AND ASSOCIATED LOCATION OF BOW WAVE FOR $M_\infty = 8, \gamma = \frac{4}{3}$.

Figure 13.

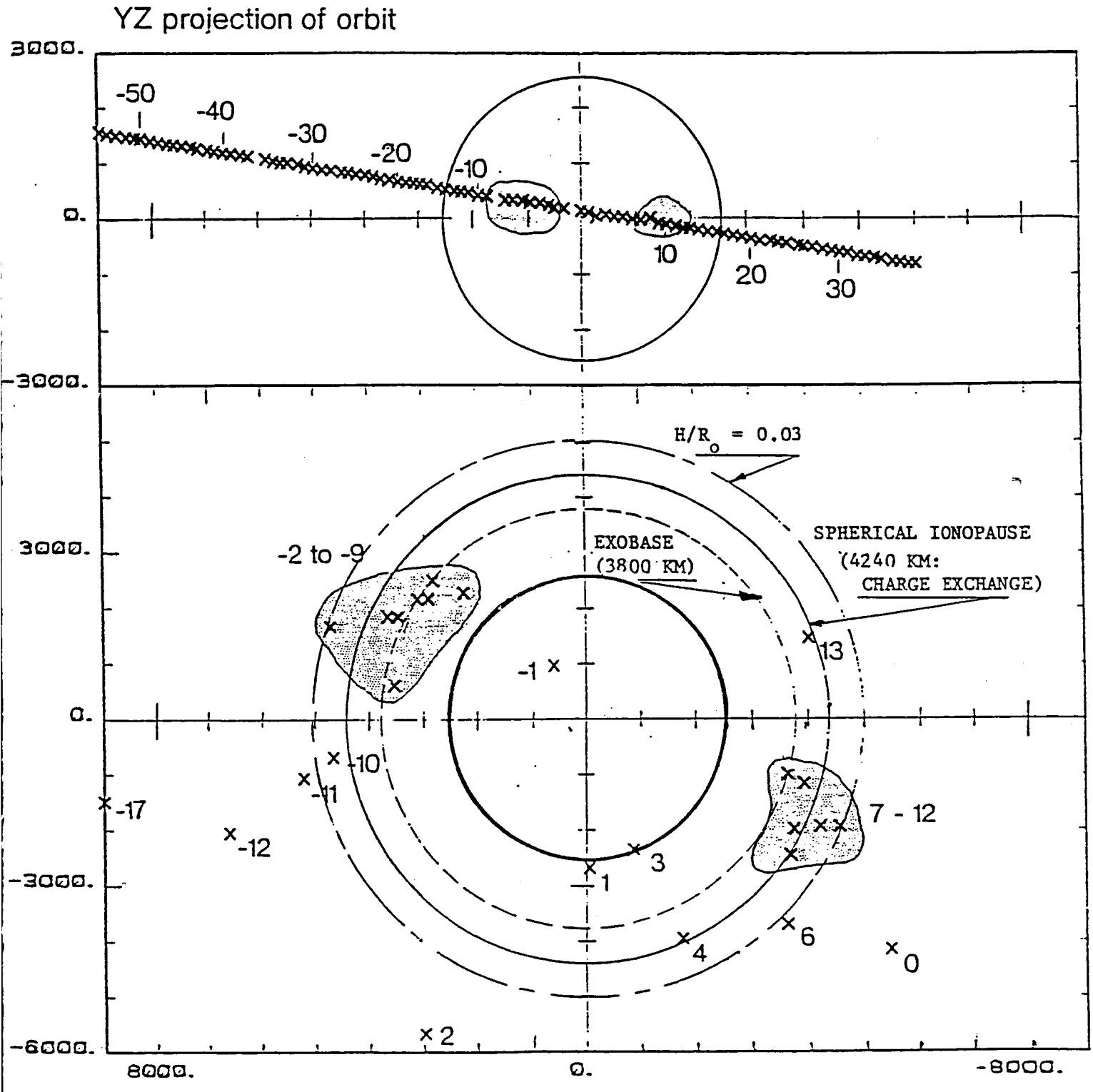

Figure 14 Y (km) relative to aberrated wake intercepts of B and X=0 plane

TITAN FLYBY: 27° ABERRATED COORDINATES

(KIVELSON AND RUSSELL, JGR 88, 49, 1983

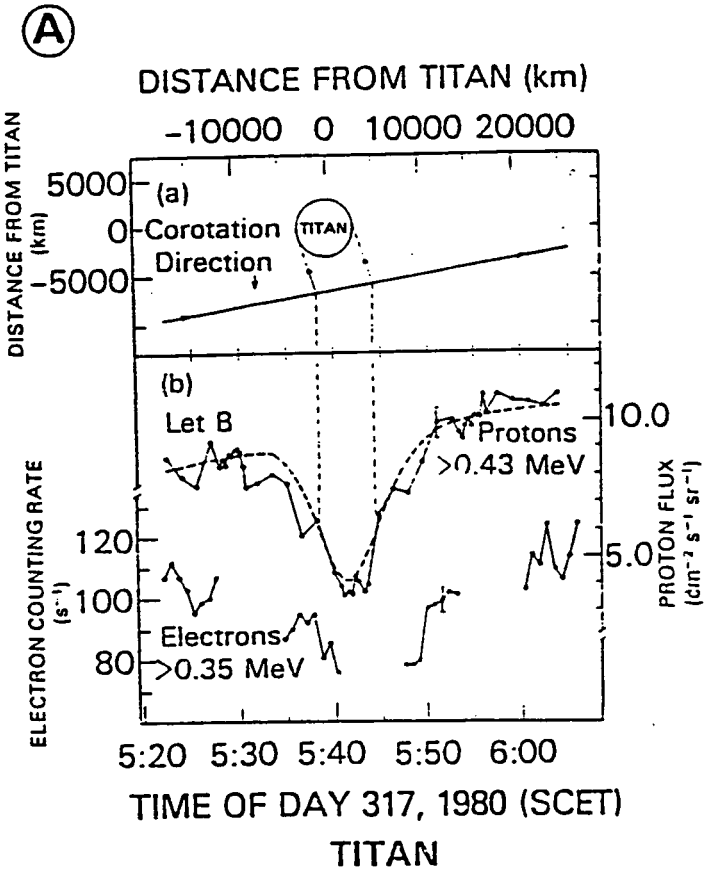

Figure 15a

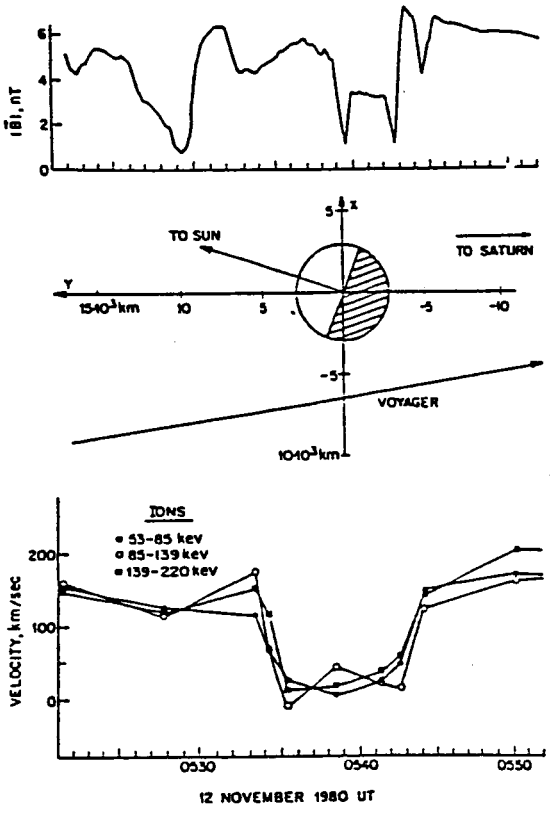

Figure 15b

TITAN'S BOW SHOCK

IN PERSPECTIVE

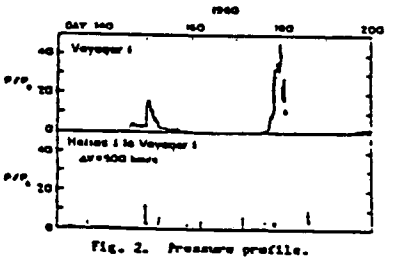

Fig. 2. Pressure profile.

(AFTER BURLAGA ET AL. 1983)

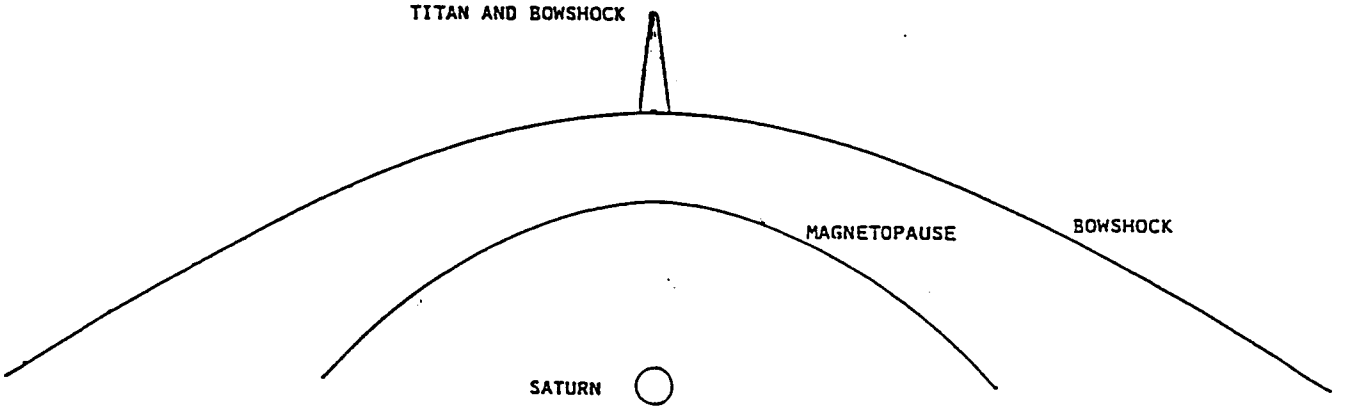

(AFTER SLAVIN ET AL. 1983)

Figure 16

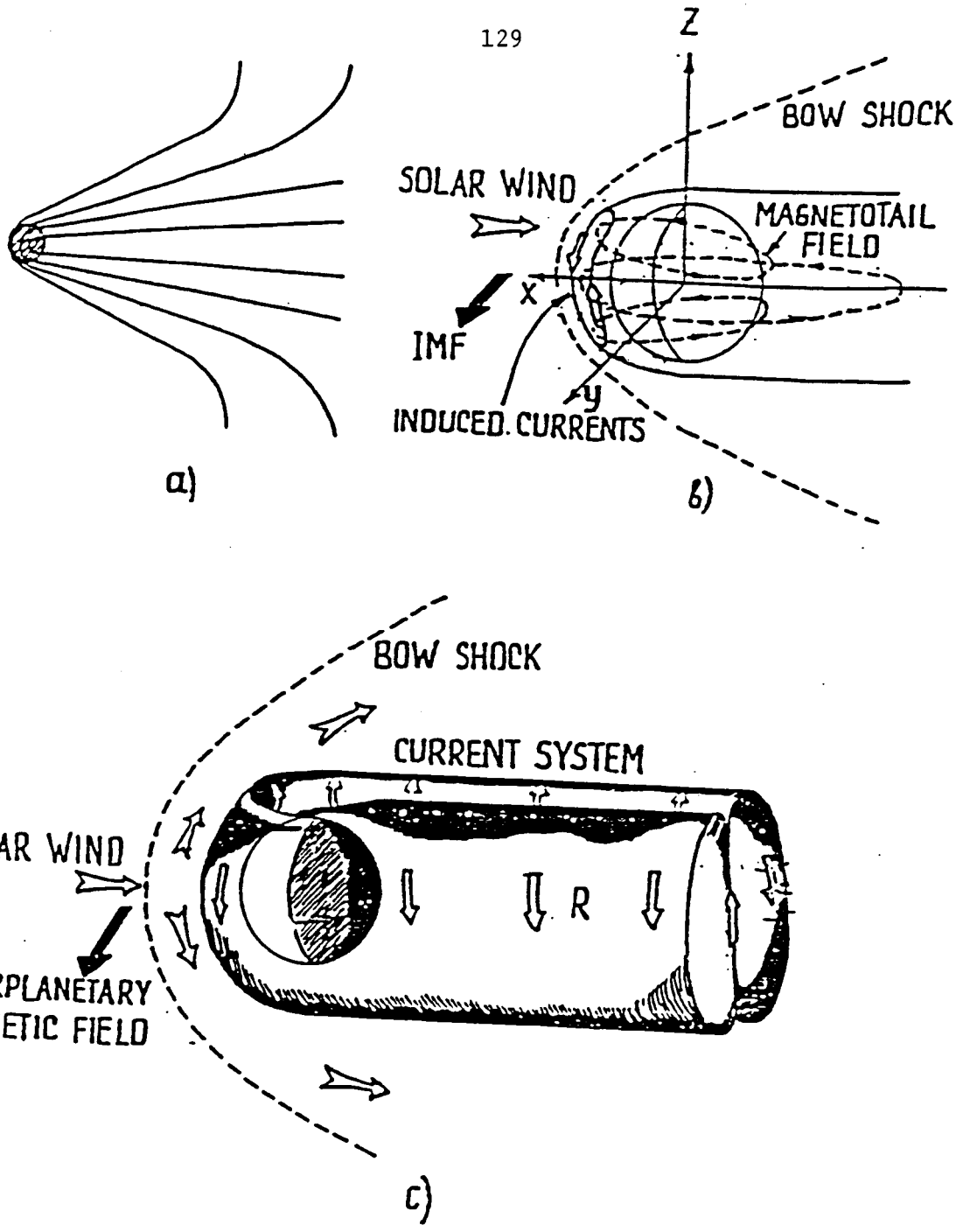

Figure 17

(Verigin, Gringauz, and Ness, 1983)

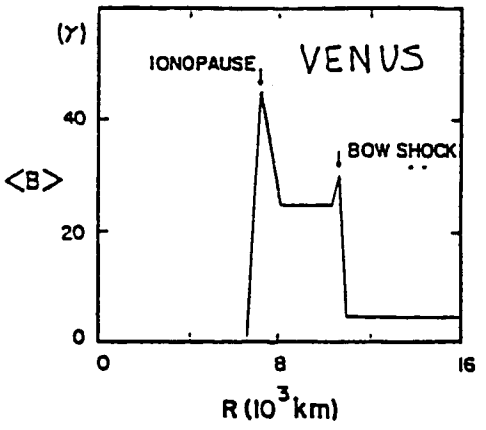

Figure 18a.

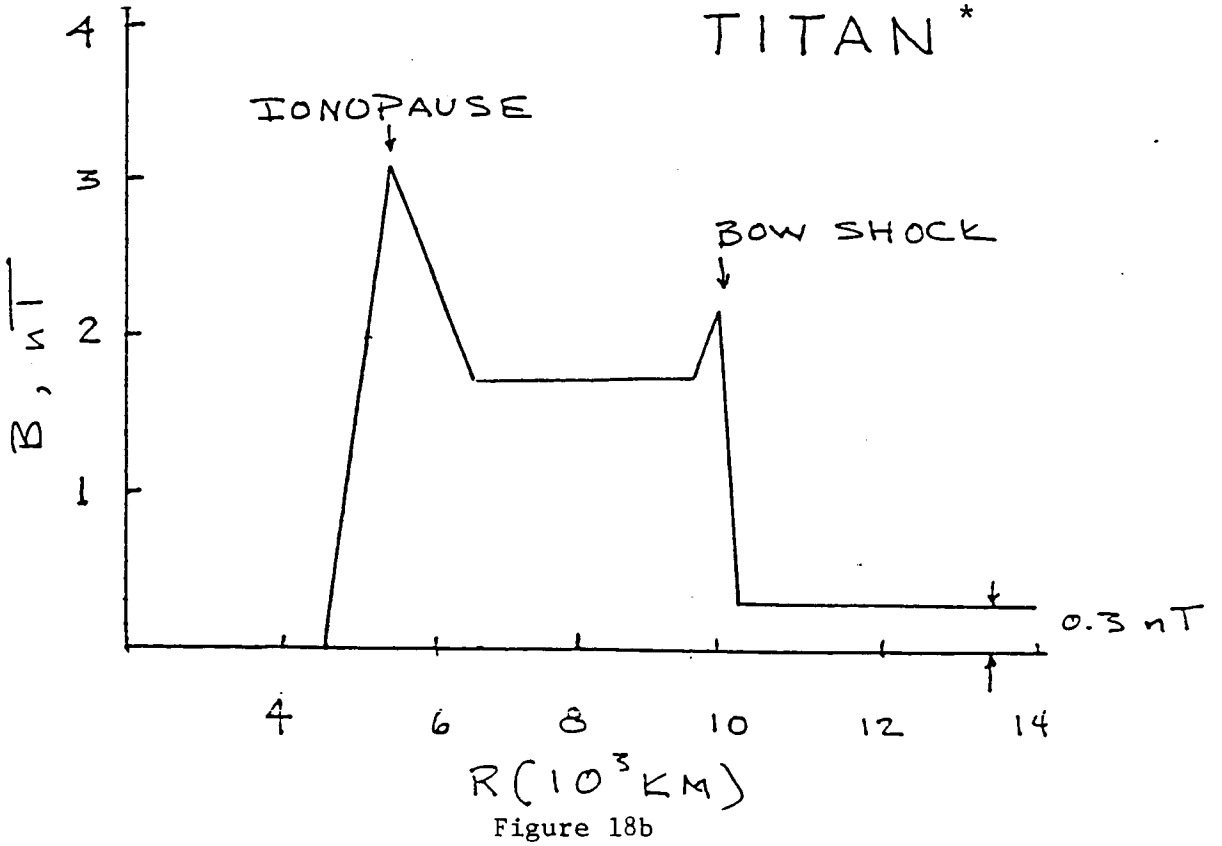

Figure 18b

* Mass loading and charge exchange neglected

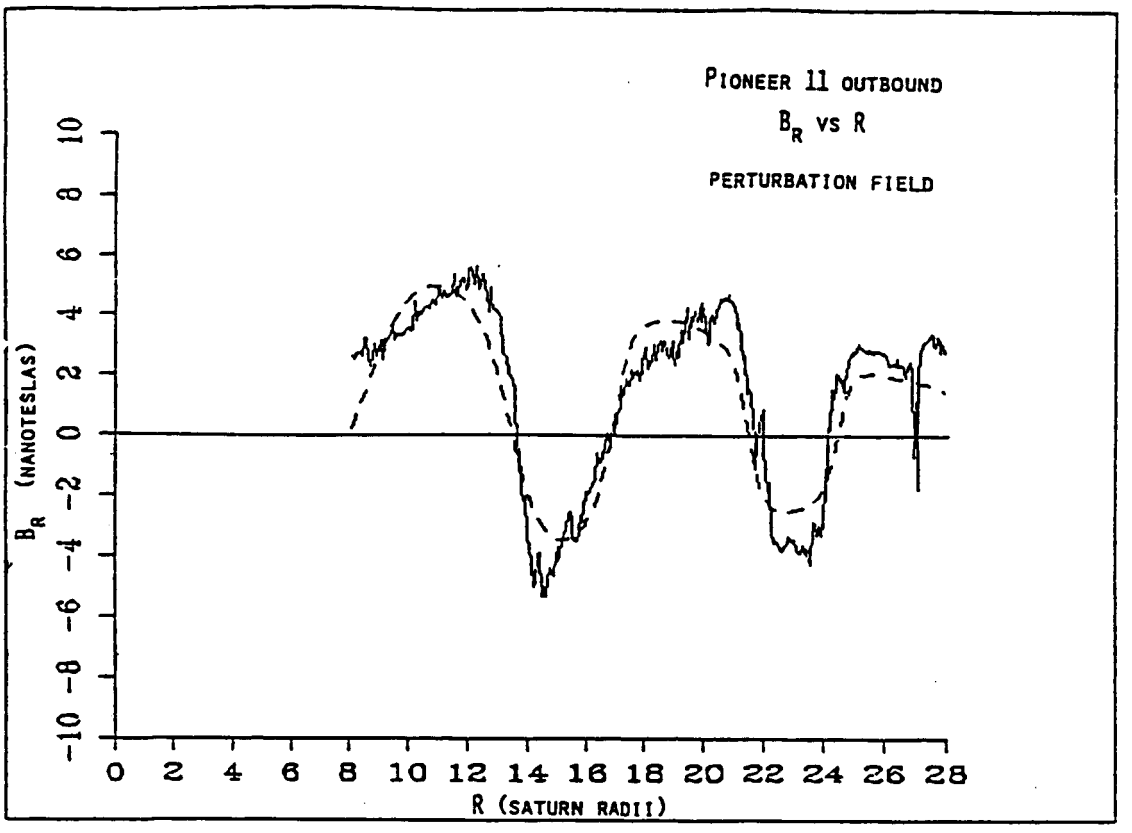

Figure 19a

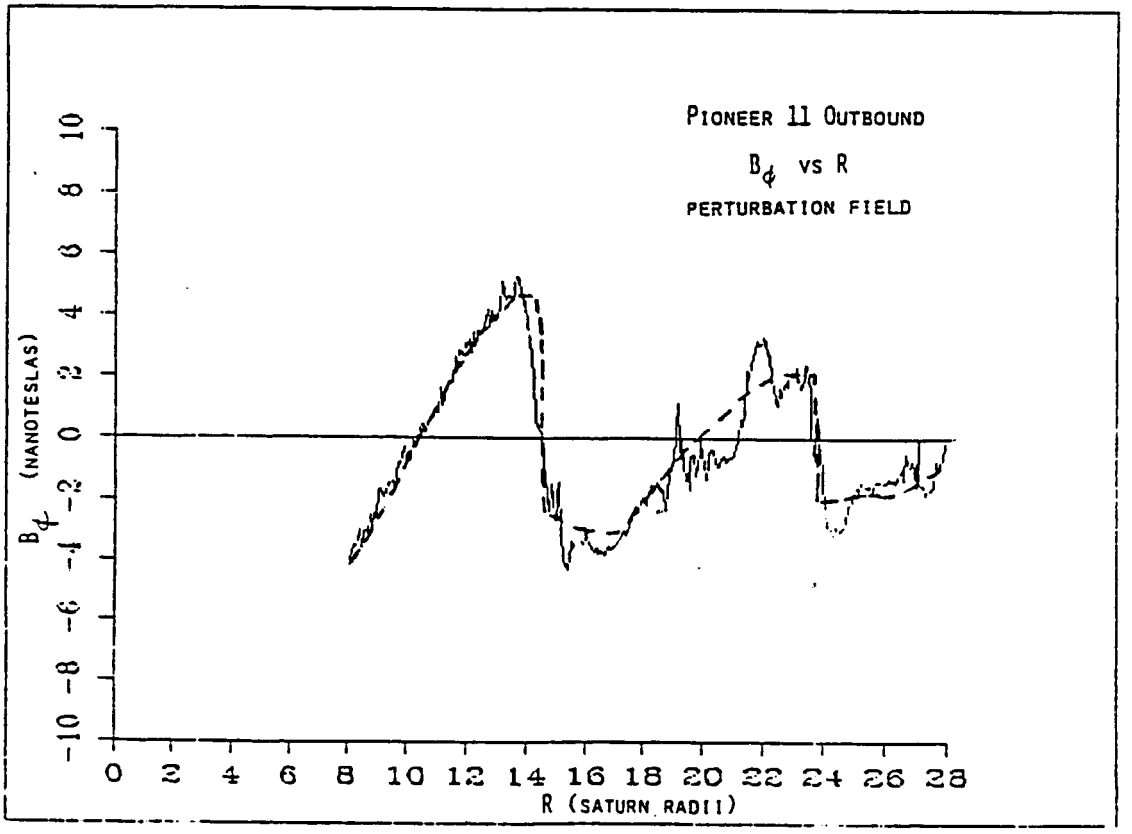

Figure 19b